Application of Vibration-based Techniques for Modal Identification and Damage Detection in Structures

Chaewoon Lim

A thesis

in

The Department

of

Building, Civil and Environmental Engineering

Presented in Partial Fulfillment of the Requirements

for the Degree of Master of Applied Science (Civil Engineering) at

Concordia University

Montreal, Quebec, Canada

October 2016

CONCORDIA UNIVERSITY
School of Graduate Studies

This is to certify that the thesis prepared

By: Chaewoon Lim

Entitled: Application of Vibration-based Techniques for Modal Identification and Damage Detection in Structures

and submitted in partial fulfillment of the requirements for the degree of

Master of Applied Science (Civil Engineering)

complies with the regulations of the University and meets the accepted standards with respect to originality and quality.

Signed by the final examining committee:

Lucia Tirca Chair

Anjan Bhowmick Examiner

Sivakumar Narayanswamy Examiner

Ashutosh Bagchi Supervisor

Approved by _____
Chair of Department or Graduate Program Director

_____
Dean of Faculty

Date _____

ABSTRACT

Application of Vibration-based Techniques for Modal Identification and Damage Detection in Structures

Chaewoon Lim

All structures such as bridges, buildings and dams are deteriorated by environmental conditions like corrosion, earthquake and traffic after they are built. Therefore, vibration-based damage identification (VBDI) techniques have attracted attention to verify the safety and functionality of structures. Conventional damage identification techniques such as non-destructive evaluation (NDE) methods have many obstacles and are not practical to be implemented in order to detect damage. One of the main obstacles is that the conventional methods are focused on local structural damage and easily affected by measurement noise. Moreover, there are several uncertainties that restrict the successful application of the damage detection. On the other hand, vibration-based techniques can be used when the global vibration characteristics is available. To do this, it is required to perform modal identification, perform model updating, and detect local changes in a structure.

The objectives of this study are: (a) to develop vibration-based techniques for modal identification by output-only information through the experimental and numerical study of bridges and frame structures; and (b) to study the VBDI techniques to perform model updating and damage detection using the changes in the dynamic characteristics of structures and determine their performance in practical structures.

Two existing bridges, a Pre-stressed Concrete Bridge (PSCB) and a Steel Box Bridge (STB) tested earlier were used here as case studies and the data from the vibration test were used to verify modal identification using output-only information. In this study, two output-only methods, Frequency Domain Decomposition (FDD) and Stochastic Subspace Identification (SSI) were studied to compare the results from the vibration test. In addition to this, laboratory experiments on three-story steel frame were carried out to generate additional data for testing the system identification and model updating methods. Further, various damage scenarios were created in the

frame to obtain the vibration signals corresponding to such conditions. The vibration data from the undamaged and damaged frame were used to study the performance of existing VBDI methods.

Based on the above study, it is concluded that both FDD and SSI techniques provide accurate results for modal identification in the case of studied structures. FDD is relatively simpler, but it may miss some modal information when two modes are closer. However, in the cases studied here, the modes are quite apart from each other. Among many available VBDI methods, the matrix update method performs better than others when the measurement noise is small. Otherwise, data-driven models such as those based on Genetic Algorithm should be used.

Acknowledgements

First, I would like to express my profound gratitude to my supervisor, Prof. (Dr.) Ashutosh Bagchi. Through my academic years, he has given guidance, suggestions and encouragement. His knowledge and motivation have helped me to write this thesis and also expanded to other things. For all of this, I will always be greatly appreciative of his assistants.

Also, I would like to thank Korea Expressway Corporation for giving me the chance to study at Concordia University and providing me the financial support.

A special thanks goes to Dr. Wontae Lee, Dr. Changgeun Lee and Mr. Bonseong Gu, researchers at KEC Research Institute for handing down their knowledge and providing me with the data for this research. My profound gratitude to Dr. Sangsoon Lee and Sanggil Seo for their teachings of my life.

I would like to extend my gratitude to my professor, Dr. Sungbo Kim at Chungbuk National University for his constant encouragement and inspiring guidance throughout my studies.

I would also like to thank my friends and colleagues at Concordia including a special thanks to Ardalan Sabamehr, Srishti Banerji, Amit Chandra and Mrinmoy Nath for their help.

Lastly, I thank my family.

Table of Contents

List of Figures

List of Tables

Nomenclature

a_n	unknown coefficients of the Fourier series
b_n	unknown coefficients of the Fourier series
Δt	time step
N	number of data
A	rectangular matrix in SVD
U	orthogonal matrix
S	diagonal matrix
V	orthogonal matrix
$\hat{G}_{yy}(jw_i)$	estimate of the output PSD
U_i	unitary matrix
u_{ij}	singular vectors
S_i	diagonal matrix
w_k	white noise vector sequences
v_k	measurement noises
$R(k)$	cross correlation function
O_n	observability matrix
C_n	extended controllability matrix
$W_1,\ W_2$	weighting matrices
$\xi_j^{(p)}$	modal damping ratio
$f_j^{(p)}$	j-th natural frequency

$\phi_j^{(p)}$	j-th mode shape
Δf_{stable_cr}	tolerance values for natural frequency
$\Delta \xi_{stable\_cr}$	tolerance values for damping ratio
$\Delta \phi_{stable\_cr}$	tolerance values for mode shape
$\psi''(x_i)$	curvature at location i
y_i	mode shape displacement at location i
F	flexibility matrix
ϕ	modal matrix
nm	number of measured mode
F_d	flexibility matrix of damaged structure
ϕ_d	modal matrix of damaged structure
ΔF	difference between flexibility matrices
δ	largest absolute value of ΔF
ψ_{dj}	jth damaged curvature
ψ_j	jth undamaged curvature
S_i	modal strain energy in ith mode
L	length of beam
EI	flexural rigidity
$\psi''(x)$	modal curvature
S_{ij}	strain energy of the jth element
γ_{ij}	damage index
k_j	stiffness matrix of member j

K	stiffness matrix of whole structure
S_i^d	total strain energy of damaged structure
K^d	global stiffness matrix of damaged structure
λ_{di}	ith eigenvalue of damaged structure
R_i	modal residual vector for ith mode
ϕ_{di}	ith mode shape of damaged structure
ne	number of elements
β	vector of unknown changes in element stiffness matrices
$\delta\lambda$	vector of measured eigenvalue changes

List of Abbreviations

AVT	Ambient Vibration Test
BFD	Basic Frequency Domain
CMS	Component Mode Synthesis
COMAC	Co-Ordinate Modal Assurance Criterion
DFT	Discrete Fourier Transform
DOF	Degree Of Freedom
EMA	Experimental Modal Analysis
ERA	Eigensystem Realization Algorithm
FDD	Frequency Domain Decomposition
FEM	Finite Element Method
FFT	Fast Fourier Transform
FVT	Forced Vibration Test
GA	Genetic Algorithm
ITD	Ibrahim Time Domain
MAC	Modal Assurance Criterion
MI	Modal Identification
MIMO	Multiple-Input-Multiple-Output
MLP	Multi-Layer Perceptron
MRPT	Minimum Rank Perturbation Theory
PP	Peak-Picking

PS	Power Spectral
PSCB	Pre-Stressed Concrete Box
PSD	Power Spectral Density
SHM	Structural Health Monitoring
SIMO	Single-Input-Multiple-Output
SISO	Single-Input-Single-Output
SPC	Sectional Property Calculator
SSI	Stochastic Subspace Identification
SSI/BR	Stochastic Subspace Identification/Balanced Realization
SSI/CVA	Stochastic Subspace Identification/Canonical Variate Analysis
STB	Steel Box
SVD	Singular Value Decomposition
VBDI	Vibration-Based Damage Identification

Chapter 1. Introduction

1.1 Background

All structures, such as bridges and buildings, deteriorate with time. The reasons of this deterioration are various including effects of environment, fatigue caused by repeated traffic loads and extreme loads like an earthquake. In recent days, this deterioration has become a global issue. Many highway bridges were built decades ago and have serious structural deficiencies. Visual inspection is the main method to maintain the safety of the bridges and this method consists of planned field inspection, typically once every several years. However this inspection has limited accuracy and efficiency. Serious damage could happen to the bridge between the gaps of inspection periods, and also, it is not easy to evaluate structural conditions after major events such as earthquakes. Therefore, structural detection and integrity assessment are necessary to ensure the serviceability and safety of structures at a higher frequency. Information on integrity and damage is especially important when the expected hazard level is high or after long-term usage.

Structural Health Monitoring (SHM) provides important tools for addressing these issues. Housner et al. (1997) defined the SHM as "the use of in-situ, non-destructive sensing and analysis of structural characteristics, including the structural response, for the purpose of detecting changes that may indicate damage or degradation". Guan et al. (2006) modified this definition as "the use of in situ, non-destructive sensing and analysis of structural characteristics, including the structural response, for the purpose of estimating the severity of damage and evaluating the consequences of damage on the structure in terms of response, capacity, and service-life. Simply, SHM represents the implementation of a Level IV (Rytter, 1993) non-destructive damage evaluation method".

Based on the above understanding, a more effective "condition-based" approach could be implemented. This condition assessment could include more quantitative content than that could be provided by visual inspection. The following assessment, for example, would be typically desired by the bridge management authority (Guan et al. 2006): (a) damage to the structure and changes in structural resistance, (b) probability of failure or of the structure's performance falling

below a certain threshold, and (c) estimation of the severity of damage and the remaining service life.

Vibration-based Damage Identification (VBDI) is a comparatively recent development in the SHM of civil engineering structures. The physical characteristics of the structure such as mass, stiffness and boundary condition affect vibration characteristics like frequencies, mode shapes, and damping. Damage can change these dynamic characteristics. Thus, the location and severity of the damage can be detected by utilizing vibration measurement (Bagchi et al. 2007). In the damage identification process, precise modeling of structure and calculation of damage detection algorithm is essential. The changes in modal parameters are generally used in VBDI techniques such as frequency changes, mode shape changes, mode shape curvature changes, flexibility matrix changes and modal strain energy changes. These changes are obtained from the monitoring of structural responses before and after damage.

Global vibration characteristics of a structure can be determined by the monitoring the whole structural system, instead of individual structural elements. Normally, a limited number of sensors are installed on a structure for monitoring purpose. The challenge is to obtain sufficient information from the limited number of sensors to locate the damage and assess its severity. VBDI is a combined method of experimental and analytical processes. The process of VBDI are: a) measurement of dynamic characteristics, b) modeling of the real structure, and c) detecting damage by the VBDI algorithm.

Frequency change method is relatively easy. Typical resolution for the natural frequencies of a lightly damped mechanical structure is 0.1% whereas typical mode shape errors are 10% or more (Friswell and Penny, 1997). However, the structural damage is generally a local damage and the frequency changes is not sensitive to small local damages (Salawu, 1997). Natural frequency of a structure relates to its global properties, and the above method cannot provide spatial information like location of damage. Theoretically, mode shape information can provide spatial information, but it is not practical because of measurement noise and requirement of high number of sensors. In addition, mode shape methods do not provide the information of damage severity (Pandey et al, 1991; Farrar and Jauregui, 1998). The modal strain energy is less affected by measurement noise, but it is difficult in practice to recognize damage location when a high noise level (e.g., 3%) can interfere with the changes due to low amount of damage (Alvandi and Cremona, 2006).

Other advantages of the monitoring the vibration characteristics are: (a) if measured periodically from the completion of the structures, the behavior of the structures could be recorded historically (b) safety changes could be identified simply by just comparing frequencies and mode shapes.

1.2 Objectives and Scopes

The main objectives of this study are: (a) to develop vibration-based techniques for modal identification by output-only information through the experimental and numerical study of bridges and frame structures; and (b) to study the VBDI techniques to perform model updating and damage detection using the changes in the dynamic characteristics of structures and determine their performance in practical structures.

In order to achieve these objectives the following tasks will be undertaken:

(i) Available modal identification methods (PSD, FDD, and SSI) will be implemented and compared using measured data from ambient vibration tests of two highway bridges and a scaled model of a steel frame tested in the laboratory. A new method will be developed based on the outcome of this study.

(ii) Finite element models of the structures will be constructed and correlated to provide the vibration response reasonably close to real bridges and test structures using the process of model updating.

(iii) A number of available VBDI techniques will be studied with respect to the above structures using the using the correlated FEM models to find the best method for systems identification and damage detection, and identify the limitations of every methods.

1.3 Layout of thesis

The thesis is composed of six chapters. Main part consists of experimental and numerical studies of modal identification and VBDI techniques. The experimental studies of modal identification are carried out for the highway bridges with output-only information (Chapter 5) and experimental and numerical studies of VBDI for the steel frame structure (Chapter 6). The brief contents of each chapter in the thesis are described below.

Chapter 1: The background of structural health monitoring and VBDI of civil structures and the objectives, scope and layout of the thesis

Chapter 2: Literature review of modal identification methods using output-only information and VBDI

Chapter 3: Theoretical review of modal identification methods (FFT, PSD, FDD, SSI)

Chapter 4: Theoretical review of VBDI techniques

Chapter 5: The details of the experimental and numerical studies of modal identification for the highway bridges

Chapter 6: The details of the experimental and numerical studies for the steel frame structure of modal identification and several VBDI methods

Chapter 7: Conclusions and recommendations for future research

Appendix: Case studies of damage identification and model updating techniques

Chapter 2. Literature Review

2.1 Modal identification methods using output-only information

The objective of Modal Identification (MI) is to identify the characteristic of structures from the experimental test especially by vibration test. There are two types of vibration tests: forced vibration test (FVT) and ambient vibration test (AVT). FVT is carried out under controllable input like shaker or dropper, but AVT is carried out under the operational condition such as traffic or wind loadings. Therefore, FVT can be used for the input and output information method, but AVT is used for the output-only information method. However, FVT method is not applicable for civil structures, because civil structures are generally massive, applied loads are not measurable and exciting massive structures with shaker is difficult. Therefore, AVT is more suitable for civil structures (Yi et el. 2004).

There are various modal identification methods using output-only information. The most frequently used method in civil structures would be the power spectral (PS) method in which the modal parameters can be identified by reading the peak frequency values and the amplitude of the power spectral density (PSD) functions (Newland 2012). The frequency domain decomposition (FDD) method was developed by using the singular value decomposition (SVD) of the power spectral density matrix (Brincker et al. 2000). This method was performed for the estimation of the modal parameters without knowing the input excitation and identification of modes with high accuracy. The power spectral (PS) method and the frequency domain decomposition (FDD) method are classified as the frequency domain method. However, there are several time domain methods assuming that the ambient loads are Gaussian white noise. Ibrahim time domain (ITD) method was developed to deal with the free vibration responses (Ibrahim and Pappa 1982). In this study, they proposed that the number of degrees of freedom to be allowed in the ITD identification algorithm can be several times larger than the number of structural modes of vibration excited in the time response functions used for the identification of modal parameters. The eigensystem realization algorithm (ERA) (Juang and Pappa 1985) was developed for modal parameter identification and model reduction of dynamic systems from test data. In this study, they compared

techniques to extract the modal parameters from output-only data. The stochastic subspace identification (SSI) method (Hermans and Van Der Auweraer 1990) was developed based on the system theory in the discrete time domain. This method uses the SVD of a block Hankel matrix with cross correlation matrix of responses.

2.2 Vibration-based Damage Identification (VBDI)

The objective of this study is to investigate the capability of vibration-based damage identification techniques to detect and locate damage in structures using vibration test. Generally, damage detection can be defined by four levels (Rytter, 1993) as described below.

Level 1: The method gives a qualitative indication that the damage might be present in the structure. (DETECTION)

Level 2: The method gives information about the probable location of the damage also. (LOCALIZATION)

Level 3: The method provides information about the size of the damage. (ASSESSMENT)

Level 4: The method provides information about the actual safety of the structure at a certain damage state. (CONSEQUENCE)

Most of the literature in VBDI is about Level 1 to Level 3 and few of them deal with Level 4 problem. Moreover, most of them deal with the application of theoretical damage identification or laboratory test. Application of this method on real structures such as bridges or buildings are very rare. Doebling et al. (1996), Sohn et al. (2004), and Farrar et al. (1994) reviewed the application of VBDI on real structures. These studies are about the possibility of VBDI method and tests time were short. There are many analytical methods to identify damage from changes of dynamic parameters. Detailed reviews of these methods have been provided by Doebling et al. (1996, 1998) and Humar et al. (2006). The following list is provided to depict various methods by Humar et al (2006),

1) Methods based on frequency changes
2) Methods based on mode shape changes
3) Mode shape curvature method
4) Methods based on change in flexibility matrix
5) Methods based on changes in uniform flexibility shape curvature
6) Damage index method
7) Method based on modal residual vector
8) Matrix update methods
9) Neural network methods
10) Genetic Algorithm

2.2.1 Methods based on frequency changes

Frequency changes are relatively insensitive to damage but natural frequencies are very sensitive to changes in temperature and other environmental conditions (Kim and Stubbs. 2003).

Salawu (1997) reviewed the natural frequency as a diagnostic parameter in structural assessment procedures using vibration monitoring. The approach is based on the fact that natural frequencies are sensitive indicators of structural integrity. In this paper, this method could provide an inexpensive structural assessment technique. However, this method requires either a theoretical model of damage or a set of sensitivity values to be computed before physical measurements. Moreover, this method might not be sufficient for a unique identification of the location of structural damage. Integrity assessment of civil engineering structures using vibration data would require a method which uses only test data from the first few modes and is based on simple assumptions about the behavior of the structure.

Kim and Stubbs. (2003) outlined the theory of a non-destructive crack localization and crack-size estimation algorithm for beam-type structures and carried out a field experiment of a full scale

plate girder bridge to verify the feasibility and applicability. The authors have provided the evidence that it was possible to localize cracks and estimate crack sizes in plate–girder bridges with the three natural frequencies and mode shapes measured before and after damage without having any prior knowledge of the material properties of the bridge

Steenackers and Guillaume (2005) presented a method to establish the correlation between variations in temperatures and the resulting resonant frequency variations. In this study, a correlation is made between the variations in temperatures and the resulting resonant frequency variations. They have investigated to check whether it is possible to distinguish changes in modal parameters due to damage from changes caused by temperature or other environmental variations.

2.2.2 Methods based on mode shape changes

Single-number measures of mode shape changes have been proposed to detect damage. A common single-number measure is the Modal Assurance Criterion (MAC) (Ewins, 2000). The MAC value varies from 0 to 1 and indicates the degree of correlation between two modes. The MAC value of 0 represents that there is no correlation and 1 is perfect correlation.

Allemang (2003) presented an overview of the use of MAC values and other similar assurance criteria to measure the correlation between two modes.

West (1986) proposed the Co-ordinate Modal Assurance Criterion (COMAC). This method is able to identify significant change and isolate the change to a particular locale in a complex structure. If the modal displacements at co-ordinate from two sets of measurements are identical, the COMAC value equals 1 for this co-ordinate while the smallest COMAC value at any point indicates the most likely location of damage.

Fox (1992) demonstrated that the single-number parameters, natural frequency and MAC value are the reasonable indicators of the presence of damage. However, it is not sufficient to locate the damage solely using these methods. Particularly, the MAC is a little insensitive when there is an experimental scatter. Graphical differences and relative changes in the mode shape provide the way of detecting the damage location when resonant frequencies and mode shapes were examined.

2.2.3 Mode shape curvature method.

Pandey et al. (1991) introduced mode shape curvature method for damage detection. In this study, finite element models of simply supported and cantilever beams have been used and it has been found that modal curvature is more sensitive damage indicator than the MAC and COMAC values. Moreover, strains have been used to obtain the experimental curvature mode shapes instead of displacement or acceleration.

Salawu and Williams (1994) evaluated the performance of some procedures for locating damage using mode shapes. They used simulated data using the finite element method to compare the effectiveness of the method in the absence of measurement errors. They found that although MAC and COMAC showed sensitivity to damage, they were unable to clearly indicate the damage location. They pointed out that the most important factor was to determine which modes to use since only some of the modes correctly identified and located the damage. They also suggested that if the methods (curvature mode shape and mode shape relative difference) were to be applied to large structures, it would be necessary to measure sufficient number of points, possibly in a grid-like format, in order to reasonably refine the identification.

Chance et al. (1994) presented that the mode curvature calculated by using accelerometer was disappointing in errors. So, they suggested to use strain gauges to closely represent an actual crack.

2.2.4 Methods based on change in flexibility matrix

Pandey and Biswas (1994) introduced this method not only for identifying the presence of the damage but also for locating the damage. Also, using a few of the lower frequency modes of vibration of the structure, the flexibility matrix can be easily and accurately estimated. The advantage of using a few lower frequency is that concerning of nonlinearity is not required. They found that this method works best when damage is located at a section where high bending moments occur, which also happens to be the probable location of occurrence of such a damage.

Jing et al. (2010) proposed a new method of changes of flexibility matrix. They found that the effect of truncating higher-order modes can be considerably reduced in the new method. They

demonstrated using a simply beam in the numerical example with only the lowest measured mode. They concluded that the proposed method was very efficient in damage locations regardless of a single or multiple damages.

Yang and Sun (2011) proposed a new method based on best achievable change to localize and quantify damage in structures. They used three examples to demonstrate the efficiency of the method and concluded that this method might be useful for structural damage identification.

2.2.5 Methods based on changes in uniform flexibility shape curvature

Zhang and Aktan (1995) used the flexibility and its derived curvature obtained from experiment and analysis as the indices for the measurement of the structural status. They applied these indices to a highway bridge and showed that these indices are very handy tool as damage indices. They proposed that absolute curvature difference of the uniform load surface together with the absolute displacement difference in uniform load surface give least error sensitive and reliable methods to detect bridge damage.

Jauregui and Farrar (1996) compared several different techniques for damage assessment including changes in uniform flexibility curvature method. They used experimental and numerical modal data gathered form the bridge.

Siddique et al. (2007) presented several VBDI techniques including this flexibility shape curvature method. They considered influence of temperature, sensor spacing on the accuracy and compared experimental and numerical modal properties.

2.2.6 Damage index method

Stubbs et al. (1995) performed this method for a full-scale structure. In this study, they used only three vibration modes and with no knowledge of the material properties of the structure, they accurately located damage in the structure.

Kim and Stubbs (1995) applied this method to the model plate girder and found that damage can be located with a relatively small error and relatively small false-negative error (i.e., missing detection of true damage locations) but a relatively large false-positive error (i.e., prediction of locations that are not damaged).

Chen et al. (1999) conducted investigation on aluminum and composite plates with different damage scenarios. They used scanning laser vibrometer to measure the mode shapes and to determine the changes in modal parameters. They found that this method was effective for damage detection on the plates and discussed the sensitivity of the technique and practicality issues in applying this technique to different structures.

Kim and Stubbs (2003) presented a damage index method to non-destructively locate cracks in full-scale bridges by using changes in modal parameters. Moreover, they found that it is feasible to accurately localize cracks in plate-girder bridges with three natural frequencies and mode shapes measured before and after damage with no knowledge of the material properties of the bridge.

2.2.7 Method based on modal residual vector

Kaouk and Zimmerman (1994) extended the concept of the minimum rank perturbation theory (MRPT) to determine the damage extent on the mass properties of undamped structures and proportionally damped structures. The MRPT method showed that this method is suitable for large-order problems. They performed the MRPT in assessing structural damage extent using numerical and experimental data.

Santos and Zimmerman (1996) presented an approach for structural damage localization using component mode synthesis (CMS) and residual modal force vector methods. In this study, they found that a) the MRPT dynamic residual vector fails in the localization of damage; b) the MRPT angle residual vector can localize the substructure damage by using analytical CMS substructured FEM even with a poor component modal base; c) the MRPT angle residual vector can localize the exact damage by using analytical CMS substructured FEM with a rich component modal base.

2.2.8 Matrix update methods

Hajela and Soeiro (1990) presented an output error approach and an equation error approach to detect structural damage. They tested on a fifteen-bar planar truss and a two-bar planar truss for these methods. Damage was detected successfully on the numerical model and physical model was not investigated.

Beck and Katafygiotis (1992) described that global health monitoring of a structure can be used to detect any significant changes in its stiffness distribution through continual updating of a structural model using vibration measurements. They used Bayesian probabilistic formulation to treat uncertainties which arise from measurement noise, modeling errors, and an inherent non-uniqueness common in this inverse problem.

Zimmerman and Kaouk (1994) presented the minimum rank update theory that makes use of an original finite element model and a subset of measured eigenvalues and eigenvectors. In this theory, first the location of structural damage is determined, then a minimum rank update algorithm is developed. If the actual damage results in a rank p change to the finite element model, then this algorithm produces exact results if p eigenvalues and eigenvectors are measured exactly. The method has been successfully used to detect the damage on an eight-bay truss, in which damage was induced by removing specified members.

Casas and Aparcio (1994) presented a method for the identification of cracking and real bearing conditions in concrete elements using analysis of dynamic response and successfully identified damage conditions. They found that at least two frequencies are required to obtain not only the cracked zone and equivalent inertia modulus, but also the real bearing conditions.

Fares and Maloof (1997) developed a probabilistic framework to detect and identify anomalies such as damage in structures. They introduced a new framework that can avoid ill-conditioning in the identification problem and clear relation between measurements and modeling. They applied an example to detect and identify part-through cracks in a plate from surface strain measurements.

Beck and Katafygiotis (1998) addressed the problem of updating a structural model and its associated uncertainties by utilizing dynamic response data using a Bayesian statistical framework. They found that this framework can handle the inherent ill-conditioning and possible non-

uniqueness in model updating applications. A large-sample asymptotic expression was given for the updated predictive probability distribution of the uncertain structural response.

Hu et al. (2001) described subspace rotation algorithm for the damage location detection. They tested a ten-bay planar truss structure for checking the present approaches numerically and used the experimental data from the vibration test of a beam with two fixed ends. They found that the method performed well in spite of the little structural information and measurement inaccuracies.

2.2.9 Neural network methods

The most common neural network in use is the multilayer perceptron (MLP) trained by backpropagation (Wu et al. 1992). They used a back-prop neural network to identify damage in a three-story shear building by earthquake excitation. The damage was introduced by reducing the stiffness of a specified member with 50% to 70%. The neural network was used to identify the level of damage in each of the members using the Fourier transform of acceleration data.

Doebling et al. (1996) described neural network-based damage identification methods. In this study, they found that damage was typically modelled by a linear process. Most studies used changes of member shape or cross-sectional area to describe damage. Therefore, the considered cases could not produce a non-linear dynamic system, which may be expected in a most real damaged structure.

Masri et al. (1996) adapted a neural network-based approach to detect small changes in structural parameters, even when the vibration measurements were polluted by noise.

2.2.10 Genetic Algorithm

Mares and Surace (1996) presented the concept of the residual force vectors to specify an objective function for an optimization procedure then, they used genetic algorithms to identify damage in elastic structures.

Friswell et al. (1998) proposed a combined genetic and eigensensitivity algorithm to locate damage in structures.

Chou and Ghaboussi (2001), Xia and Hao (2001) applied genetic algorithm in structural damage identification. Au et al. (2002) proposed the two-level search strategy and the micro-genetic algorithm to identify structural damage severity. When there are too many candidates in the possible damage domain, they used this method to reduce the computational complexity of traditional genetic algorithms involved in evaluating the fitness functions for large populations.

Chapter 3. Modal Identification

3.1 Modal Identification

Modal Identification means to identify the properties of real structures from the experimental vibration test. Modal Identification can be classified as time domain analysis, frequency domain analysis and time-frequency domain analysis of a signal. Traditional Experimental Modal Analysis (EMA) makes use of measured input excitation and output response. Various modal identification algorithms, such as Single-Input-Single-Output (SISO), Single-Input-Multiple-Output (SIMO) and Multiple-Input-Multiple-Output (MIMO) techniques, have been developed both in the Time Domain and the Frequency Domain. Traditional EMA has been applied in various fields like vibration control, structural dynamic modification, and analytical model validation, as well as vibration-based structural health monitoring in mechanical, aerospace and civil applications. However, for large civil structures such as bridges and buildings, it is very difficult to excite the structure using controlled input. It is also impossible to measure all the inputs under operational conditions, especially those from ambient sources.

Vibration tests are usually divided into the forced vibration tests (FVT) and the ambient vibration tests (AVT). AVT is carried out under ordinary operating conditions with uncontrollable and immeasurable ambient loads such as traffic and wind loadings, while FVT is performed using the controllable and measurable loads such as droppers and shakers. FVT usually requires more expensive equipment and controlled operating conditions. However, AVT may be carried out under normal operating conditions and require simpler equipment. FVT is usually used for input and output information, while AVT is used for output information. Input and output method is not enough for civil structures because these structures are massive, immeasurable input sources and difficult to shake structures efficiently. Therefore, the output only method is more appropriate than input and output method. In this regard, AVT may be more suitable testing methods for civil structures like bridges, buildings and dams. The non-stationarity in ambient loads would be one obstacle to apply AVT to modal testing; however, the undesirable non-stationary effect can be

minimized by collecting a sufficiently long data or deleting any parts of the response data under the non-stationary ambient loads (Yi et al. 2004).

3.2 Discrete Fourier Transform (DFT) and Fast Fourier Transform (FFT)

The acquired signal form vibration measurement is typically obtained in the time domain. However, we use changes of the dynamic properties such as natural frequencies, mode shapes, and damping ratio when we perform VBDI to identify the damage. This is because it is more convenient to identify the dynamic properties of a structure from a frequency response spectrum than from the time domain data. DFT and FFT are generally used to convert the signal from the time domain to the frequency domain.

The vibration responses of a structure are continuous in time, but the raw data recorded in a computer through a data acquisition system are sampled at discrete intervals. Therefore, a discrete Fourier transform (DFT) is required. A DFT is a discrete approximation of the Fourier integral, which is the analog counterpart of the DFT. The fast Fourier transform (FFT) is an algorithm for computing the DFT. The major advantage of the FFT is the speed with which it analyzes large numbers of waveform samples. By making use of periodicities in the sinusoidal functions that are multiplied to do the transforms, the FFT greatly reduces the amount of calculation required. Ramirez (1985) and Brigham (1988) gave the details of the implementation of the FFT.

Storey (2002) explained FFT analysis with MATLAB easily as follows; assuming a signal that last for 1 second, the signal can be represented by the infinite series

$$f(t) = a_0 + \sum_{n=1}^{\infty}(a_n\,(\sin(2\pi nt) + b_n\cos(2\pi nt)) \tag{3.1}$$

where $f(t)$ is the signal in the time domain, a_n and b_n are unknown coefficients of the series. The Fourier representation is formally periodic, this means that the beginning of the cycle is always equal to the end ($f(t = 0) = f(t = 1)$).

Unknown coefficients can be calculated as follows;

$$\int_0^1 f(t)\sin(2\pi nt)\,dt = \frac{a_n}{2}$$

$$\int_0^1 f(t)\cos(2\pi nt)\,dt = \frac{b_n}{2} \qquad (3.2)$$

$$\int_0^1 f(t)\,dt = a_0$$

However, the data form measurement are discrete data, not an analytical function. Therefore, taking a Fourier transform of discrete data (DFT) is done by taking a discrete approximation to the integrals (3.2). This discrete integral can be computed using the trapezoidal rule. However this DFT method requires so many operations to perform DFT using the trapezoidal rule.

$$a_n = \Delta t\left[\sin(2\pi t_1)\,f(t_1) + \sin(2\pi t_N)\,f(t_N) + 2\sum_{j=2}^{N-1}\sin\left(2\pi t_j\right)f\left(t_j\right)\right] \qquad (3.3)$$

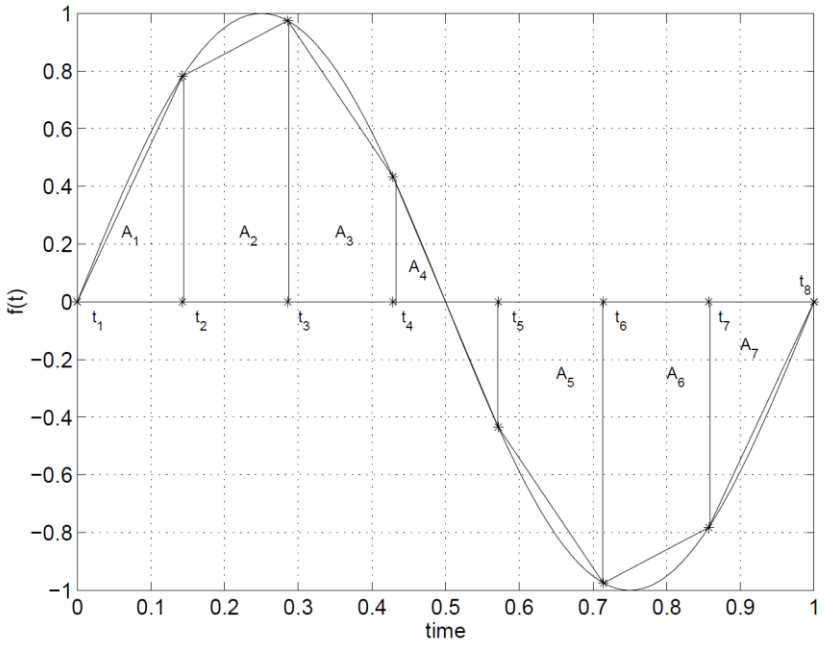

Fig. 3.1 Schematic of trapezoidal rule (Storey)

The FFT algorithm can reduce the computation times enormously. The FFT in MATLAB uses complex numbers and the FFT computes positive and negative frequencies. The real part of the FFT corresponds to the cosines series and the imaginary part corresponds to the sine. The MATLAB FFT returns data that needs to be divided by N/2 to get the coefficients. To obtain the coefficients a_n and b_n, we use the following formulas,

$$a_n = -\frac{1}{2N} imag(c_n), 0 < n < \frac{N}{2}$$

$$b_n = \frac{1}{2N} real(c_n), 0 < n < \frac{N}{2} \tag{3.4}$$

where c_n is the coefficient of the MATLAB FFT. The Eq. (3.4) are appropriate for $0 < n < N/2$. The values of negative frequencies provide no new information because the coefficients are simply complex conjugates.

3.3 Power Spectral Density

The simplest method to estimate modal parameters from operation data in the frequency domain is the so-called Peak-Picking (PP) or Basic Frequency Domain (BFD) method. In this method, the natural frequencies are simply taken from the observation of the peaks on the power spectrum plots. The method yields estimations of acceptable accuracy when the structure exhibits low damping, and structural modes are well separated in frequency. However, a violation of these conditions leads to erroneous results. Another disadvantage is that the method does not given any estimate of modal damping.

Storey (2002) explained power spectrum analysis with MATLAB as follows; we are interested in the absolute value of the FFT coefficients. This absolute value gives the total amount of information contained at a given frequency, the square of the absolute value is considered as the power of the signal. Fig. 3.2 shows an example of 10 Hz sine wave ($f = sin(2 * 10 * \pi t)$).

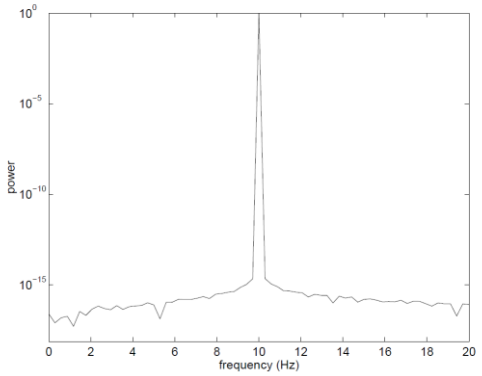

Fig. 3.2 Power spectrum of a 10 Hz sine wave (Storey)

3.4 Frequency Domain Decomposition (FDD)

FDD is an output-only modal analysis method in the frequency domain, proposed by Brincker et al. (2000). Taking the Singular Value Decomposition (SVD) of the spectral matrix, the spectral matrix is decomposed into a set of auto spectral density functions, each corresponding to a single degree of freedom system.

SVD is based on a theorem from linear algebra which says that a rectangular matrix A can be broken down into the product of three matrices (an orthogonal matrix U, a diagonal matrix S, and the transpose of an orthogonal matrix V) (Baker 2005). The theorem is usually presented something like this:

$$A_{mn} = U_{mm} S_{mn} V_{nn}^{T} \tag{3.5}$$

where $U^T U = I$, $V^T V = I$; the columns of U are orthonormal eigenvectors of AA^T, the columns of V are orthonormal eigenvectors of $A^T A$, and S is a diagonal matrix containing the square roots of eigenvalues from U or V in descending order. For S we take the square roots of the non-zero eigenvalues and populate the diagonal with them, putting the largest in s_{11}, the next largest in s_{22} and so on until the smallest value ends up in s_{mm}. The non-zero eigenvalues of U and V are always the same.

FDD method is used in a lightly damped structures, when the loading is white noise and the mode shapes of close modes are geometrically orthogonal. In order to obtain the natural frequencies and mode shapes, the power spectral density matrix is estimated, then the estimate of the output PSD $\hat{G}_{yy}(jw_i)$ is decomposed by taking the SVD of the matrix.

$$\hat{G}_{yy}(jw_i) = U_i S_i U_i^H \tag{3.6}$$

where the matrix $U_i = [u_{i1}, u_{i2}, \dots, u_{im}]$ is a unitary matrix including the singular vectors u_{ij} and S_i is a diagonal matrix including the scalar singular values s_{ij}. If singular values obtained from outputs of the structure are plotted in an SVD diagram, dominant peaks are natural frequencies of the structure and the corresponding singular vectors are mode shapes (Brincker et al. 2000).

3.5 Stochastic Subspace Identification (SSI)

There are two kinds of the SSI methods (Yi et al. 2004); one is SSI/BR (balanced realization) and the other is SSI/CVA (canonical variate analysis). The SSI method utilizes the SVD of a block Hankel matrix with cross correlation matrix of responses. The deterministic models are not appropriate to output-only system such as bridges and dams. In this system, the noise components from uncertainty have to be removed by considering stochastic components w_k and v_k.

$$x_{k+1} = Ax_k + w_k \tag{3.7}$$

$$y_k = Cx_k + v_k \tag{3.8}$$

where w_k is statistically uncorrelated white noise vector sequences with zero means representing the process and v_k is measurement noises. The covariance between the outputs and a limited set of reference outputs is used instead of inputs, because the input components are not available in output-only methods. So, impulse responses are replaced by output covariance and the inputs by reference outputs.

The cross correlation function $R(k)$ can be calculated using the Eq. (3.9)

$$R(k) = E[y(k+m)y(m)^T] = CA^{k-1}E[z(m+1)y(m)^T] = CA^{k-1}G \tag{3.9}$$

The block Hankel matrix can be decomposed into an observability matrix (O_n) and an extended controllability matrix (C_n) as in the last equality of Eq. (3.10)

$$H_{n_1 n_2}^{SSI} = \begin{bmatrix} y(1+m)y(m)^T & \cdots & y(n_2+m)y(m)^T \\ \vdots & \ddots & \vdots \\ y(n_1+m)y(m)^T & \cdots & y(n_1+n_2+m)y(m)^T \end{bmatrix} = \begin{bmatrix} R_1 & \cdots & R_{n_2} \\ \vdots & \ddots & \vdots \\ R_{n_1} & \cdots & R_{n_1+n_2-1} \end{bmatrix}$$

$$= \begin{bmatrix} CG & \cdots & CA^{n_2-1}G \\ \vdots & \ddots & \vdots \\ CA^{n_1-1}G & \cdots & CA^{n_1+n_2-1}G \end{bmatrix} = \begin{bmatrix} C \\ \vdots \\ CA^{n_1-1} \end{bmatrix} [G \quad \cdots \quad A^{n_2-1}G] = O_{n_1} C_{n_2}^{ext} \tag{3.10}$$

Weighting matrices W_1 and W_2 multiply to Hankel matrix. SSI/BR is using identify matrix as weighting matrices, while SSI/CVA is using the weighting matrices by maximizing the correlation between the measured time history data at different locations.

$$W_1 = L^{+-1},\ W_2 = L^{--1} \tag{3.11}$$

where $R^+ = \begin{bmatrix} R_0 & \cdots & R_{p-1}^T \\ \vdots & \ddots & \vdots \\ R_{p-1} & \cdots & R_0 \end{bmatrix} = L^+L^{+T},\ R^- = \begin{bmatrix} R_0 & \cdots & R_{q-1}^T \\ \vdots & \ddots & \vdots \\ R_{q-1} & \cdots & R_0 \end{bmatrix} = L^-L^{-T}$

After pre and post-multiplying of invertible weighting matrices W_1 and W_2 to the block Hankel matrix and decomposing it into $W_1O_{n_1}$ and $C_{n_2}^{ext}W_2$ by SVD, the observability matrix can be obtained as follows

$$W_1H_{n_1n_2}^{SSI}W_2 = [U_1 \quad U_2]\begin{bmatrix}\sum_1 & 0\\ 0 & 0\end{bmatrix}\begin{bmatrix}V_1^T\\ V_2^T\end{bmatrix} \approx U_1\sum_1 V_1^T \Leftrightarrow W_1O_{n_1}C_{n_2}^{ext}W_2$$

$$U_1\sum_1^{1/2}\sum_1^{1/2}V_1^T = W_1O_{n_1}C_{n_2}^{ext}W_2 \tag{3.12}$$

$$U_1\sum_1^{1/2} = W_1O_{n_1},\ \sum_1^{1/2}V_1^T = C_{n_2}^{ext}W_2$$

$$\therefore\ O_{n_1} = W_1^{-1}U_1\sum_1^{1/2}$$

Finally, the system matrix A can be obtained using the upper (n_1-1) block matrix deleting the last block row of O_{n_1} and lower (n_1-1) block matrix of the upper-shifted matrix by one block row as

$$O_{n_1-1}^{\uparrow} = O_{n_1-1}A \tag{3.13}$$

where $O_{n_1-1}^{\uparrow} \triangleq \begin{bmatrix} CA \\ CA^2 \\ \vdots \\ CA^{n_1-1} \end{bmatrix},\quad O_{n_1-1} \triangleq \begin{bmatrix} C \\ CA \\ \vdots \\ CA^{n_1-2} \end{bmatrix}$

The modal parameter such as natural frequencies, mode shapes and damping ratios can be determined from system matrix A.

In the cases of time domain identification techniques such as ERA and SSI, an appropriate system order should be determined. The size of system matrix A is theoretically 2n, if the structural model has n-DOFs. However, a real structure has infinite number of DOFs. So the meaningful system order should be determined to carry out engineering problems. The singular values have the following relationship as

$$\sigma_1 \geq \sigma_2 \geq \cdots \geq \sigma_{2n} \gg \sigma_{2n+1} \geq \sigma_{2n+2} \geq \cdots \geq 0 \tag{3.14}$$

Therefore, it would be possible to find out the suitable system order by looking into the trend of singular values. However in reality, it may be very difficult to find out a large drop in singular values due to the effect of the measurement noise. In such cases, the proper system order may be determined by looking into the trend of the estimated modal parameters in a stabilization chart, as the system order increases sequentially. The following criteria can be used to classify a mode as stable mode, unstable mode and noise mode.

Noise mode: if the estimated modal damping ratio is larger than a prescribed value

$$\xi_j^{(p)} > \xi_{noise\_cr} \tag{3.15}$$

where $\xi_j^{(p)}$ is j-th identified modal damping ratio at the system order p and ξ_{noise_cr} is the prescribed critical value for damping ratio.

Stable modes

$$\begin{aligned} \frac{f_j^{(p)} - f_j^{(p+1)}}{f_j^{(p)}} &< \Delta f_{stable\_cr} \\ \frac{\xi_j^{(p)} - \xi_j^{(p+1)}}{\xi_j^{(p)}} &< \Delta \xi_{stable\_cr} \\ 1 - \frac{\left\| \phi_j^{(p)} \cdot \phi_j^{(p+1)} \right\|^2}{\left\| \phi_j^{(p)} \right\|^2 \left\| \phi_j^{(p+1)} \right\|^2} &< \Delta \phi_{stable\_cr} \end{aligned} \tag{3.16}$$

where $f_j^{(p)}$ and $\phi_j^{(p)}$ are j-th natural frequency and mode shape at the system order p, and Δf_{stable_cr}, $\Delta \xi_{stable\_cr}$, $\Delta \phi_{stable\_cr}$ are the tolerance values for the natural frequency, damping ratio and mode shape. The tolerance values may be determined by considering the structural type and the confidence level of the measurement data.

Chapter 4. Vibration-based Damage Identification

4.1 General

There are a number of methods for vibration-based damage identification in literature (Doebling et al. 1997, Humar et al. 2006, and Bagchi et al. 2007). In this part, several methods of VBDI reviewed in literature will be introduced. These include methods reviewed in literature review (section 2.2) and other relevant areas.

4.2 Methods based on frequency changes

Frequency changes come from structural property changes such as mass, stiffness and damping. However, this technique has significant practical limitations for application for real structures. There are two reasons. First, very precise frequency measurements are required to detect small levels of damage. Second, environmental elements, especially temperature, have an important effect on frequency changes. Therefore, it is difficult that frequency changes can be used to detect more than Level 1 damage. If higher modal frequencies are used, this method may be useful because these modes are associated with local responses. However, it is difficult to excite and extract these higher local modes.

4. 3 Methods based on mode shape changes

Damage reduces the stiffness of structures and it alters the mode shapes. Mode shape changes are good indicators as the damage identification and the location of the damage. Single-number measures of mode shape changes such as the Modal Assurance Criterion (MAC) are suggested to detect damage in a beam with a saw cut (Fox, 1992). The MAC can be mathematically summarized

by the following equation (Allemang and Brown, 1982). This MAC value compares between two mode shapes (damaged and not damaged or measured and computed).

$$MAC_{cdr} = \frac{\left|\{\phi_{cr}\}^T\{\phi_{dr}^*\}\right|^2}{\{\phi_{cr}\}^T\{\phi_{cr}^*\}\{\phi_{dr}\}^T\{\phi_{dr}^*\}} \tag{4.1}$$

A value close to 1 suggests that the two mode shapes are well correlated, while a value close to 0 indicates that the mode shapes are not correlated. However, mode shape changes are usually so small that detection of damage is impractical (Humar et al. 2006).

4.4 Mode shape curvature method

Instead of using methods based on mode shape changes to obtain spatial information, mode shape curvature method is an alternative method. This method is better than mode shape changes to detect damage for a beam type structure.

The curvature values can be computed from the measured displacement mode shapes by using a central difference operator. Therefore, the curvature $\psi''(x_i)$ at location i along a beam is obtained from

$$\psi''(x_i) = \frac{y_{i+1}-2y_i+y_{i-1}}{h^2} \tag{4.2}$$

where y_i is the mode shape displacement at location i and $h = x_{i+1} - x_i$. An advantage of this Eq. (4.2) is that an analytical model is not required when healthy mode shapes are obtained from measurement. Modal curvatures are easily affected by measurement errors (Humar et al. 2006).

4.5 Methods based on change in flexibility matrix.

In this flexibility change method, damage is detected by comparing the flexibility matrix measured from the mode shapes of the damaged and undamaged structure. The flexibility matrix is the inverse matrix of the static stiffness matrix. Therefore, the flexibility matrix is relations between the applied static force and displacement. The measured flexibility matrix can be estimated from the mass-normalized measured mode shapes and frequencies. The flexibility matrix F of the undamaged structure is obtained from the Eq. (4.3) (Humar et al. 2006).

$$F \approx \phi\Omega^{-1}\phi^T = \sum_{j=1}^{nm} \frac{1}{\lambda_j}\phi_j\phi_j^T \tag{4.3}$$

where ϕ is the modal matrix of the mass-normalized mode shapes ϕ_j and nm is the number of measured mode shapes. This equation of the flexibility matrix is approximate because only the first few modes of the structure can be measured (Deobling et al. 1997). The flexibility matrix F_d of the damaged structure is obtained from the Eq. (4.4) (Humar et al. 2006)

$$F_d \approx \phi_d\Omega_d^{-1}\phi_d^T = \sum_{j=1}^{nm} \frac{1}{\lambda_{dj}}\phi_{dj}\phi_{dj}^T \tag{4.4}$$

where ϕ_d is the modal matrix of the damaged structure.

The difference between flexibility matrices of the damaged and undamaged structure is obtained from

$$\Delta F = F_d - F \tag{4.5}$$

Let δ as the row vector whose jth element is equal to the element with the largest absolute value in the jth column of ΔF.

$$\delta_j = max\left|\Delta F_{ij}\right| i = 1, \dots, N \tag{4.6}$$

The large value of δ is relevant to the location of damage.

4.6 Methods based on changes in uniform flexibility shape curvature

As mentioned before, the flexibility matrix is relations between the applied static force and the displacement of the corresponding degree of freedom. Therefore, a displacement curvature shape can be obtained corresponding to each column of F and F_d. The difference of curvatures between damaged and undamaged can be obtained from

$$\delta = \sum_j |\psi_{dj} - \psi_j| \tag{4.7}$$

where ψ_{dj} is the jth damaged curvature, ψ_j is the jth undamaged curvature (Humar et al. 2006).

4.7 Damage index method

This damage index method was proposed by Stubbs et al. (1995) to identify damage in a beam-type structure. Damage index is defined as the change in strain energy of the structure when it is deformed. This modal strain energy can be derived from the curvature of the measured mode shapes. In a linear elastic beam of NE elements, damage causes reduction in the flexural rigidity of one or more elements. The lowest nm mode shapes of the structure have been made both of the undamaged and the damaged structure. In the process of the numerical differentiation method such as the central difference operation, modal curvature can be derived. The modal strain energy in the ith mode is obtained from

$$S_i = \int_0^L EI(x)[\psi_i''(x)]^2 dx \tag{4.8}$$

where L is the length of the beam, EI is the flexural rigidity, and $\psi''(x)$ is modal curvature.

With the above case, the strain energy of the jth element between a and b is

$$S_{ij} = \int_a^b EI_j[\psi_i''(x)]^2 dx \tag{4.9}$$

Total strain energy contributed by element j is given by the ratio $F_{ij} = S_{ij}/S_i$. For the damaged structure, the above equations are changed into

$$S_i^d = \int_0^L EI^d(x)\left[\psi_i^{d\prime\prime}(x)\right]^2 dx$$

$$S_{ij}^d = \int_a^b EI_j^d\left[\psi_i^{d\prime\prime}(x)\right]^2 dx \tag{4.10}$$

$$F_{ij}^d = S_{ij}^d / S_i^d$$

Assuming that damage is limited to a few elements, the damaged and undamaged flexural rigidity would be approximately same $EI^d(x) \approx EI(x)$. It is also assumed that $F_{ij}^d \approx F_{ij}$.

Substituting Eq. (4.8) through (4.10), we get

$$\gamma_{ij} = \frac{EI_j}{EI_j^d} = \frac{\int_0^L EI(x)\left[\psi_i''(x)\right]^2 dx \cdot \int_a^b \left[\psi_i^{d\prime\prime}(x)\right]^2 dx}{\int_0^L EI^d(x)\left[\psi_i^{d\prime\prime}(x)\right]^2 dx \cdot \int_a^b \left[\psi_i''(x)\right]^2 dx} \tag{4.11}$$

where γ_{ij} is the damage index for the jth element in mode no. i. This damage index is changed as follows to use the information available from the nm measured modes

$$\gamma_j = \frac{\sum_{i=1}^{nm} f_{ij}^d}{\sum_{i=1}^{nm} f_{ij}} \tag{4.12}$$

where

$$f_{ij} = \frac{\int_a^b \left[\psi_i''(x)\right]^2 dx}{\int_0^L EI(x)\left[\psi_i''(x)\right]^2 dx}$$

$$f_{ij}^d = \frac{\int_a^b \left[\psi_i^{d\prime\prime}(x)\right]^2 dx}{\int_0^L EI^d(x)\left[\psi_i^{d\prime\prime}(x)\right]^2 dx}$$

Elements with relatively large γ_j are likely to be damaged.

When the strain energy contributed by the jth member in the modes is very small, the denominator will be very small in magnitude too. This may arise numerical problems in the evaluation of Eq. (4.11) and (4.12). In that case, Eq. (4.12) is modified as follows

$$\gamma_j = \frac{1+\sum_{i=1}^{nm} f_{ij}^d}{1+\sum_{i=1}^{nm} f_{ij}} \tag{4.13}$$

The above method can be applied to a general structure. The undamaged structure's strain energy of member j in mode i is given by

$$S_{ij} = \phi_i^T k_j \phi_i \tag{4.14}$$

The total strain energy of the structure deforming in its mode i is obtained from

$$S_i = \sum_j \phi_i^T k_j \phi_i = \phi_i^T K \phi_i \tag{4.15}$$

where k_j is the stiffness matrix of member j and K is the stiffness matrix of the whole structure. Similarly, the total strain energy of damaged structure can be obtained from

$$S_i^d = \sum_j \phi_i^{dT} k_j^d \phi_i^d = \phi_i^{dT} K^d \phi_i^d \tag{4.16}$$

where K^d is the global stiffness matrix of the damaged structure and it can be taken as approximately equal to undamaged global stiffness matrix K. Similarly, the damage index can be obtained from

$$f_{ij} = \frac{\phi_i^T k_j \phi_i}{\phi_i^T K \phi_i} \tag{4.17}$$

$$f_{ij}^d = \frac{\phi_i^{dT} k_j \phi_i^d}{\phi_i^{dT} K \phi_i^d} \tag{4.18}$$

4.8 Method based on modal residual vector

This method uses both the frequencies and mode shapes of the damaged structure (Humar et al. 2006). The eigenvalue equation for the damaged structure is

$$(K + \delta K)\phi_{di} - \lambda_{di} M \phi_{di} = 0 \tag{4.19}$$

where λ_{di} is the ith eigenvalue of the damaged structure and mass is constant. This equation can be rewritten in the following form to obtain δK

$$K\phi_{di} - \lambda_{di} M \phi_{di} = R_i = -\delta K \phi_{di} \tag{4.20}$$

where R_i is the modal residual vector for the ith mode. Damage location can be determined by perception of the affected degree of freedom and the connecting relation between the elements and the degree of freedom. Once the damaged elements are identified, δK can be expressed as the

weighted sum of the damaged elements' stiffness matrices. This weighting factors show the severity of damage. If the stiffness reduction of element j is expressed as $\beta_j k_j$, then

$$\delta \boldsymbol{K} = -\sum_j \beta_j \boldsymbol{k}_j \tag{4.21}$$

where the summation is carried out over the all damaged elements. Then this equation can be expressed as

$$\left(\sum_j \beta_j \boldsymbol{k}_j\right)\phi_{di} = \boldsymbol{R}_i \text{ or } H_i\beta = \boldsymbol{R}_i \tag{4.22}$$

4.9 Matrix update methods

This method was first developed by Kabe (1985). The basic eigenvalue equation for a undamaged structural system is given by

$$\boldsymbol{K}\phi_i = \lambda_i \boldsymbol{M}\phi_i \tag{4.23}$$

Damage in structure change both the stiffness and the mass matrices, and these change the frequencies and mode shapes. Therefore the above equation can be modified as

$$(\boldsymbol{K} + \delta\boldsymbol{K})(\phi_i + \delta\phi_i) = (\lambda_i + \delta\lambda_i)(\boldsymbol{M} + \delta\boldsymbol{M})(\phi_i + \delta\phi_i) \tag{4.24}$$

where $\phi_{di} = \phi_i + \delta\phi_i$ is the ith mode shape of the damaged structure. If the mass is not altered and $\delta \times \delta$ is minimal

$$\boldsymbol{K}\delta\phi_i + \delta\boldsymbol{K}\phi_{di} = \lambda_i \boldsymbol{M}\delta\phi_i + \delta\lambda_i \boldsymbol{M}\phi_{di} \tag{4.25}$$

As $\boldsymbol{K}\delta\phi_i = \lambda_i \boldsymbol{M}\delta\phi_i$ and multiplying both sides of Eq. (4.25) by ϕ_i^T, Eq. (4.26) is obtained.

$$\frac{\phi_i^T \delta\boldsymbol{K}\phi_{di}}{\phi_i^T \boldsymbol{M}\phi_{di}} = \delta\lambda_i \tag{4.26}$$

If the damage severity is small, $\phi_{di} \approx \phi_i$, then Eq. (4.26) reduces to

$$\phi_i^T \delta\boldsymbol{K}\phi_{di} = \delta\lambda_i \tag{4.27}$$

Using Eq. (4.21) and Eq. (4.27) can be expressed as

$$\delta\lambda_i = \frac{-\sum_{j=1}^{ne} \phi_i^T \boldsymbol{k}_j \phi_{di} \beta_j}{\phi_i^T \boldsymbol{M} \phi_{di}} \tag{4.28}$$

or

$$\boldsymbol{D}\beta = -\delta\lambda \tag{4.29}$$

where ne is the number of elements, D is an nm by ne matrix whose elements are $d_{ij} = \phi_i^T \boldsymbol{K}_j \phi_{di} / \phi_i^T \boldsymbol{M} \phi_{di}$, β is the ne-vector of unknown changes in element stiffness matrices, and $\delta\lambda$ is the m-vector of measured eigenvalue changes. For damage of low severity the expression d_{ij} can be simplified as $d_{ij} = \phi_i^T \boldsymbol{K}_j \phi_i$.

If $nm = ne$, β can be obtained from Eq. (4.29). However, nm is much smaller than ne, the solution is under deterministic and has infinite number of solutions. There are some method to solve this problem. One method is to apply a least square technique and another method is minimization of an objective function subjected to specific constraints. The other method is the "Pseudo-Inverse" method and the equation is given by

$$\beta = -D^T (DD^T)^{-1} \delta\lambda \tag{4.30}$$

This solution is effective in updating the analytical model of the undamaged structure to compare with damaged structure. Updated model can be used as basic and reference model in the future evaluation of the structure.

4.10 Method based on genetic algorithm

In this model updating method, structural model matrices such as mass, stiffness, and damping of the initial finite element model are updated to reproduce as closely as possible measured dynamic parameters of the baseline structure. Then, this updating process is continued for each set of measured response from each damage stage using the changes of finite element model properties between stages.

Genetic Algorithm (GA) is one of widely used Evolutionary Optimization (EO) method. GA is a strategy that guide the search process by mimicking the nature. The goal is to efficiently explore the search space to avoid getting trapped in confined area of the search space. It uses probabilistic decisions for reproduction of next generation and mutation for a diverse search during the generation. This randomness based on the probability can make it to explore the search space globally and is not used blindly. GA uses search experience to guide the search. This is the main difference from classical trajectory optimizations. The basic idea of GA is "survival of fitness". The general procedure (Marwala, 2010) and flowchart (Xia and Hao, 2001) of GA are as follows,

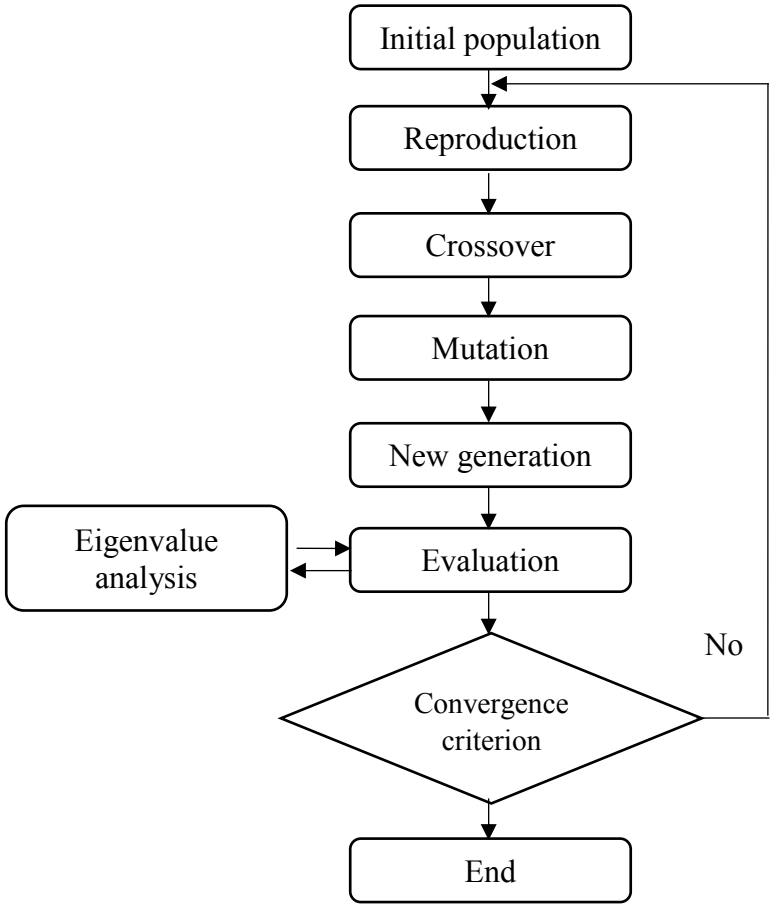

Fig 4.1 Flowchart of Genetic Algorithm

4.10.1 Initialization

In the beginning, a large number of possible individual solutions are randomly generated to form an initial population. This initial population is sampled so that it covers a good representation of the updating solution space. For example, if there are two variables to be updated, the size of the population must be greater than when there is only one variable to be updated.

4.10.2 Crossover

Crossover is an algorithmic operator used to alter the programming of a potential solution to the updating problem from one generation to the other.

Simple crossover: one crossover point is selected, a binary string from the beginning of a chromosome to the crossover point is copied from one parent, and the rest is copied from the second parent. a = 11001011 and b = 11011111 undergo a one-point crossover at the midpoint, then the resulting offspring is c = 11001111

Arithmetic crossover: a mathematical operator is performed to make an offspring. AND operator, a = 11001011 and b = 11011111 to form an offspring 11001011

4.10.3 Mutation

The mutation operator picks a binary digit of the chromosomes at random and inverts it. It prevents the genetic-algorithm simulation from being stuck in a local optimum solution.

Binary mutation: a number written in binary form is chosen and one bit value is converted. The chromosome 11001011 may become the chromosome 11000011

Non-uniform mutation: increasing the probability of mutation in such a way that it will be close to 0 as the generation number increases sufficiently. It prevents the population from stagnating in

the initial stages of the evolution process, and then permits the algorithm to refine the solution in the end stages of the evolution.

4.10.4 Selection

For every generation, a selection of the proportion of the existing population is chosen to breed a new population. This selection is conducted using the fitness based process, where solutions that are fitter and are given a higher probability of being selected. Some selection methods rank the fitness of each solution and choose the best solutions, while other procedures rank a randomly chosen sample of the population for computational efficiency.

4.10.5 Termination

The process described above is repeated until a termination condition has been achieved, either because a desired solution that satisfies the objective function or a specified number of generations has been reached or the solution's fitness converged.

In GA based population, the optimization reproduces the new generation by GA operator, so that it spreads the parameters widely in the search space. By this reason, GA can search the solutions globally in the search space.

Chapter 5. Modal Identification for the Highway Bridges

5.1 Introduction

In this chapter, the theoretical and practical modal identification techniques on highway bridges will be described to identify each modal identification method. First, the selected bridge and measurement system are described, then, modal identification resulted from field test is presented.

For effective damage identification, undamaged FE model should be modeled to reflect identically the real behavior of the structures (Brownjohn et al. 2001). It would be difficult to detect damage, if a small amount of experimental data were used. To avoid an under-determined or ill-conditioning problem, sufficient information is required. Aktan et al. (1998) and Catbas et al. (2007) proposed that different types of measurement methods are required to identify for large structures. Generally, when we test vibration of the real bridge, limited number of sensors are used and we don't know the excitation level when ambient vibration test is performed. So, if the excitation level is very low and performance of sensors is not suitable to measure vibration, the test results must be unreliable.

The number and location of sensors are related to the spatial information such as mode shape. Spatial information is very important to match the correlated modes. The importance of spatial information is shown in Fig. 5.1. If the sensors are installed in only one array, only bending modes in low order are identified and torsional or lateral behavior may be not verified.

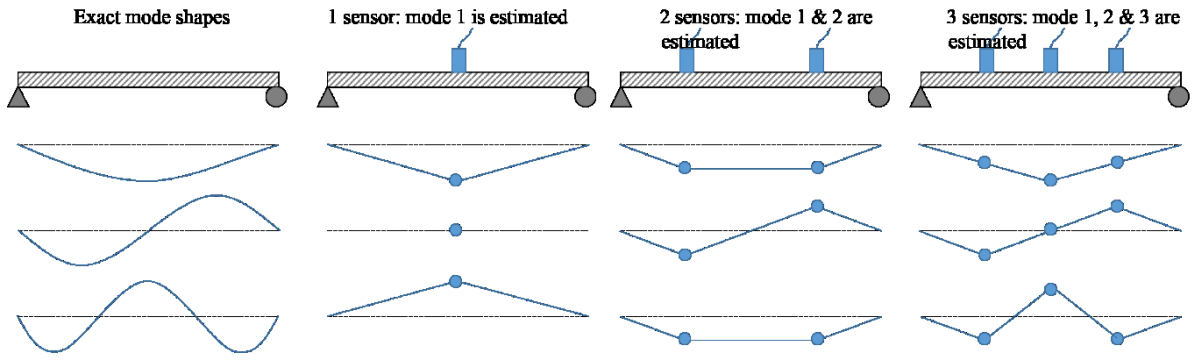

Fig. 5.1 Sensor quantity and mode shape

5.2 Pre-stressed Concrete Box (PSCB) Bridge

5.2.1 Description of Bridge

The Pre-stressed Concrete Box (PSCB) bridge considered here is composed of 16 continuous spans (40 m + 14@50 m + 40 m) with deck width 12 m and its curve radius is 3000 m. It was built in 1994 and its location is Gangwon province of South Korea. An ambient vibration test was performed in September 2012 with normal traffic loads by the Smart Load Rating Team of Korea Expressway Corporation.

Fig. 5.2 PSCB bridge

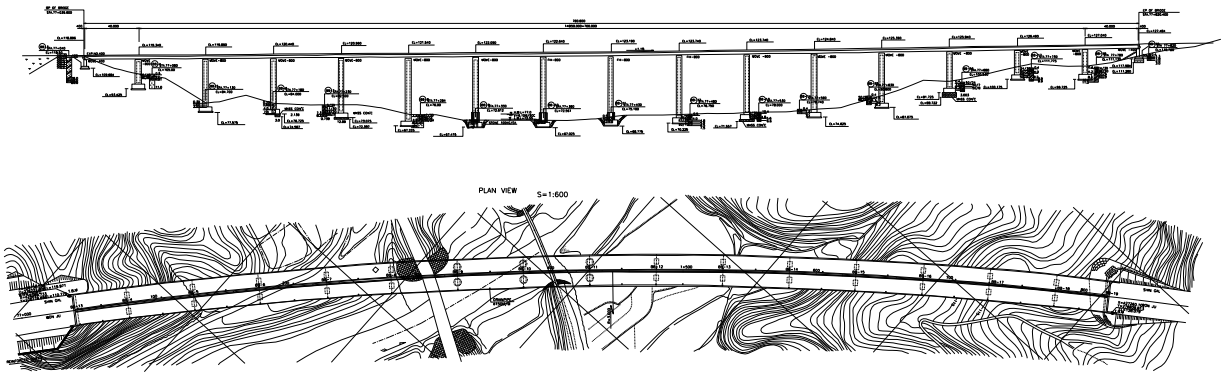

Fig. 5.3 Overview of PSCB bridge

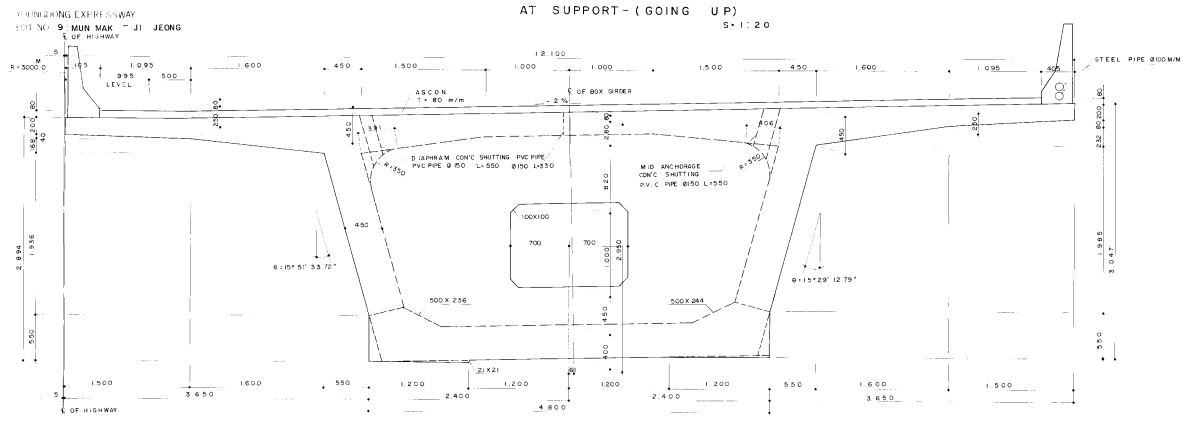

(a) At support

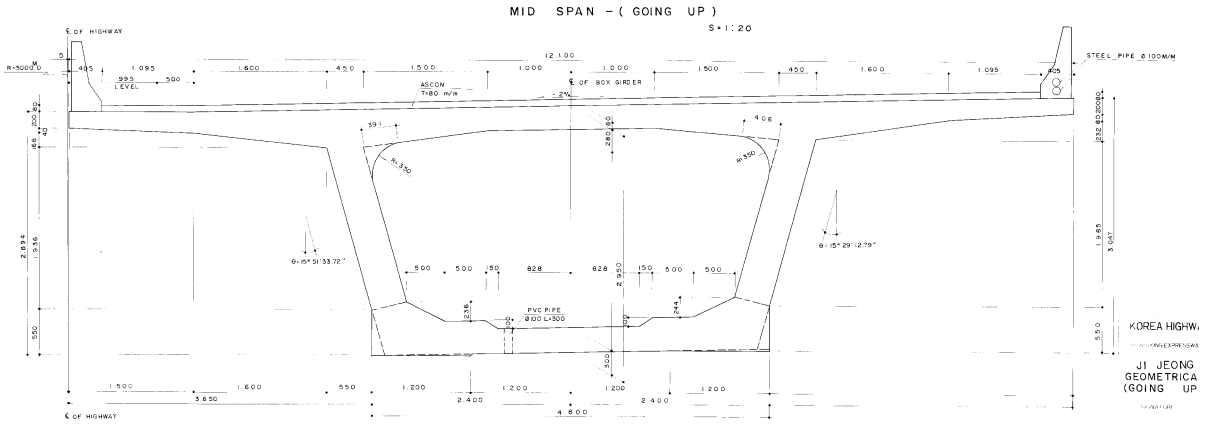

(b) At mid span

Fig. 5.4 Cross-section of the PSCB bridge

5.2.2 Vibration Test

Normal traffic over the bridge was used when the ambient vibration test was carried out on the bridge. The installation of accelerometers is shown in Fig. 5.5. To measure the ambient vibration of the bridge, 30 wireless loggers and PCB 393B12 accelerometers (10,000 mV/g sensitivity, ±0.5 g range) were used. Accelerometers with magnetic base were mounted firmly on the bridge using heavy steel plates to prevent moving from surface of the slab and adjusted horizontally with the bubble inclinometer. Accelerometers were placed only longitudinal direction because no torsional

modes were anticipated. The measurement time was 100 minutes with sampling rates of 256 Hz in order to collect sufficient vibration data for modal parameter extraction. As it is shown in Fig. 5.5, two sensors in each span were placed in a row to measure bending modes because FEM analysis prior to the test showed that the primary modes were only bending modes. Only one sensor was placed in the first and last span because of the lack of sensor, but it was sufficient to measure vibration characteristics.

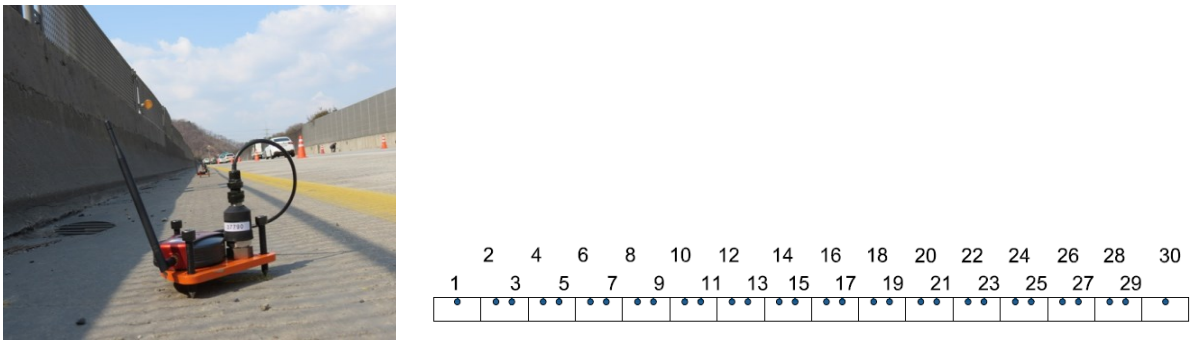

Fig. 5.5 The array of sensors

5.2.3 Modal Identification

Some acceleration time histories recorded during the modal test and their PSD are plotted in Fig. 5.6. In this PSD graph, most peaks are between 2 and 4 Hz. Other time history and PSD graphs are appended in the end of this thesis as Appendix A.

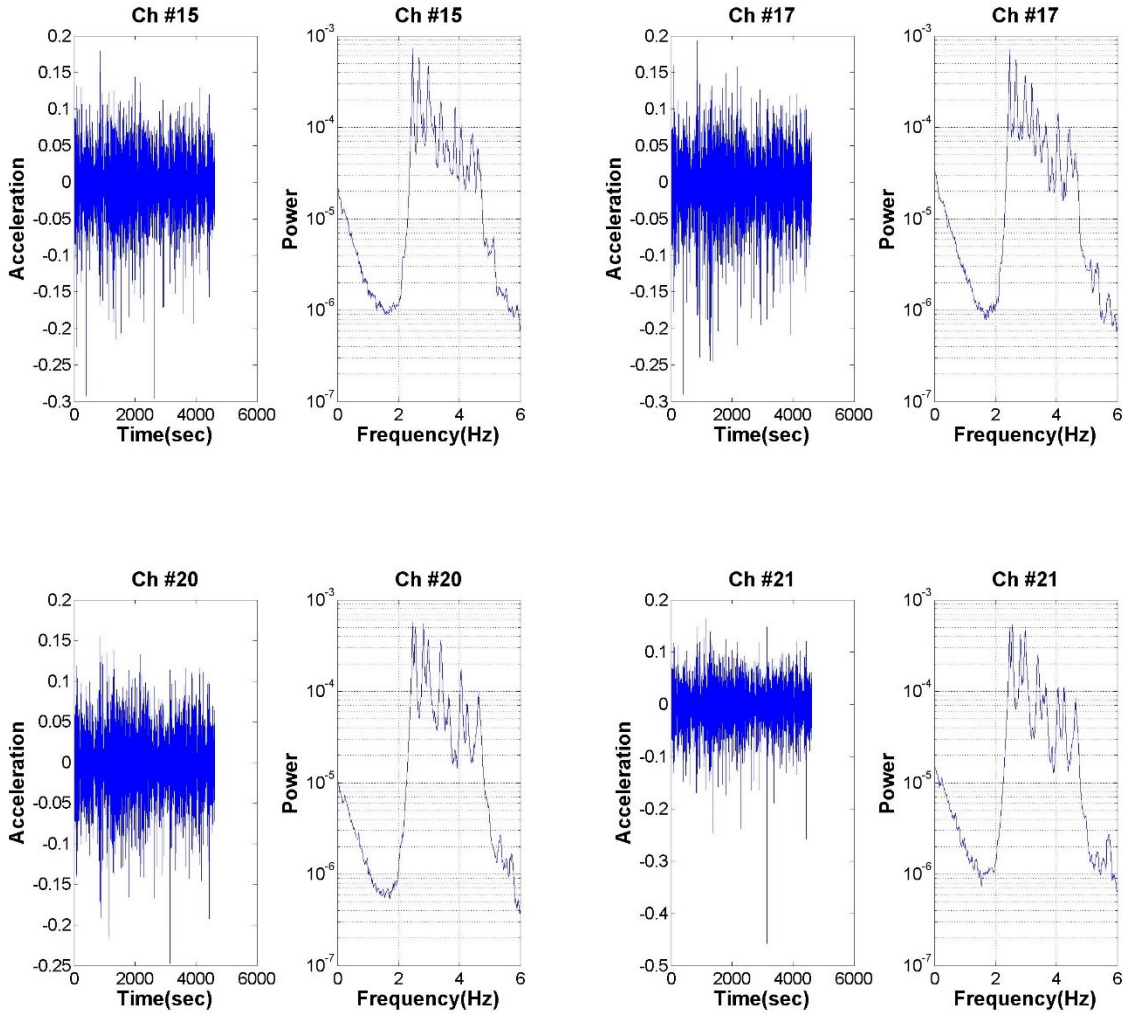

Fig. 5.6 Acceleration response and PSD of the PSCB bridge

The excitation of the bridge was sufficient during the measurement, because there were a lot of heavy traffics on the bridge and the measurement time was long. As shown in Fig. 5.7, many stable poles of SSI and peaks of FDD are found, and all of modes were bending mode. The range of considered frequencies are 2.4 ~ 3.2 Hz.

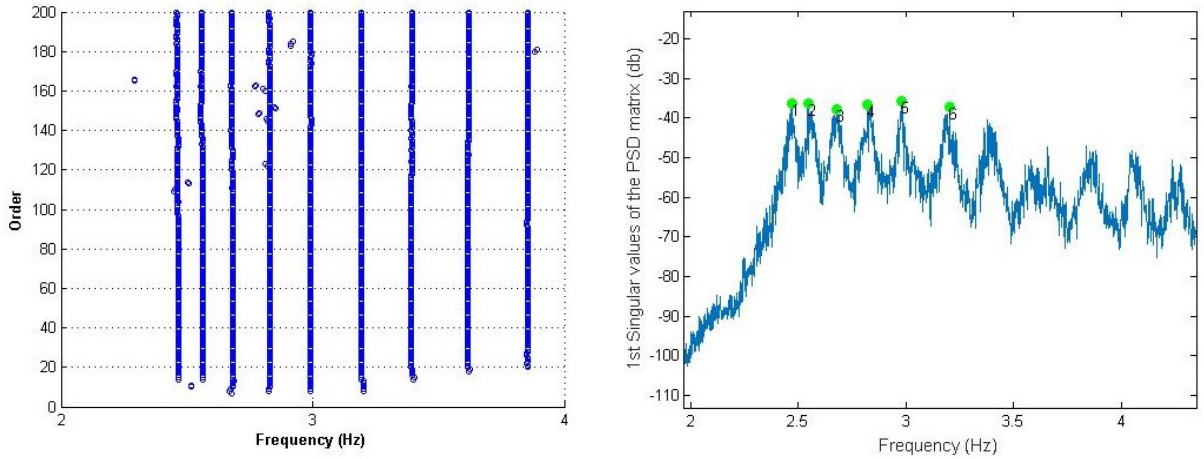

(a) Stable poles of SSI (b) Peaks of FDD (Farshchin)

Fig. 5.7 SSI and FDD

Table 5.1 shows comparison of the calculated modal frequencies for the FDD and SSI. The results are very similar.

Table 5.1 Frequencies of FDD and SSI

Mode no	FDD (Hz)	SSI (Hz)	Difference (%)
1st	2.47	2.46	0.40
2nd	2.55	2.56	-0.39
3rd	2.68	2.68	0.00
4th	2.82	2.83	-0.35
5th	2.98	2.99	-0.34
6th	3.20	3.19	0.31

Fig. 5.8 shows the MAC values to verify the orthogonality. The estimated modes are evaluated each other.

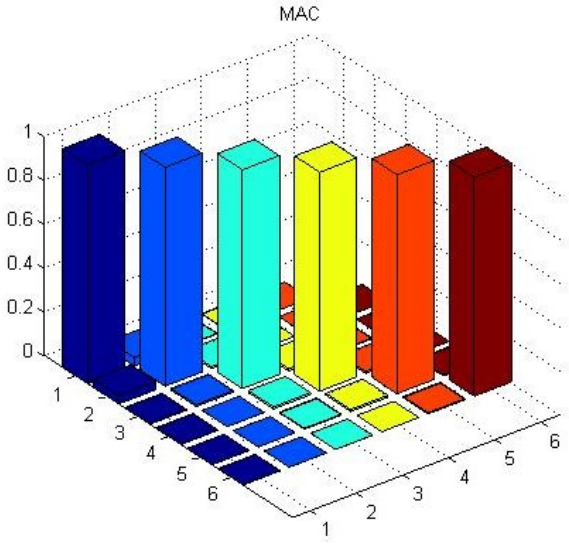

Fig. 5.8 Orthogonality check of estimated modes

Fig. 5.9 and Fig. 5.10 show modes shapes estimated by SSI and FDD. Mode shapes are very similar in two methods as frequencies. There are only bending modes because this bridge is slander. Six vertical modes are considered and these modes are concentrated between 2.4 and 3.2 Hz. Although the difference of frequency between modes is small, the mode-shapes clearly show each mode is evident.

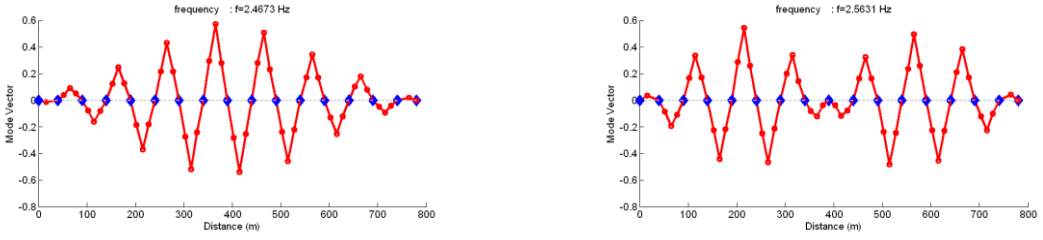

Fig. 5.9 Estimated mode shapes by SSI (continue)

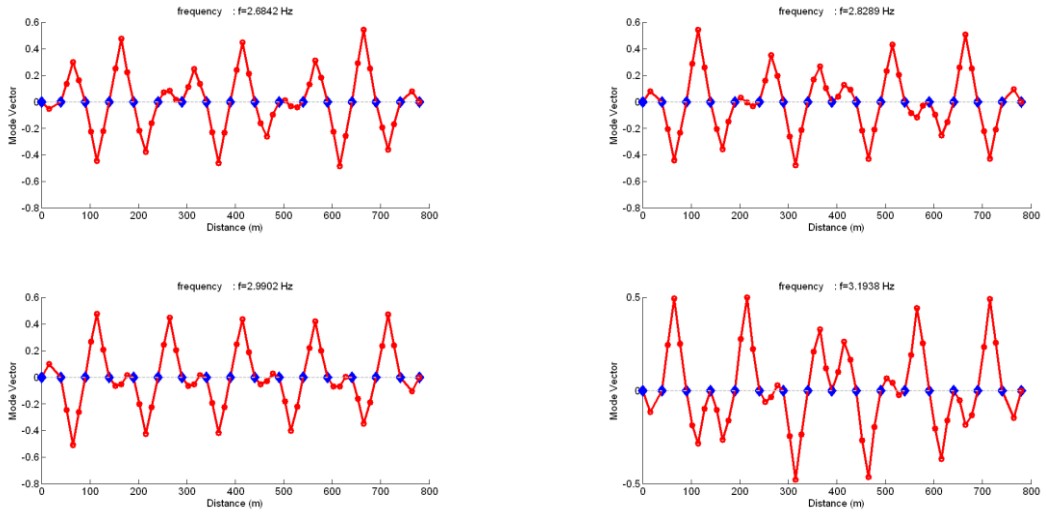

Fig. 5.9 Estimated mode shapes by SSI

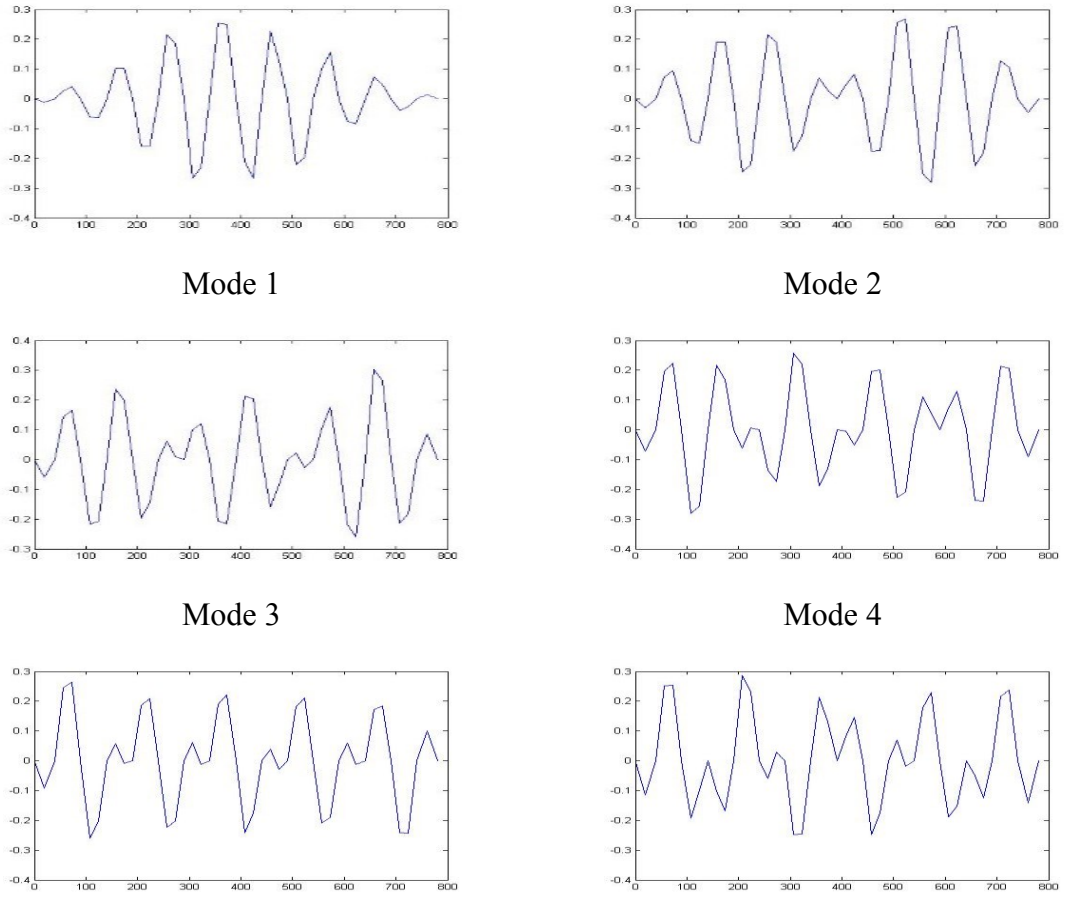

Mode 1 Mode 2

Mode 3 Mode 4

Mode 5 Mode 6

Fig. 5.10 Estimated mode shapes by FDD

5.2.4 Finite element analysis

Finite element analysis was performed to verify the results of modal identification. Midas Civil 2012 finite element software was used to carry out the simulations. This software was developed in Korea for application in many engineering fields. All spans of the bridge was simulated in the finite element models. It was expected that all modes of vibrations are only flexural bending modes because the section is slim and the span length is relatively long. Appropriate boundary conditions were considered to account for pier and abutment components of the bridge. The section was modeled by using Midas Sectional Property Calculator (SPC) software that can calculate any shape of section by input the coordinates. All box girders including slab were modeled using 780 frame elements. The material and sectional properties of frame elements (concrete) are listed in Table 5.2 and 5.3. The FE model of the bridge is shown in Fig. 5.11.

Table 5.2 Material properties of the PSCB bridge

Material properties	Young's modulus (MPa)	Compressive strength (MPa)	Density (kg/m^3)	Poisson's ratio
Box girder	28,000	40	2,500	0.167

Table 5.3 Sectional properties of the PSCB bridge

Sectional properties	Area (m^2)	Moment of inertia (m^4)	
		I_{xx}	I_{yy}
Box girder	9.54	22.07	11.73

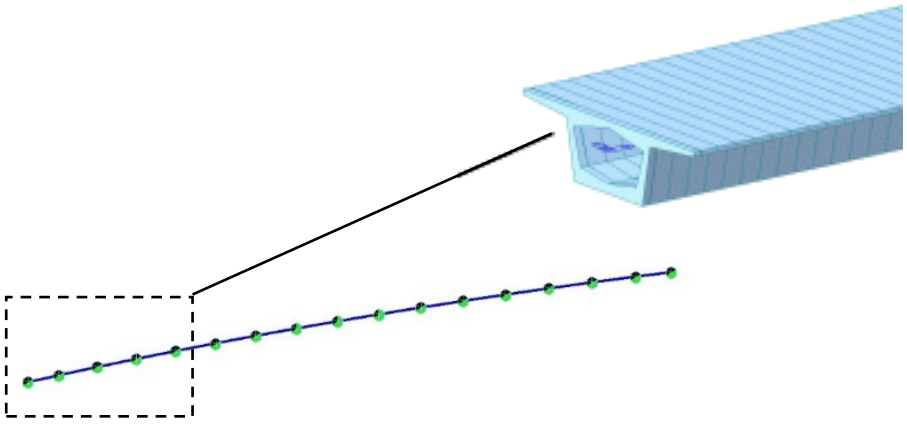

Fig. 5.11 FE model of the simulated bridge

An eigenvalue analysis of the model was performed to identify the natural frequencies and mode shapes of the bridge. The measured natural frequencies and mode shapes of the bridge are presented in Fig. 5.12. As it can be seen, the calculated mode shapes are in a very good agreement with the partial mode shapes measured in Fig. 5.9 and Fig. 5.10. The calculated natural frequencies are also reasonably close to the measured natural frequencies. The largest deviation can be observed in the 3rd calculated natural frequency which is about 8.6% different from the measured natural frequencies. The FE model is constructed well because all frequency differences are evenly distributed about 8%. This difference is perhaps caused by the difference between the design strength and strength of the real structure, and also the normal traffic load present during the ambient vibration test which was not considered in the FE model. The traffic is insignificant and that is not expected to influence the ambient vibration signals. These differences can be removed by model updating method which is not performed in this study. In Appendix D, a case study of model updating method is provided. Moreover, the main object of this section is to verify the modal identification, and it is sufficient to check the correspondence of the mode shapes and the trends of the natural frequencies.

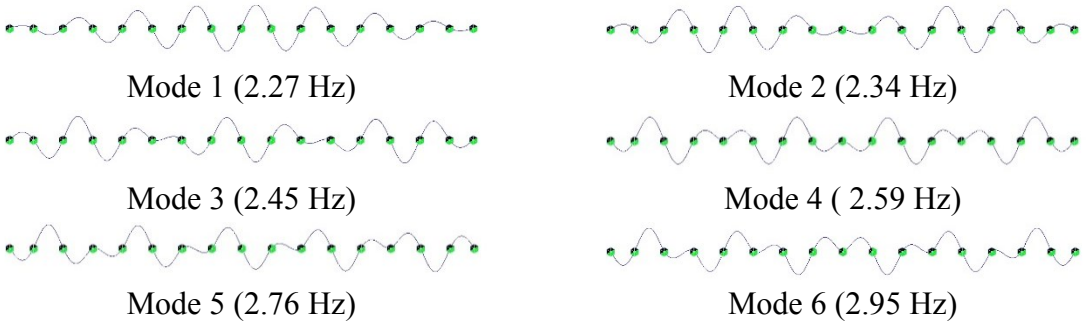

Fig. 5.12 First six mode shapes of the bridge

Table 5.4 Frequencies of test and FEM

Mode no	SSI (Hz)	FEM (Hz)	Difference (%)
1st	2.46	2.27	7.72
2nd	2.56	2.34	8.59
3rd	2.68	2.45	8.58
4th	2.83	2.59	8.48
5th	2.99	2.76	7.69

6th	3.19	2.95	7.52

5.3 Steel Box (STB) Bridge

5.3.1 Description of Bridge

The Steel Box (STB) bridge considered here is composed of 4 spans (4@47.5 m) with deck width 12. It was built in 1995 and its location is Gangwon province of South Korea. The test was performed in March 2013 with normal traffic loads by the Smart Load Rating Team of Korea Expressway Corporation.

Fig. 5.13 STB bridge

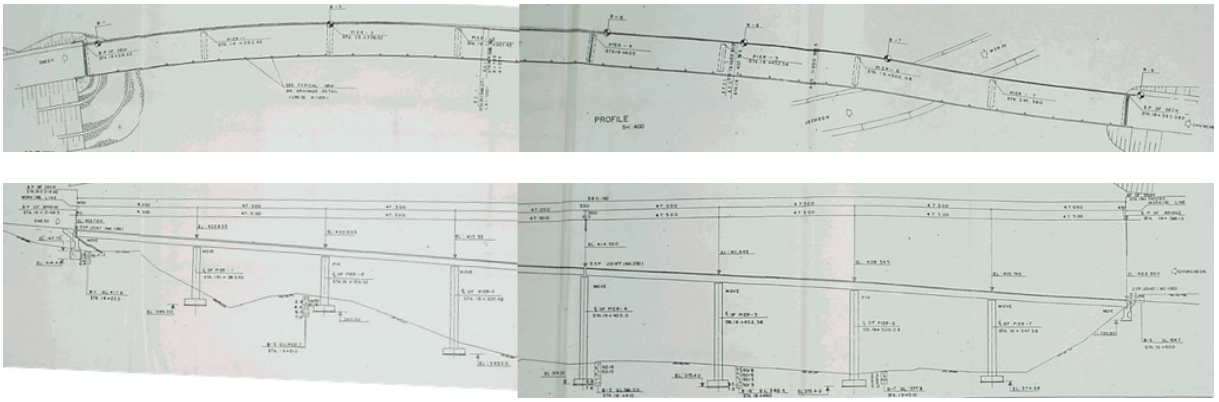

Fig 5.14 Overview of STB bridge

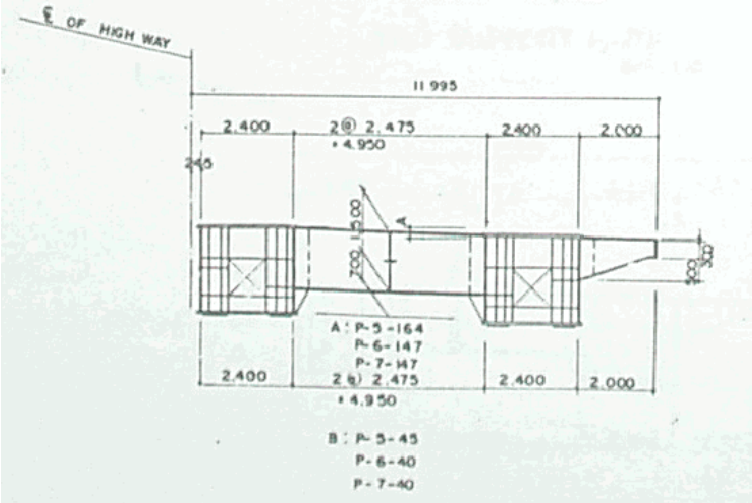

Fig. 5.15 Cross-section of STB bridge

5.3.2 Vibration Test

The ambient vibration test was carried out on both sides to detect vertical bending and torsional modes. The installation of accelerometers is shown in Fig 5.16. To measure the ambient vibration of the bridge, 24 wireless loggers and PCB 393B12 accelerometers (10,000 mV/g sensitivity, ±0.5 g range) were installed. Accelerometers with magnetic base were mounted firmly on the bridge using heavy steel plates to prevent moving from surface of the slab and adjusted horizontally with the bubble inclinometer. The measurement time was 100 minutes with sampling rates of 128 Hz in order to collect sufficient vibration data for modal parameter extraction. As it is shown in Fig. 5.16, six sensors in each span were placed on both sides of the bridge to measure bending and torsional modes which were predicted from the FEM analysis prior to the field test.

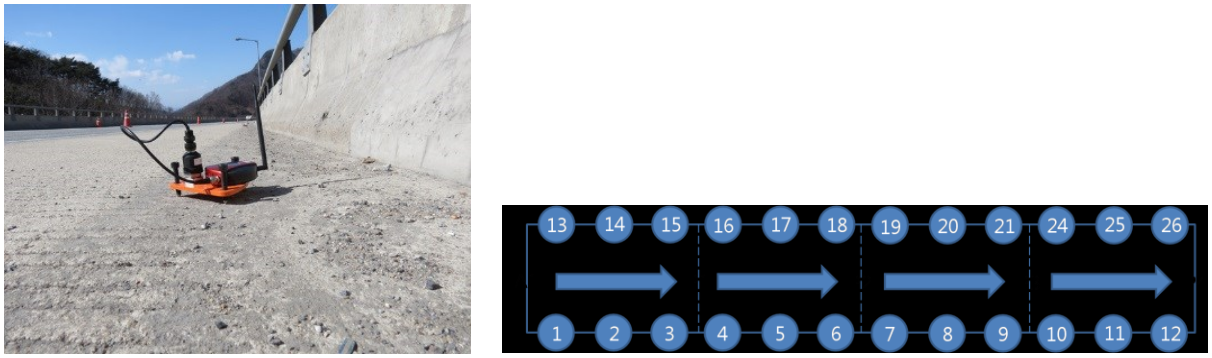

Fig. 5.16 The array of sensors

5.3.3 Modal Identification

Some acceleration time histories recorded during the modal test and their PSD are plotted in Fig. 5.17. In this PSD graph, most peaks are between 2 and 5. Other time history and PSD graphs are appended in the end of this thesis as Appendix B.

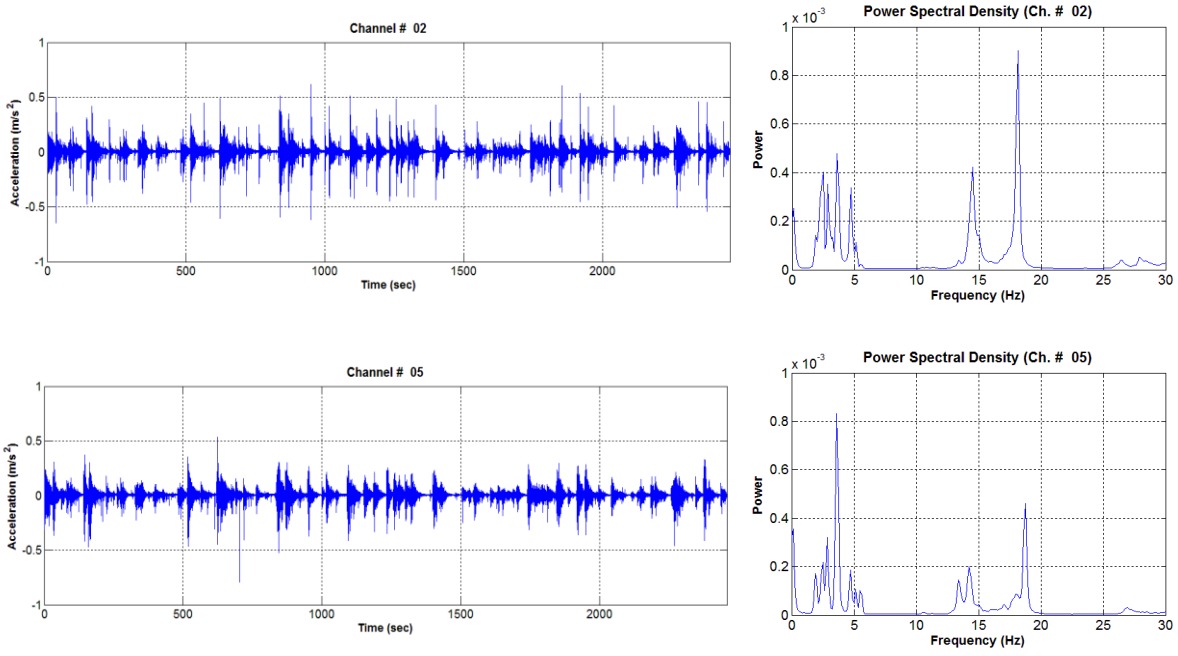

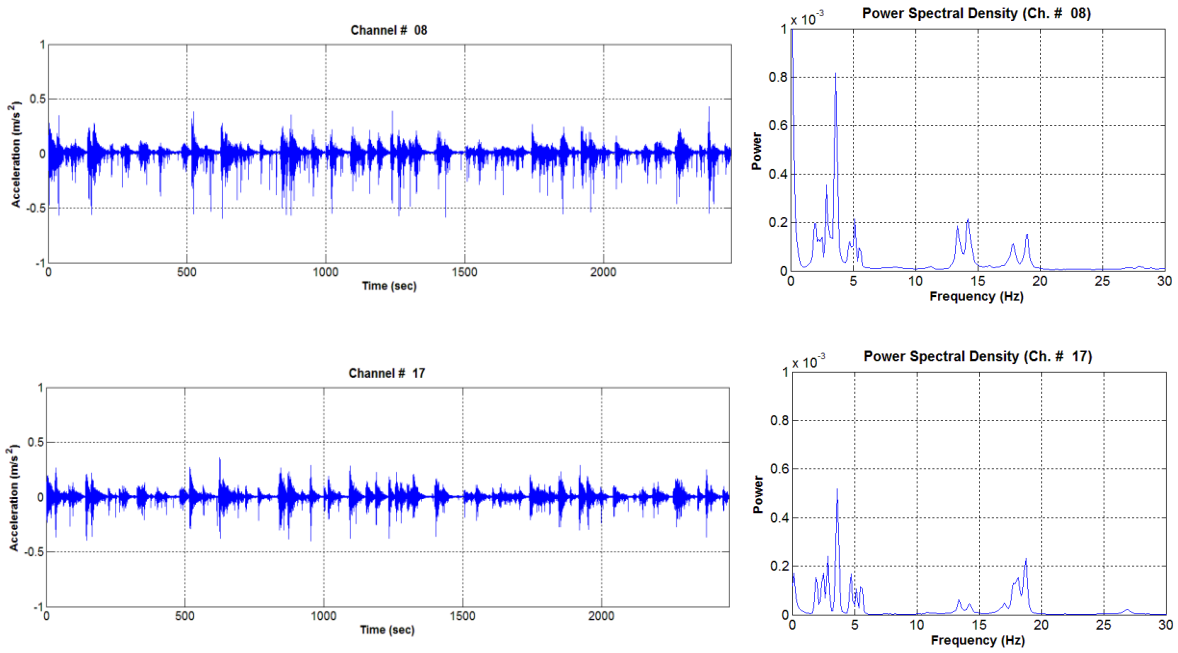

Fig. 5.17 Acceleration response and PSD of the STB bridge

The excitation of the bridge was sufficient during the measurement, because there were a lot of heavy traffics on the bridge and the measurement time was long. There were the closed modes 5th and 6th, and these were torsional modes. Closed modes are chosen as different modes of the real modal behaviors, because the mode shapes are clearly different as shown Fig. 5.18.

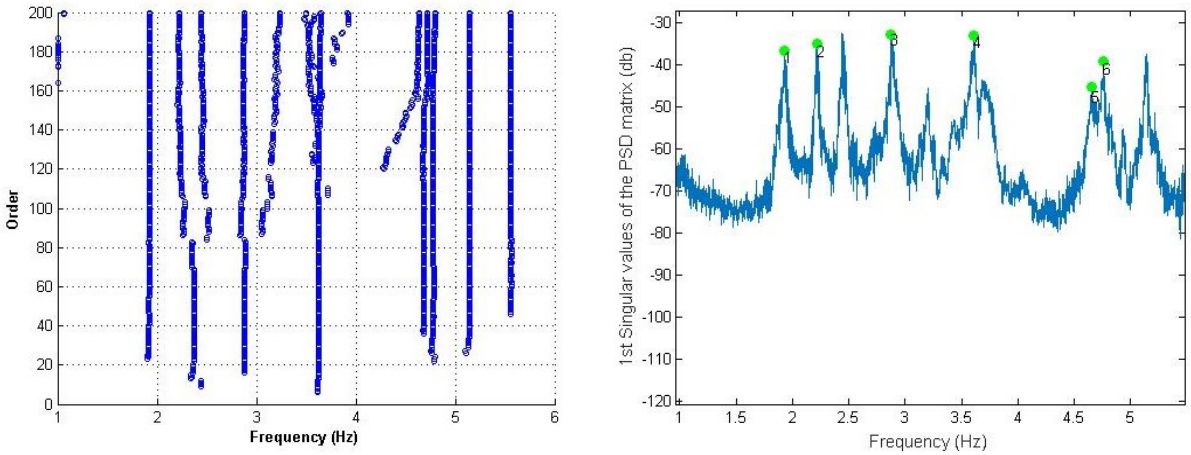

(a) Stable poles of SSI (b) Peaks of FDD (Farshchin)

Fig. 5.18 SSI and FDD

Table 5.3 shows comparison of the calculated modal frequencies for the FDD and SSI. The results are very similar.

Table 5.5 Frequencies of FDD and SSI

Mode no.	FDD (Hz)	SSI (Hz)	Difference (%)
1st	1.93	1.92	0.52
2nd	2.22	2.23	-0.45
3rd	2.88	2.87	0.35
4th	3.60	3.62	-0.56
5th	4.65	4.68	-0.64
6th	4.76	4.78	-0.42

Fig. 5.19 shows the MAC values to verify the orthogonality. The estimated modes are evaluated each other.

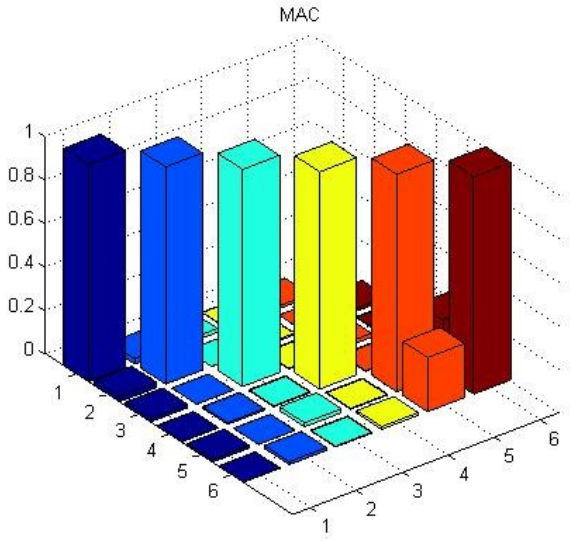

Fig. 5.19 Orthogonality check of estimated modes

Fig. 5.20 and Fig. 5.21 show modes shapes estimated by SSI and FDD. Mode shapes are very similar in two methods as frequencies. There are four bending modes and two torsional modes.

The poles of mode 5 and mode 6 are very close in the SSI stabilization chart and FDD peaks. The relative difference between frequencies is 2.14 % and their modes are torsional. Generally, closed modes might be true mode or mode from the noise. The FDD method is generally more vulnerable to the measurement noise than the SSI method, and the estimates by the FDD method is less accurate than the SSI method particularly when the two adjacent modes are closely spaced (Yi et al. 2004). In this test, mode 5 could be ignored by FDD method because the peak of mode 6 is higher than mode 5, but in the SSI stabilization chart, it is apparent that these two adjacent modes are different modes. Mode 5 is typical torsional mode (up-down-up-down), but mode 6 is up-down-down-up. As this bridge is curved bridge, this bridge may have the closed modes.

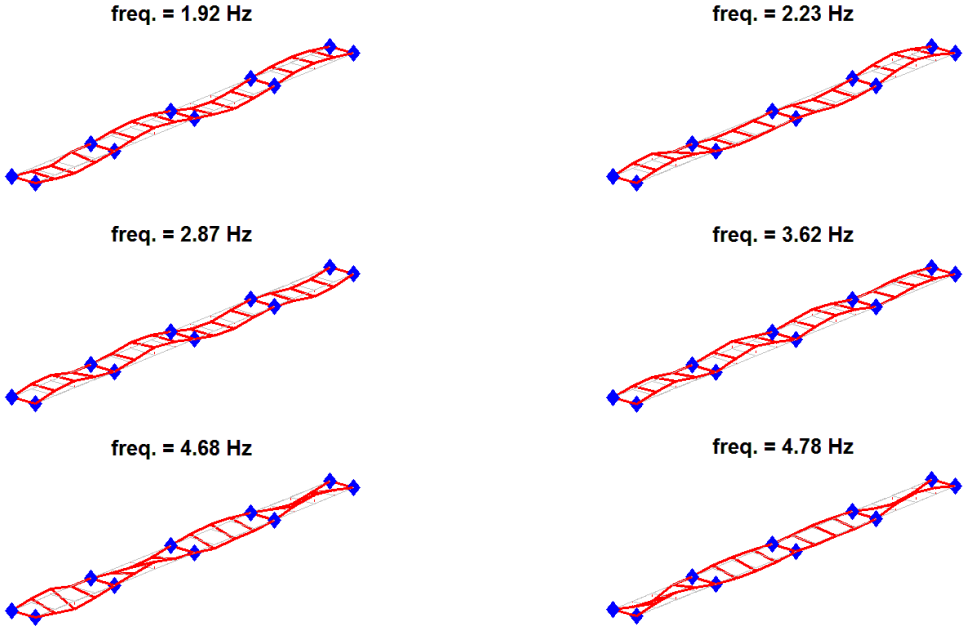

Fig. 5.20 Estimated mode shapes by SSI

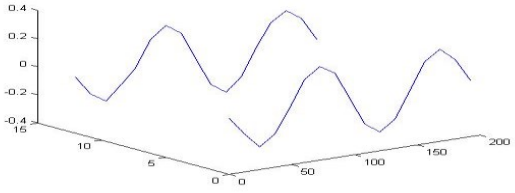

Mode 1

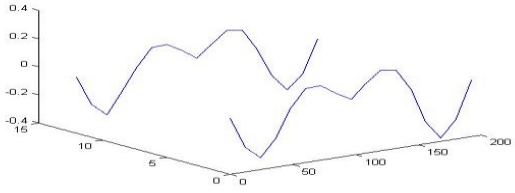

Mode 2

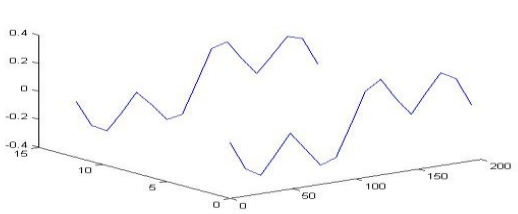

Mode 3

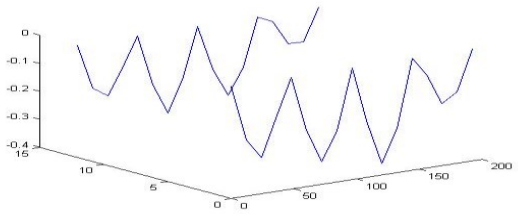

Mode 4

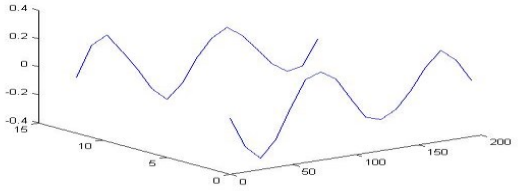

Mode 5

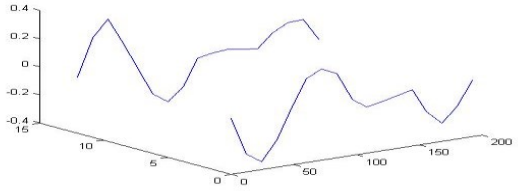

Mode 6

Fig. 5.21 Estimated mode shapes by FDD

5.3.4 Finite element analysis

Finite element analysis was performed to verify the results of modal identification. Midas Civil 2012 finite element software was used to carry out the simulations. Only first four spans of the bridge were simulated in the finite element models because other parts of the bridge are structurally independent by expansion joints. It was expected that the initial modes of vibration are due to flexure and torsion of the deck. Appropriate boundary conditions were considered to account for pier and abutment components of the bridge. The two steel box girders were modeled by using Midas composite section data function that can calculate composite steel box by input dimensions, quantities and material properties. All steel boxes, stringers and diaphragms were modeled using 2062 frame elements and the concrete slab was modeled using 1920 four-node shell elements. Although the frame and shell elements were modeled in the same plane, an offset was considered between them to account for their eccentric centroids. Also, a rigid connection was considered between the frame and shell elements to consider fully composite behavior. The intermediate and end bent diaphragms between the steel boxes were simulated using link elements with an idealized longitudinal and vertical stiffness of the real diaphragms. The material and sectional properties of elements are listed in Table 5.6 and 5.7. The FE model of the bridge is shown in Fig. 5.22.

Table 5.6 Material properties of the STB bridge

Material properties	Young's modulus (MPa)	Compressive strength (MPa)	Density (kg/m^3)	Poisson's ratio
Steel box	210,000	-	7,500	0.3
Slab	24,000	27	2,500	0.167

Table 5.7 Sectional properties of the STB bridge

Sectional properties	Area/Thickness (m^2/m)	Moment of inertia (m^4)	
		I_{xx}	I_{yy}
Steel box	0.104	0.123	0.0897
Slab	0.25	-	-

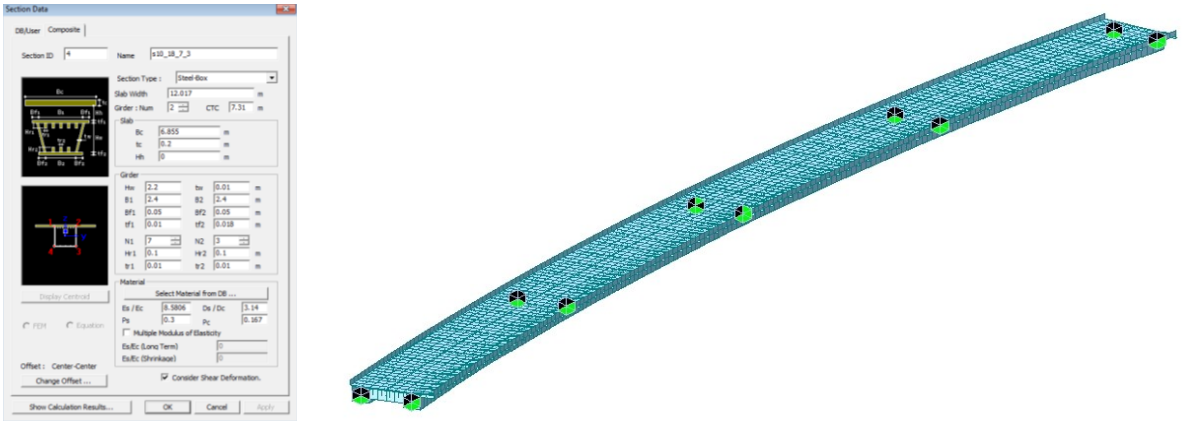

Fig. 5.22 FE model of the simulated bridge

An eigenvalue analysis of the model was performed to identify the natural frequencies and mode shapes of the bridge. The measured natural frequencies and mode shapes of the bridge are presented in Fig. 5.23. As it can be seen, the calculated mode shapes are in a very good agreement with the partial mode shapes measured in Fig. 5.20 and Fig. 5.21. The calculated natural frequencies are also reasonably close to the measured natural frequencies. The largest deviation can be observed in the 5th calculated natural frequency which is about 8.3% different from the

measured natural frequencies. The FE model is considered to be constructed well because first four modes are bending modes and their differences are relatively small. Although the differences of last two modes (torsional modes) are relatively large, the important modes are the first few modes. This difference is caused by the difference in design strength and current real strength of the concrete. Also the traffic load used in the ambient vibration test was not considered because the effect of the traffic is insignificant. In addition, these differences can be removed by model updating method which is no performed in this study. Moreover, the main object of this section is to verify the modal identification, it is sufficient to check the correspondence of the mode shapes and the trends of the natural frequencies.

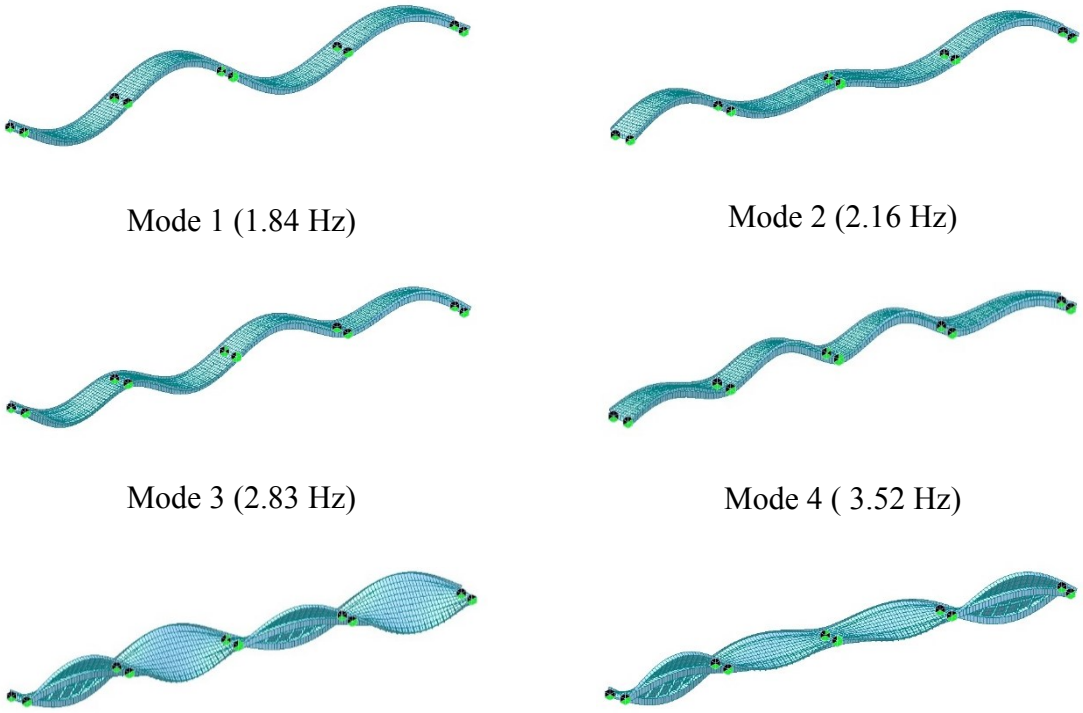

Fig. 5.23 First six mode shapes of bridge

Table 5.8 Frequencies of test and FEM

Mode no.	SSI (Hz)	FEM (Hz)	Difference (%)
1st	1.92	1.84	4.17
2nd	2.23	2.16	3.14
3rd	2.87	2.83	1.39
4th	3.62	3.52	2.76
5th	4.68	4.29	8.33
6th	4.78	4.44	7.11

5.4 Summary

In this chapter, SSI and FDD methods for identifying modal parameters from ambient vibrations of two types of bridges are examined. These two methods are fast and efficient methods to obtain modal parameters. The results of these two types of methods in real bridges is found to be reasonably accurate. From this case study and my personal experiences, FDD is relatively faster and easier than SSI for modal identification. However, SSI is more accurate method. Therefore, FDD method can be used for the preliminary estimation of modal properties, and SSI method can be used for the final stage to extract more accurate results. In addition, vibration-based damage identification for the PSCB bridge with simulated damages is presented here.

Chapter 6. Description of Experimental Program

6.1 Introduction

This thesis is composed of Modal Identification and Vibration-based Damage Identification using experimental test and numerical studies. This chapter focuses on a description of the experimental test. It is more difficult to perform an experimental test than numerical study, because experimental test is influenced by many uncertainties including measurement, excitation, material properties and support conditions.

Over the past several years, numerous experiments have been undertaken to perform VBDI techniques. However, many of them were for small size specimens, such as small steel or aluminum plates, because vibration measurement and excitation were easy and material and section properties were easy to calculate. Although some researchers have applied VBDI techniques to real structures such as bridges, it is still uncertain that small scale damage in large structures can be reliably detected and located by VBDI techniques.

The object of this experimental test was to investigate the applicability of the VBDI technique to the real structures. For this application, the dynamic properties such as natural frequency and

mode shape of a structure before and after damage were used to detect the damage. This chapter includes the dimensions of the target structure, excitation methods, sensor and logger specifications, damage type, modal identification and applications of various types of VBDI methods.

6.2 Test setup and procedures

VBDI techniques make use of changes of dynamic properties to identify damage in the structure. In this study, three-story frame was used as the target structure to measure the dynamic properties of the undamaged and damaged structure. The test was performed in the Structures Laboratory of Concordia University.

6.2.1 Target structure

The frame used in the test was three-story and its dimensions were height: 1.4 m, width: 0.6 m, depth: 0.27 m. The frame was composed of a galvanized steel angle section, L 25 × 2.5 and a steel plate of which the thickness was 2.5 mm. Each support of the frame was assumed as fully fixed with concrete slab and tightened to the lab strong floor for fixed boundary condition. Fig. 6.1 shows the fixed supports of the target structure used in this study. In this figure, there are braces in each story used to maintain the structure in the stable form when it was constructed, these braces were removed and not considered when the test was performed.

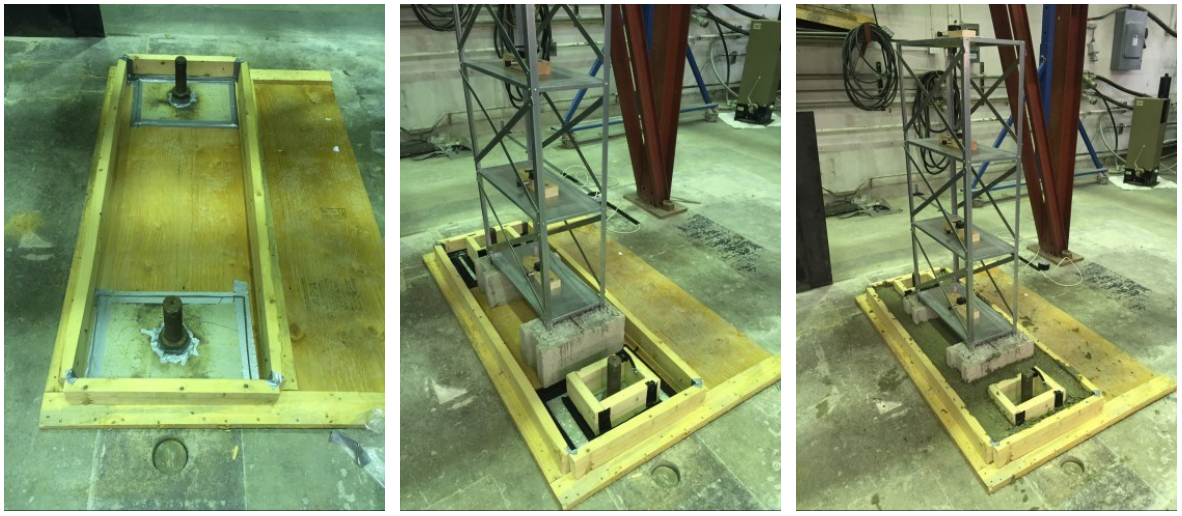

(a) Cast (b) Before pouring (c) After pouring

Fig. 6.1 Setup of the boundary condition

6.2.2 Finite Element Modelling

In order to determine the properties of the accelerometers and their placement on the frame, a finite element analysis was carried out to obtain the vibration response of the frame with the same properties of the test frame with an impact load to find the measurement range. The FEM model for the frame and impact load is shown in Fig. 6.2. The frame was modeled using beam elements and the plate was modeled as shell elements using Midas Civil 2012. Its boundary conditions were assumed as fully fixed at the supports of the frame and this was modelled as 3D to reflect the real behavior of the frame structure. An impact load was simulated in the model by applying a triangular load which reaches to 50 N in 0.5 ms because the weight of the impact hammer used in this test was about 2 kgf (20N) and safety factor was considered not to exceed the hammer's impact. The finite element model of the frame and the applied load have been shown in Fig. 6.3. After building the model, a transient dynamic analysis was performed to obtain dynamic responses of the frame due to the applied impact load.

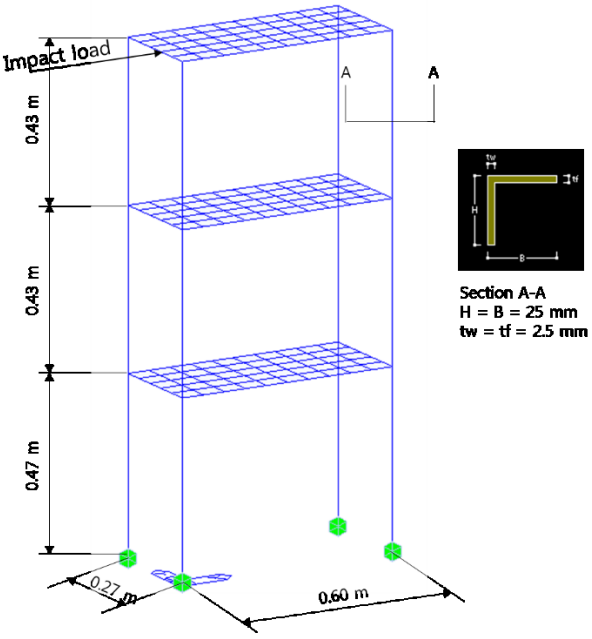

Fig. 6.2 Geometry of the modeled frame

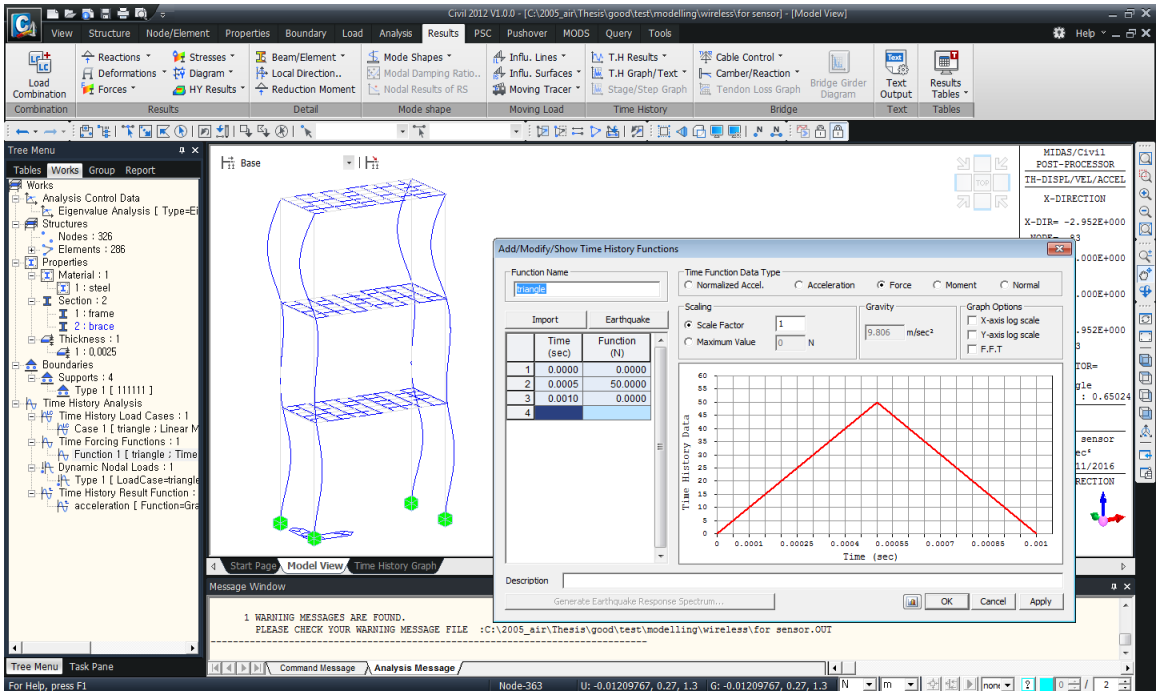

Fig. 6.3 FE model of the frame and applied impact load

The acceleration of the frame was obtained at the center node of the shell on the top floor. Fig. 6.4 shows that the maximum acceleration is about 2 g. The acceleration response does not decrease

because damping was not considered in this FE model. This result helps to select the appropriate accelerometers.

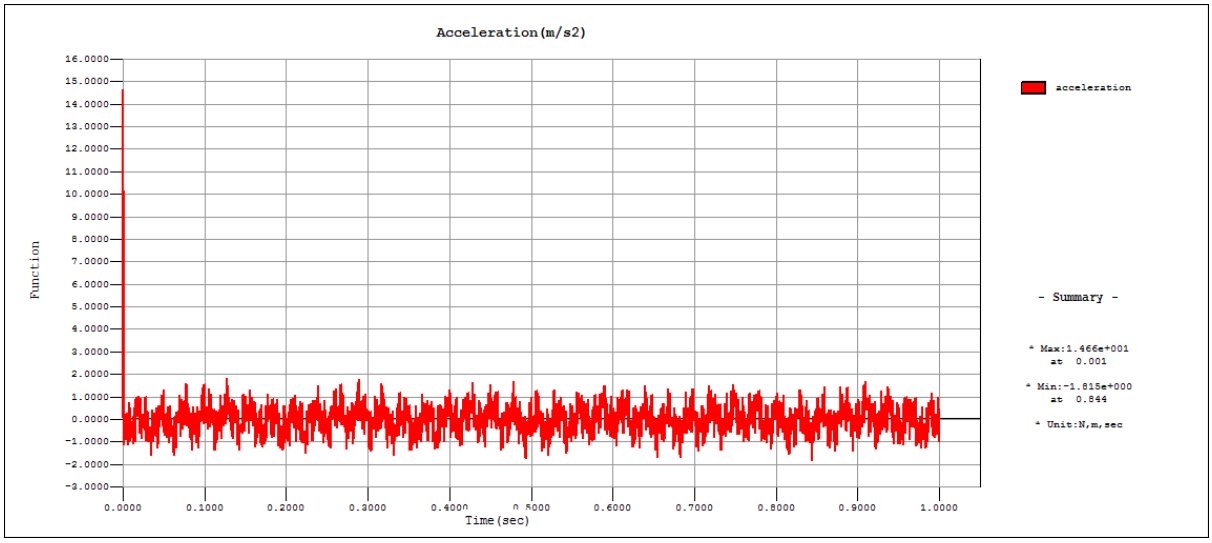

Fig. 6.4 The maximum acceleration time history (max = 14.66 m/s^2 ≈ 2g)

Generally, the sensitivity of sensor is high, the measurement range of sensor is low. It means that the higher is the sensitivity, the lower is the range of measurements. As a result of above result, the range of the accelerometer was selected as 2 g because the maximum acceleration of the frame was calculated as 2 g in the FE analysis under an impact load of 50 N. Three wireless accelerometers of MicroStrain® were used for this test. The accuracy is 10 mg and measurement range is ±2 g. An installed accelerometer is shown in Fig. 6.5. Accelerometers were fixed by bolts and installed on the surface of the each floor to measure horizontal acceleration. Accelerometers must have a lower weight because the test frame was small and its weight was light too, so that the weight of the accelerometer could affect the response of the frame.

Fig. 6.5 Wireless accelerometer and gateway

6.2.3 Measurement of vibration

As mentioned in chapter 4, some of the VBDI methods are relied only on the change of mode shape to detect damage, while others relied on both of the change natural frequencies and mode shapes. In these experiments, natural frequencies and mode shapes were identified by the response of the system to a random vibration. Data were acquired using a wireless accelerometers of MicroStrain®. Sampling rates were 512 Hz and measurement time was 20 sec. Natural frequencies were identified from the average of three normalized frequency response spectra obtained from tests. A sampling rate of 512 Hz is appropriate for natural frequency identification because the natural frequencies of the first three modes were range from 6 Hz to 110 Hz. The fundamental mode was used for damage detection because the accuracy of the second and third modes was much lower than that of the first mode. However, the first three modes were used for calibration of the finite element (FE) models described in subsequent sections.

6.2.4 Description of the induced damage conditions

The damages were induced in the frame by loosening the bolts of the second floor in each direction as shown in Fig. 6.6. These damages might reduce the stiffness of the frame in bending modes. In fact, there are other ways of inducing damage such as cutting the frame section or removing one of the members. But these methods are not used here because these methods cause permanent damage and could not be recoverable when another test is required.

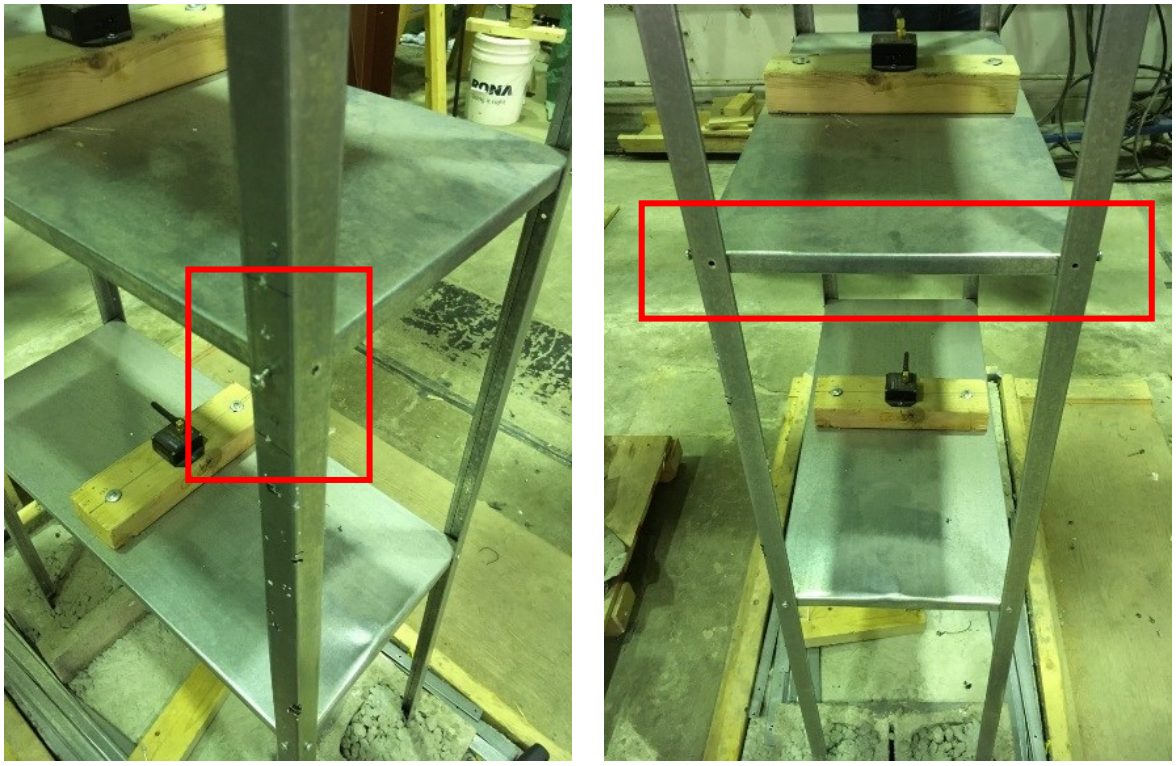

Fig. 6.6 Location of the induced damages

6.3 Modal Identification

The objective of this test was to detect damages by VBDI techniques using measured mode shapes and natural frequencies. The raw data from accelerometers acquired from the data acquisition system were recorded in the form of voltage with respect to the test time for each channel. These data must first be converted to acceleration, then these values are transformed using FFT from discrete time-domain to frequency response spectra. Then, mode shapes and natural frequencies can be obtained from this frequency response spectra.

However, there are many causes of noise such as environmental electromagnetic noise and the fluctuation and drift inherent in a measurement device. The effects of drift may be eliminated by calibration. These noise can be a cause of errors in the mode shapes and natural frequencies. In VBDI techniques, high quality and reliable mode shapes and natural frequencies are essential because small scale damage causes only very small changes to mode shapes and natural frequencies. Plenty of errors may affect the result of VBDI techniques. These noises can be eliminated by filtering techniques.

The objective of modal identification in this section is to convert the time domain raw data to frequency domain data to obtain mode shapes and natural frequencies.

6.3.1 Numerical study

The numerical study was done before performing the experimental study. The purpose of the numerical study was to confirm the capabilities of the damage identification. This helped an assessment of the possibility of proceeding with the experimental. In addition, this aided to determine if a limited number of measurement points could identify the mode shapes with enough accuracy to detect small damage.

The finite element (FE) software Midas Civil 2012 was used to perform dynamic analyses to generate the natural frequencies and mode shapes of the structure. The frame was modelled as beam elements divided by 10, and the plate was modeled as shell elements divided by 5 transversely and 10 longitudinally. Its boundary conditions were assumed as fully fixed at the supports of the frame. The mass of wooden mounts and sensors were not considered in this test because these were very small comparing to the weight of the structure (3% of the structure mass). The material properties and sectional properties used in the FE model are shown in Table 6.1 and 6.2.

Table 6.1 Material properties of the structure used in FE model

Material properties	Young's modulus (GPa)	Density (kg/m^3)	Poisson's ratio

Column	200	7,850	0.29
Plate	200	7,850	0.29

Table 6.2 Sectional properties of the structure used in FE model

Sectional properties	Shape (mm)	Area (mm^2)	I (mm^4)
Column (angle)	25×2.5	118.75	7031.42
Plate (thickness)	2.5	-	-

The first three flexural mode shapes generated by the FEM are shown in Fig. 6.7. Four elastic springs were considered at the connections of the frame and the plate to reflect damages. All bolts were loosed, we don't know the exact value of these connections. Mode shapes of the frame are three-dimensional, only portions of the mode shape defined along centers of plate were used in this study to detect damage, because accelerometers were located in the center of the plate in the experimental study. Therefore, mode shapes referred to in subsequent discussions are those along the center of the plate not columns.

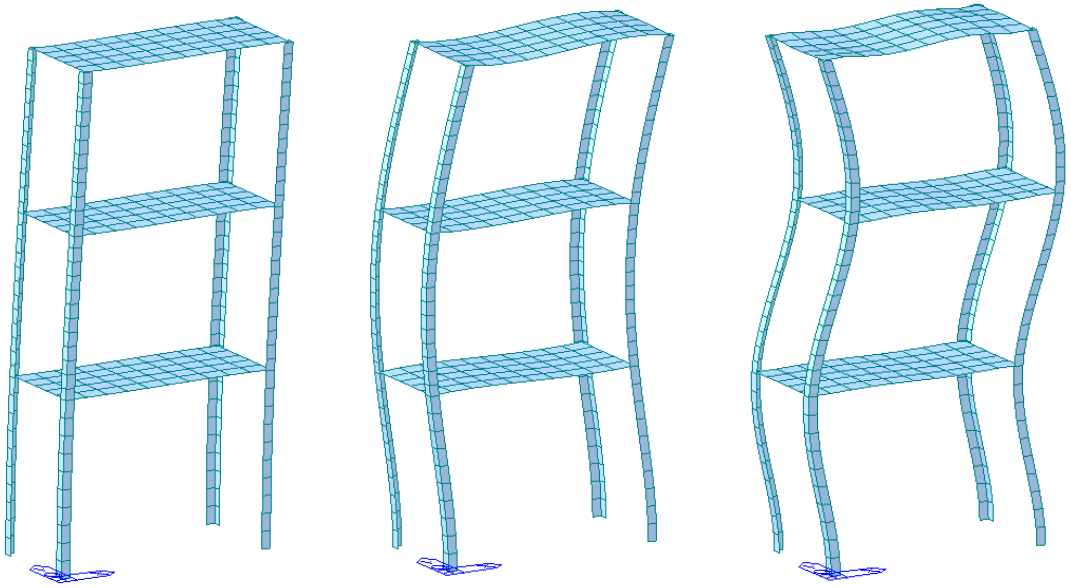

(a) First mode (b) Second mode (c) Third mode

Fig. 6.7 The first three mode shapes generated by FEM for undamaged structure

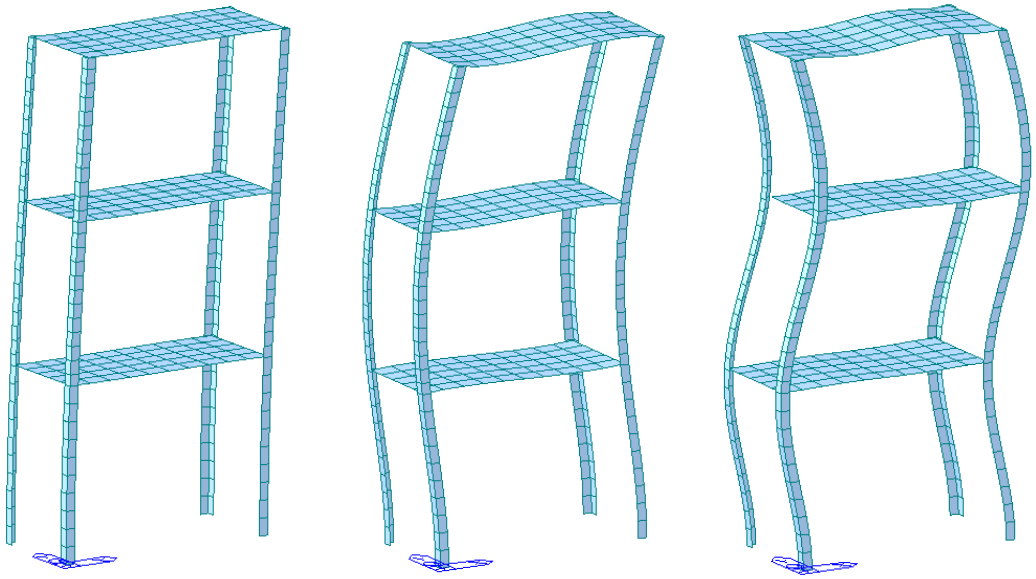

(a) First mode (b) Second mode (c) Third mode

Fig. 6.8 The first three mode shapes generated by FEM for damaged structure

6.3.2 Modal Identification

The acceleration time histories before and after damage recorded during the modal test are plotted in Fig. 6.9 and Fig. 6.10.

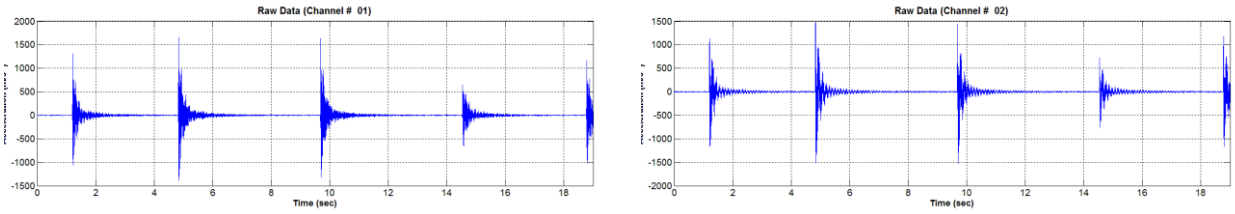

(a) Channel 1 (b) Channel 2

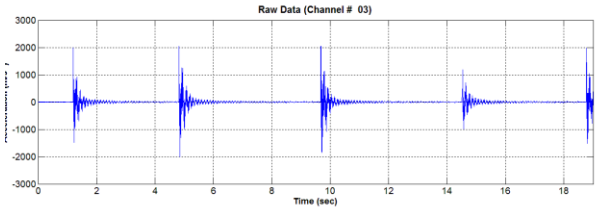

(c) Channel 3

Fig. 6.9 Acceleration response of the undamaged frame

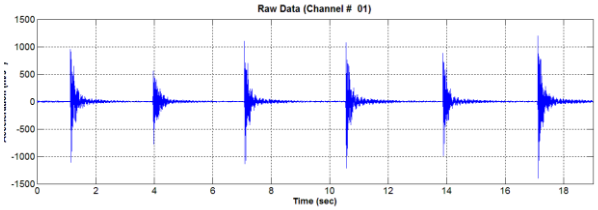

(a) Channel 1

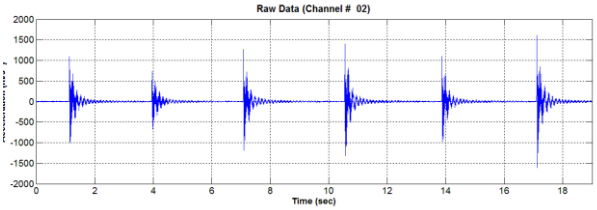

(b) Channel 2

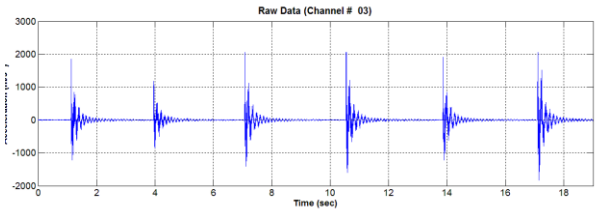

(c) Channel 3

Fig. 6.10 Acceleration response of the damaged frame

As shown in Fig. 6.11, many stable poles of SSI and peaks of FDD were found, and the range of considered frequencies were very wide (6 Hz ~ 110 Hz).

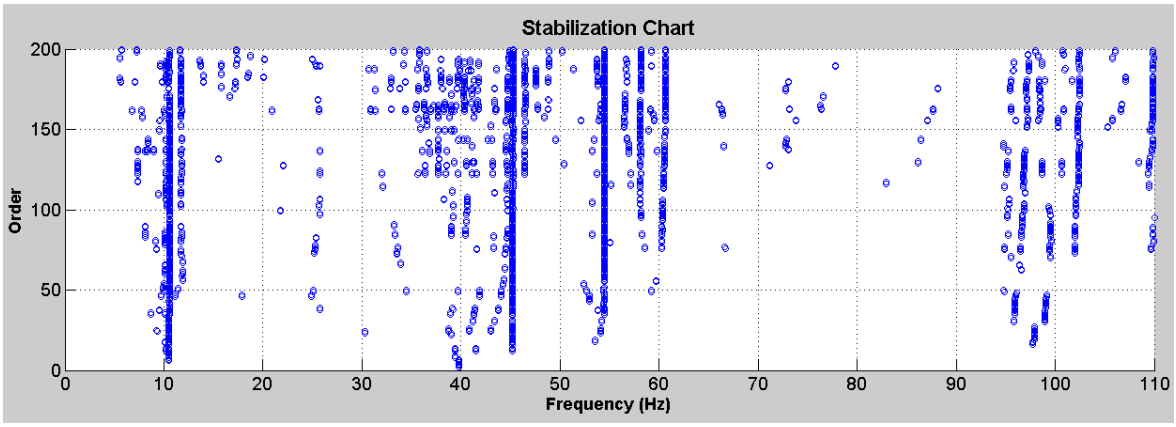

(a) Stable poles of SSI

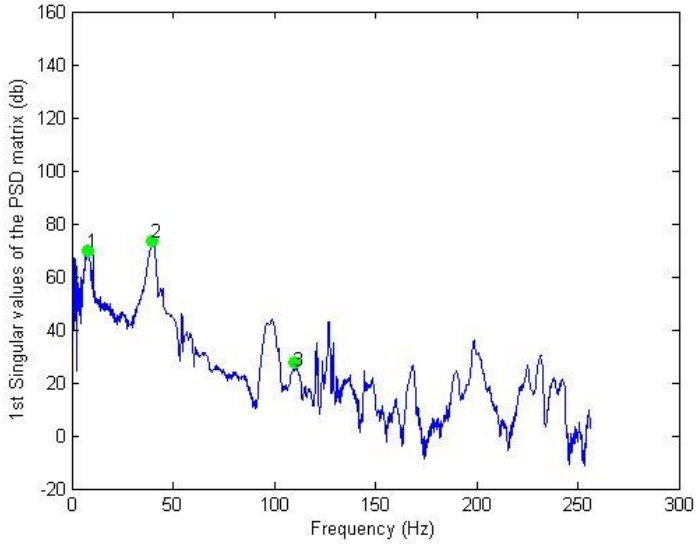

(b) Peaks of FDD

Fig. 6.11 SSI and FDD results of undamaged frame

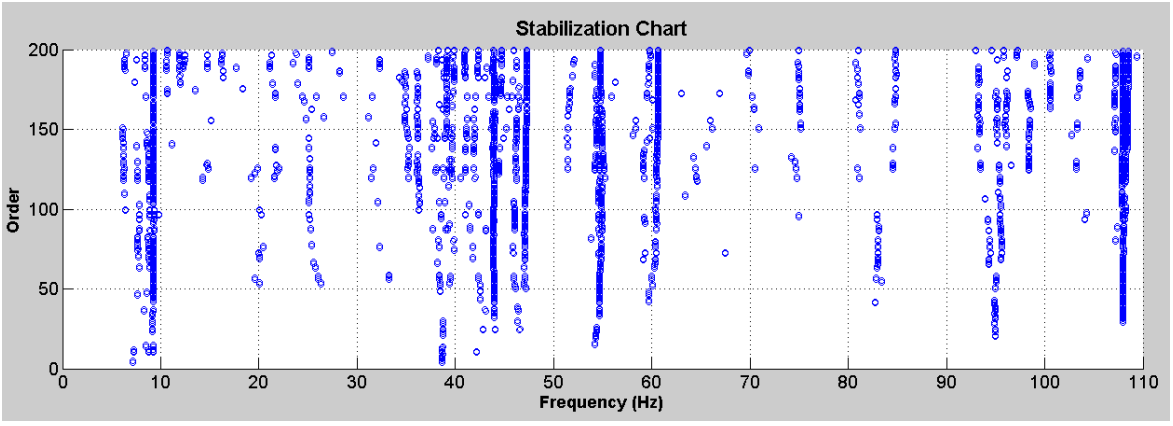

(a) Stable poles of SSI

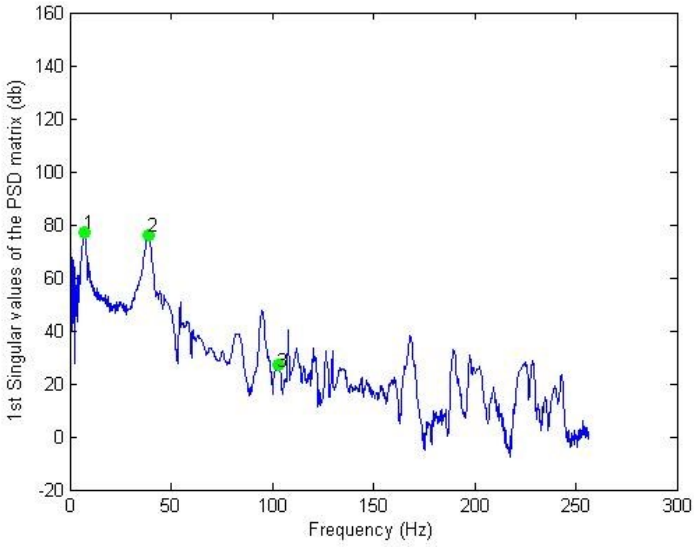

(b) Peaks of FDD

Fig. 6.12 SSI and FDD results of damaged frame

As shown in Table 6.3, the maximum difference between FEM and measured natural frequencies was 1.18%. This difference is because the material properties and sectional properties are not exact. As demonstrated in Fig. 6.13, the angle section is not exact angle and the plate has additional section. Moreover, the differences between damaged FEM and measured were over 10%. As mentioned in 6.3.1, damaged FE model used elastic spring elements to consider damages. The objective of these FEM analysis were just to identify the trend of mode shapes.

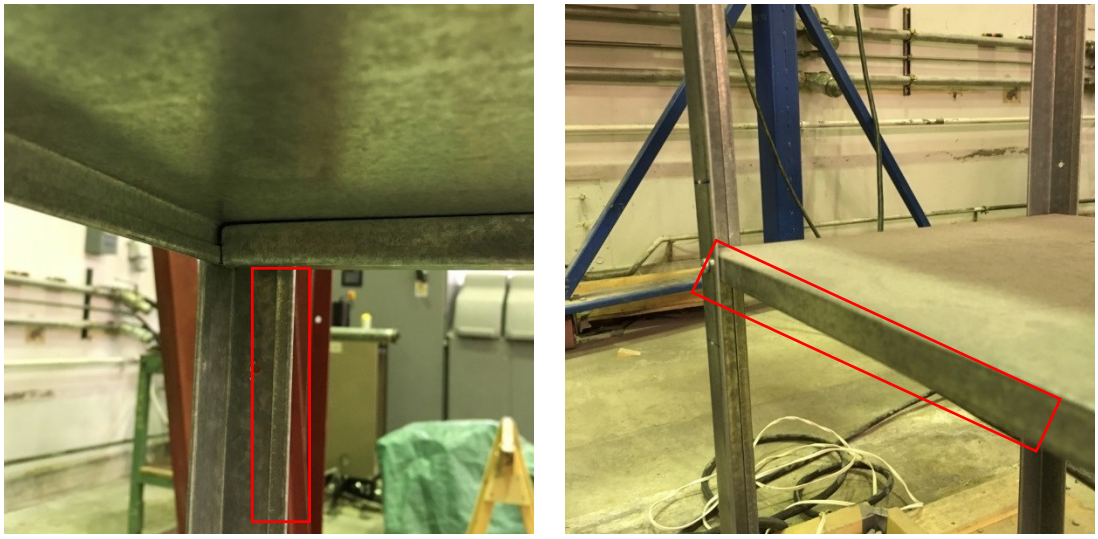

Fig. 6.13 Additional section of structure

Table 6.3 Comparison of FDD, SSI and test results for the undamaged structure

	Test (Hz)		FEM	Difference (%)	
	FDD	SSI		FDD:SSI	FEM:Test
1st Mode	6.75	6.63	6.76	1.78	-0.15
2nd Mode	39.75	39.73	39.78	0.05	-0.08
3rd Mode	108.38	107.20	107.12	1.09	1.16

Table 6.4 Comparison of FDD, SSI and test results for the damaged structure

	Test		FEM	Difference	
	FDD	SSI		FDD:SSI	FEM:Test
1st Mode	6.00	6.28	6.71	-4.67	-11.83
2nd Mode	38.50	38.68	39.47	-0.47	-2.52
3rd Mode	103.38	103.42	101.95	-0.04	1.38

In addition, the modal assurance criteria (MAC) values for FEM and measured mode shapes for the first three modes were nearly 1.00, except for third mode. A MAC value of 1.0 means perfect correlation between the corresponding measured and numerical mode shapes.

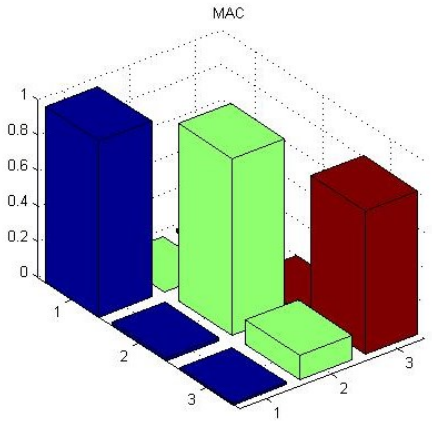

Fig. 6.14 MAC (undamaged)

Table 6.5 MAC (undamaged)

Mode no.	1st	2nd	3rd
1st	0.99	0.00	0.01
2nd	0.02	1.00	0.00
3rd	0.01	0.14	0.81

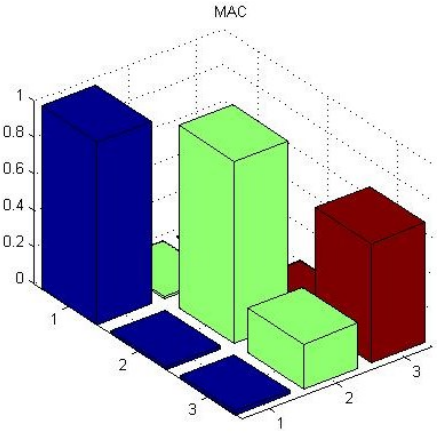

Fig. 6.15 MAC (damaged)

Table 6.6 MAC (damaged)

Mode no.	1st	2nd	3rd
1st	1.00	0.01	0.00
2nd	0.02	1.00	0.00
3rd	0.02	0.25	0.65

Through Fig. 6.16 and Fig. 6.19 show modes shapes estimated by SSI and FDD. Mode shapes are very similar in two methods as frequencies.

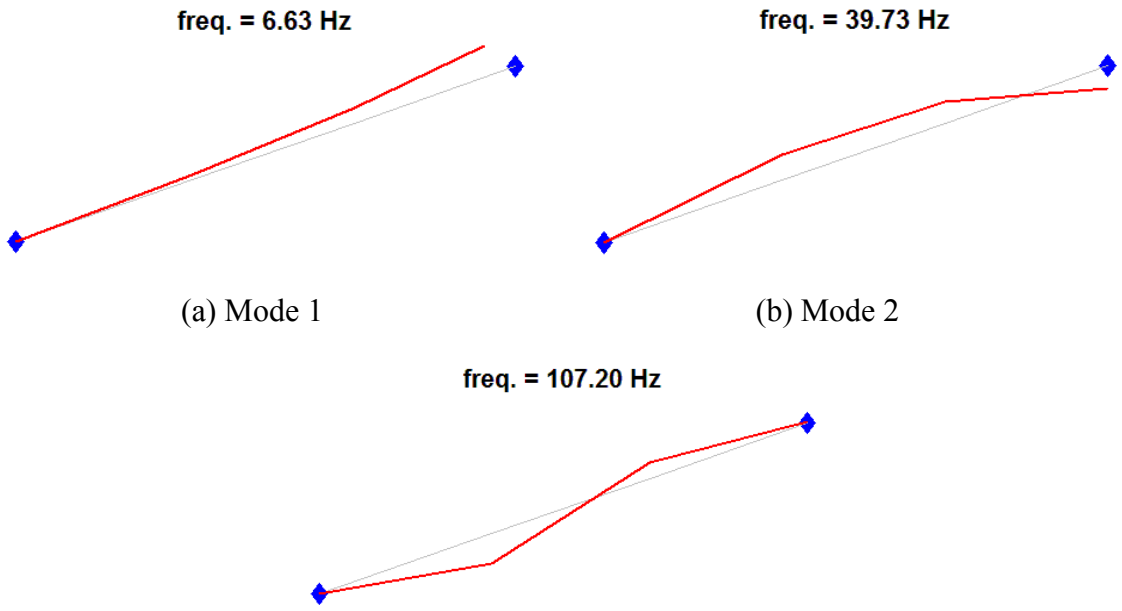

(a) Mode 1 (b) Mode 2

(c) Mode 3

Fig. 6.16 Estimated mode shapes of undamaged structure by SSI

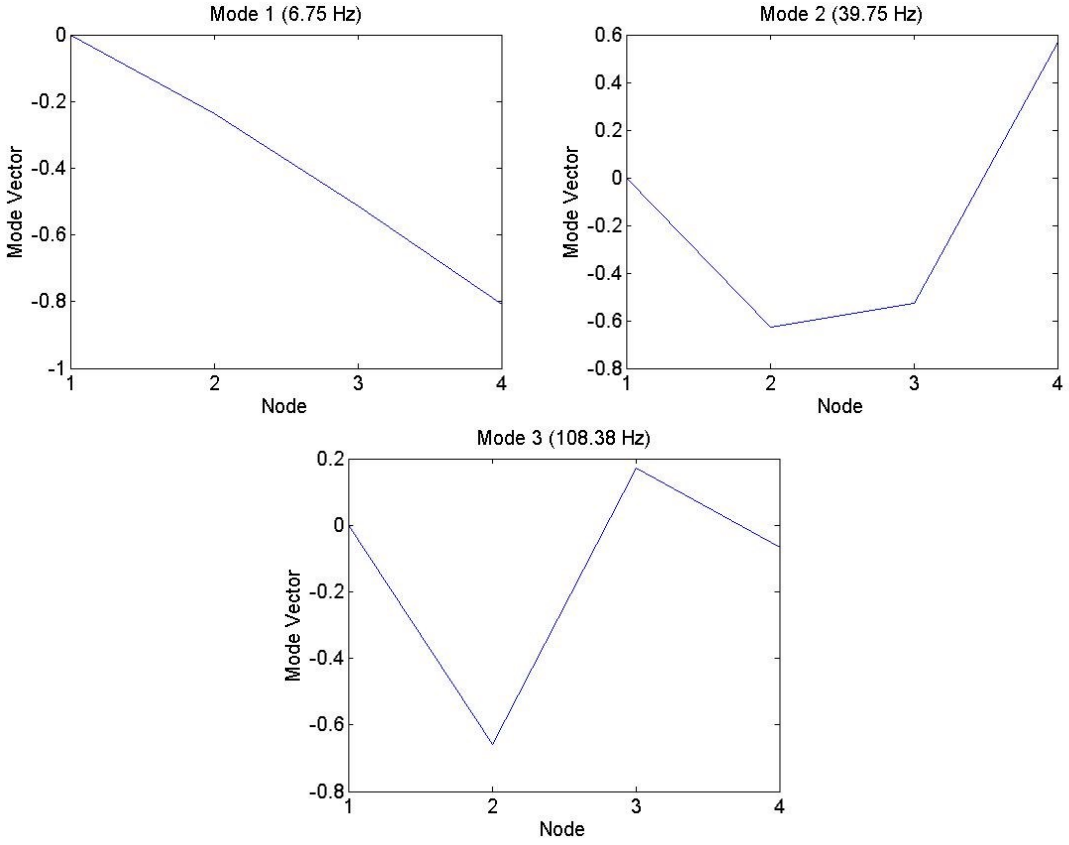

Fig. 6.17 Estimated mode shapes of undamaged structure by FDD

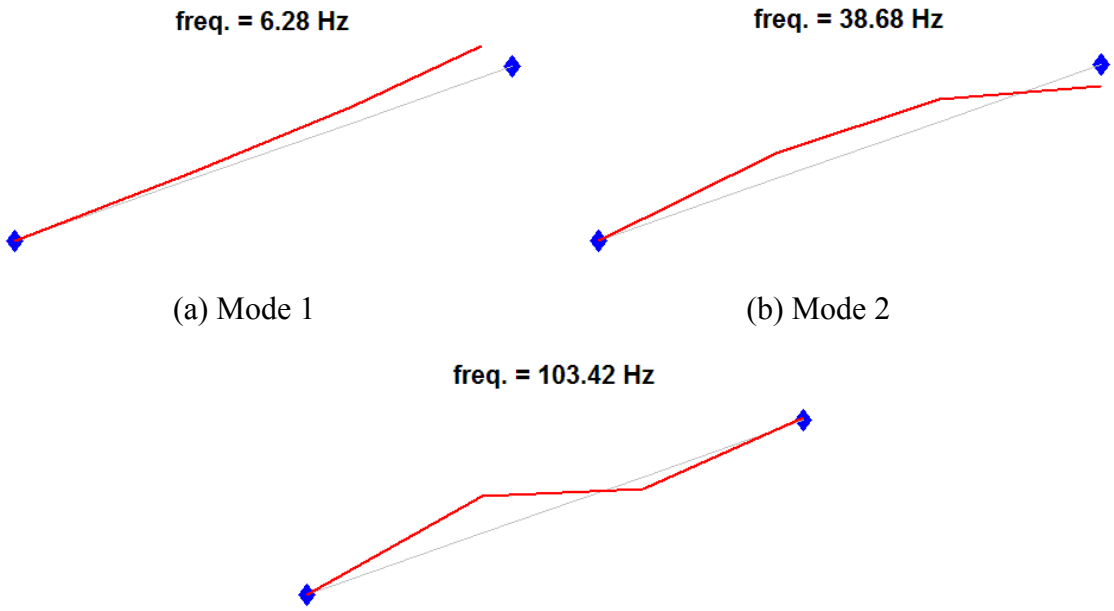

(a) Mode 1 (b) Mode 2

(c) Mode 3

Fig. 6.18 Estimated mode shapes of damaged structure by SSI

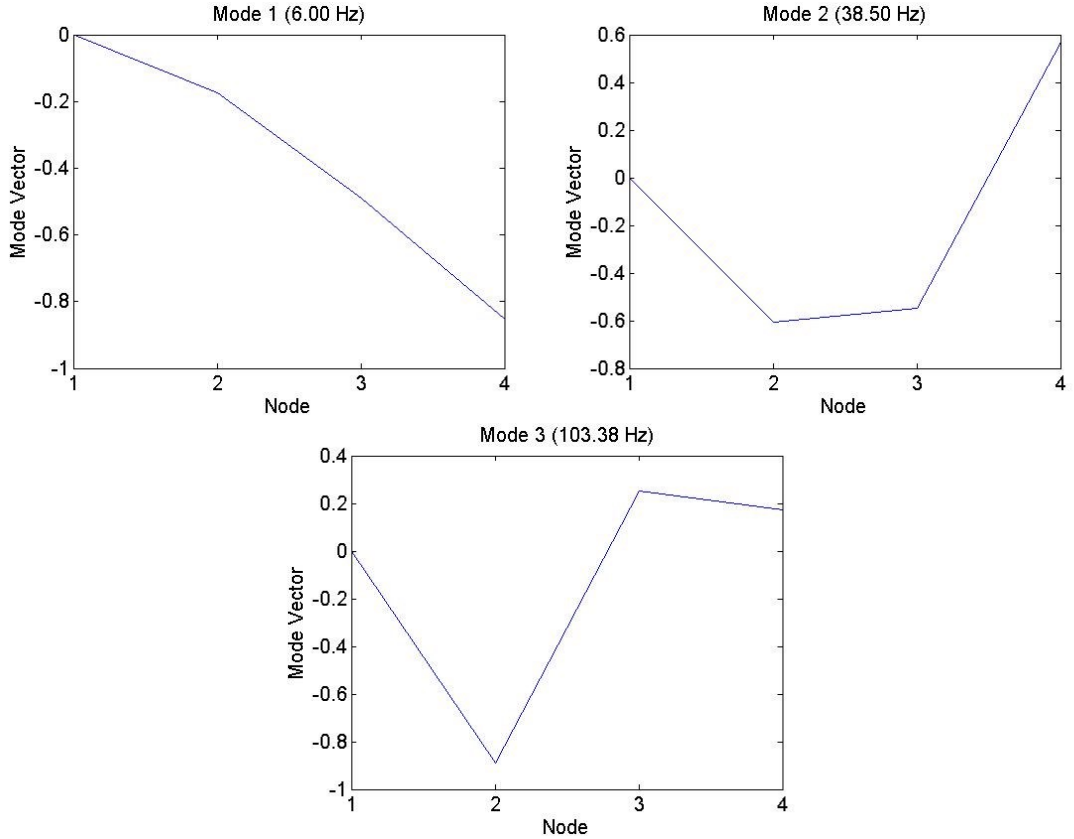

Fig. 6.19 Estimated mode shapes of damaged structure by FDD

6.4 Damage Identification

The VBDI techniques in this study use directly or indirectly the change of mode shape to locate damage and the damage indices include the change of mode shape, the change of mode shape curvature, the change of flexibility, and others. The highest peak for damage will be occurred at the location of damage when damage index plotted along the length of the frame. Practically, a very limited number of measurement points are available. In this test, only three accelerations were used for measurement. Moreover, it is possible that the damage is located between two measurement points not the exact point of measurement. This means that the highest peak should occur between the two measurement points when the damage is located between them. In such a case, it is necessary to estimate the values of a mode shape between the measurement points and interpolation can be used to make a smooth curve passing through given measurement points to improve the precision. Each VBDI technique is performed with MATLAB R2012b.

6.4.1 Methods based on frequency changes

In the initial stage of damage detection, this frequency change method was the only reliable because of the immature modal identification techniques. The advantage of this method is that the identification is relatively easy and can be performed by using a few sensors. However, to get accurate frequency changes, very precise measurements and large level of damages are required. Also, this method is not effective for spatial information of damages. Table 6.7 shows frequencies of undamaged and damaged frame. All frequencies are reduced after damage, but this does not give enough information of severity and location of damage.

Table 6.7 Frequencies of undamaged and damaged structure

Mode no.	Undamaged (Hz)	Damaged (Hz)	Difference (%)
1st	6.75	6.00	11.11
2nd	39.75	38.50	3.14
3rd	108.38	103.38	4.61

6.4.2 Methods based on mode shape changes

The large change in mode shapes would be occurred in the vicinity of damage, and it is possible to expect the location of damage. The most commonly used method to compare two sets of measured mode shapes is the modal assurance criterion (MAC). This MAC indicates the correlation between the intact structure and damaged structure. When damages are subtle, mode shape method is not available because MAC values are close to 1. Fig. 6.20 and Table 6.8 show MAC values between the undamaged and damaged mode shapes. These show that the first and second modes are correlated but the third mode is somewhat correlated. From these values, damages are expected but severity and location of damages are not possible to know.

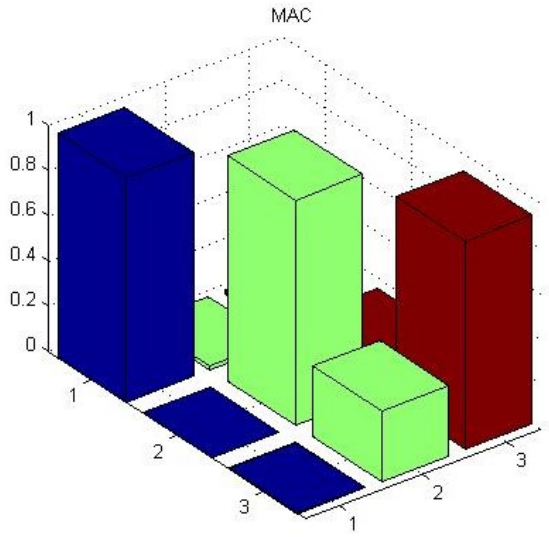

Fig. 6.20 MAC (undamaged and damaged)

Table 6.8 MAC (damaged and undamaged)

Mode no.	1st	2nd	3rd
1st	0.99	0.01	0.02
2nd	0.00	1.00	0.16
3rd	0.00	0.31	0.92

Fig. 6.21 shows the first three mode shapes. The first and second mode shapes of undamaged and damaged structure are similar but the difference of the third mode is somewhat large. This is because the difference of the mode shape change remarkably increases as the mode number increases. So, to get better results, measuring of higher modes will require more sensors.

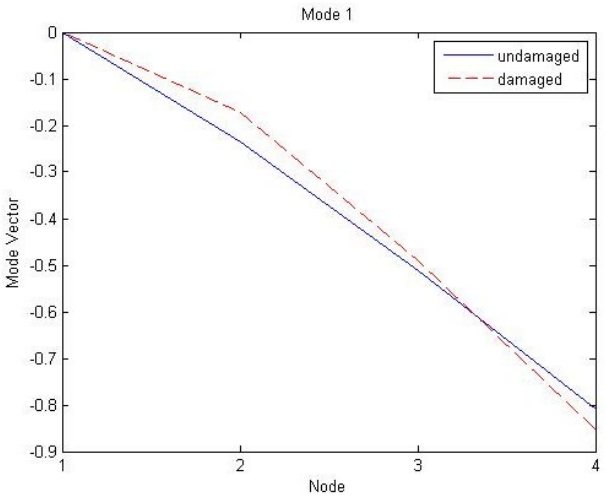

(a) Mode 1

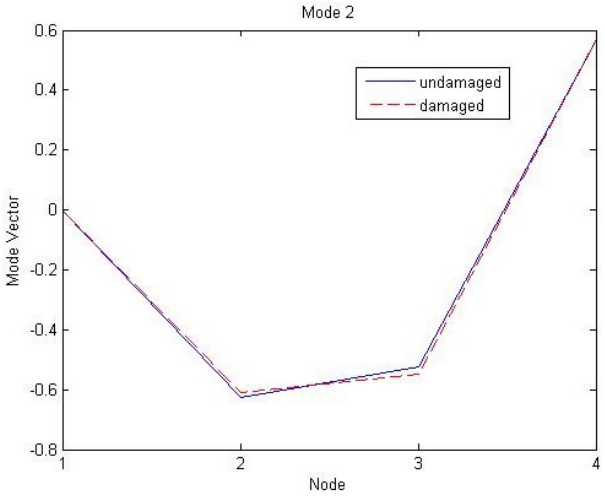

(b) Mode 2

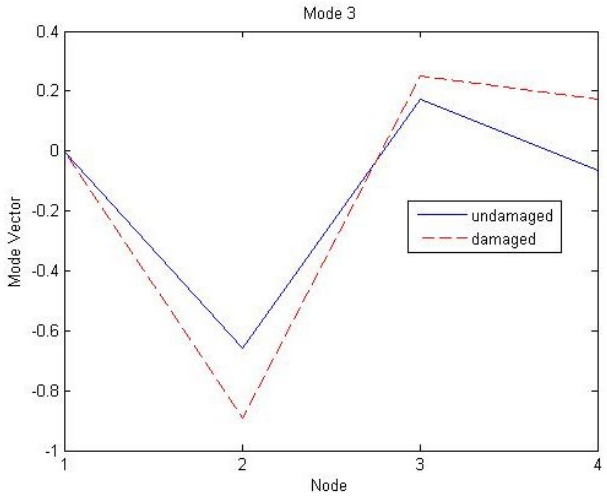

(c) Mode 3

Fig. 6.21 Mode shapes of undamaged and damaged

6.4.3 Mode shape curvature method

Fig. 6.22 shows the mode shape curvature calculated by Eq. (4.2) for first three modes both before and after damage. A reduction of the stiffness from damage increases the curvature of the mode shapes near the damage. However in this test, it is impossible to detect damages with this method. At the first mode, mode shape curvature is reduced at node 2 and node 3. At the second mode, mode shape curvature is reduced at node 2 and increased at node 3. At the third mode, damaged curvature of node 2 is increased but reduced at node 3. However the damage is located at node 3. This results show that modal curvatures are very sensitive to measurement errors and, in practice, damage cannot be detected with reliability on the basis of observed changes in the modal curvature.

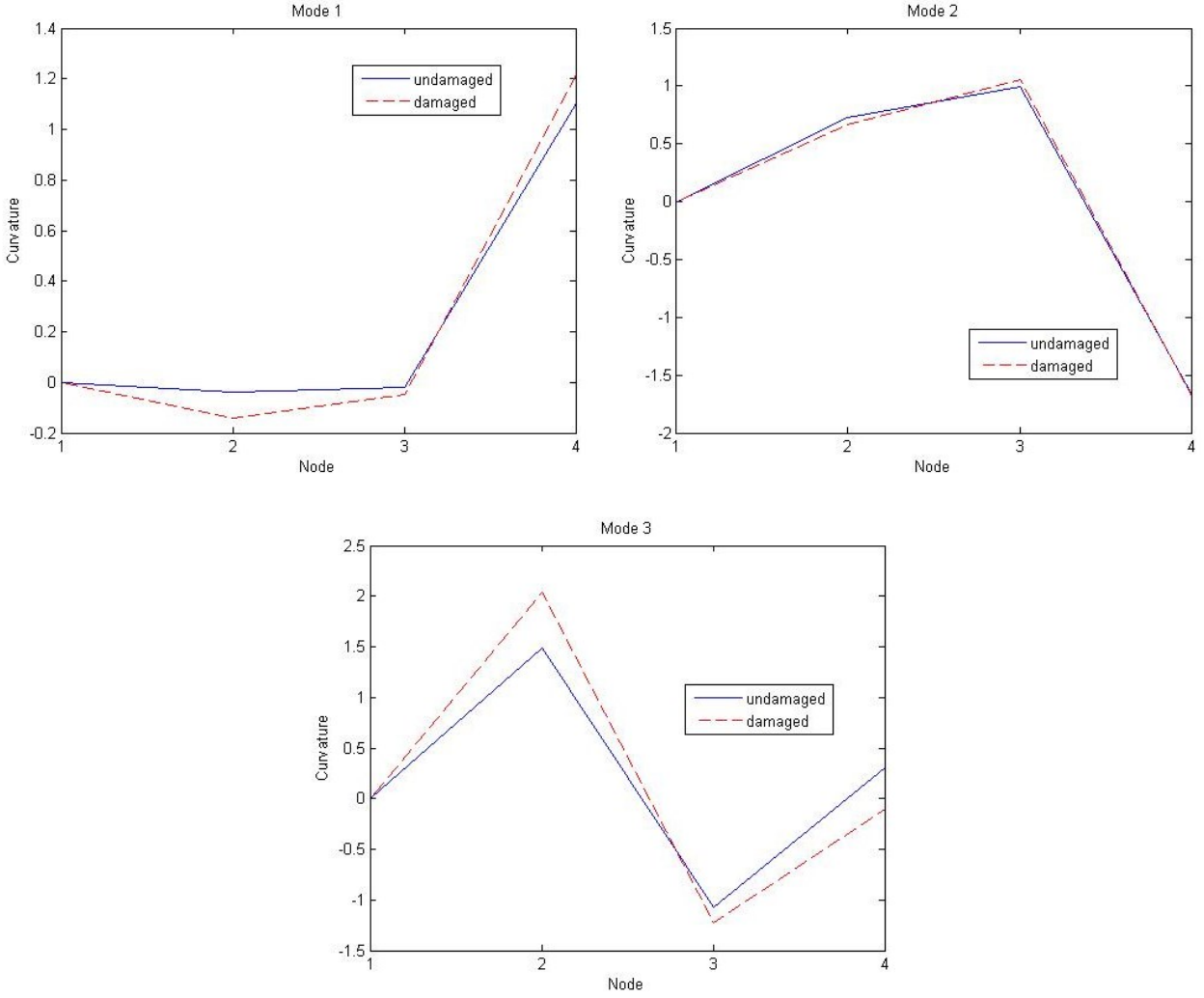

Fig. 6.22 Mode shape curvatures of undamaged and damaged

6.4.4 Methods based on change in flexibility matrix

This method is more effective when lower modes are used because the accuracy of the flexibility matrix is mostly affected by high-frequency modes. The flexibility differences δ_j obtained from Eq. (4.6) are plotted in Fig. 6.23. This figure shows that the degrees of freedom 2, 3 and 4 have been affected by damage, which means that element 2 and 3 have suffered damage because induced damage at degree of freedom 3 has affected to the adjacent degree of freedom 2 and 4.

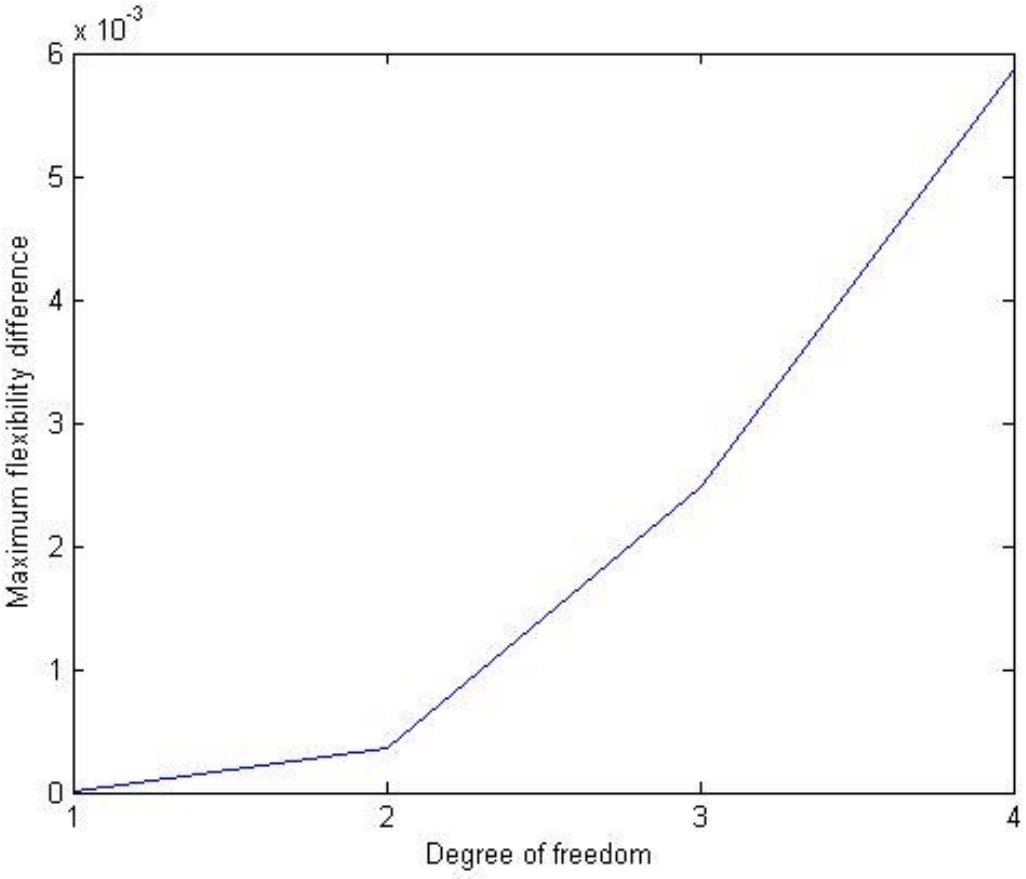

Fig. 6.23 Maximum differences of flexibility matrices

6.4.5 Methods based on changes in uniform flexibility shape curvature

This method is applied to the detection of damage in the frame structure. The number of modes is 3. The uniform flexibility shape curvature differences obtained from the flexibility matrix using Eq. (4.7) are plotted in Fig. 6.24. . This figure shows that the degrees of freedom 2, 3 and 4 have been affected by damage, which means that element 2 and 3 have suffered damage because induced damage at degree of freedom 3 has affected to the adjacent degree of freedom 2 and 4.

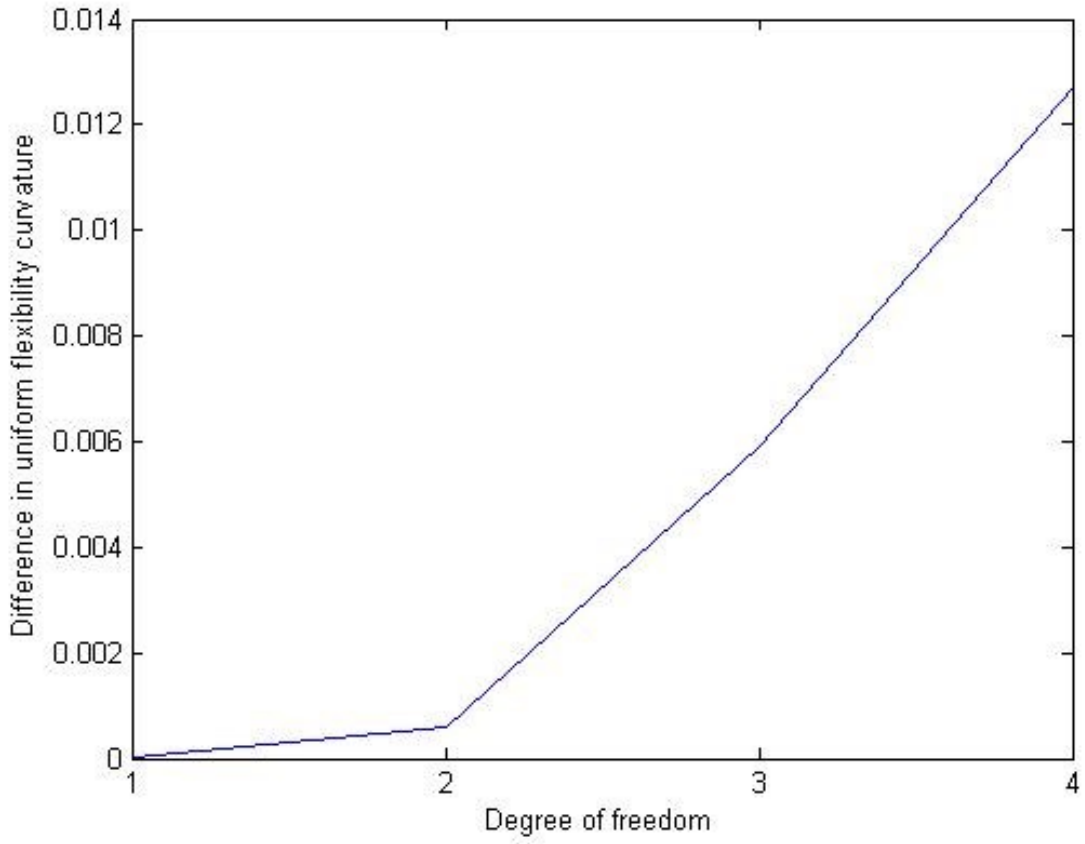

Fig. 6.24 Differences in uniform flexibility curvatures

6.4.6 Damage index method

The damage index method is applied to detect damage for the frame structure. Three mode shapes are used for this method. Using Eq. (4.12) and (4.13), damage indices are obtained for the elements and are plotted in Fig. 6.25. Larger damage indices of element 2 and 3 represent damage in these elements because induced damage at node 3 has affected to these elements.

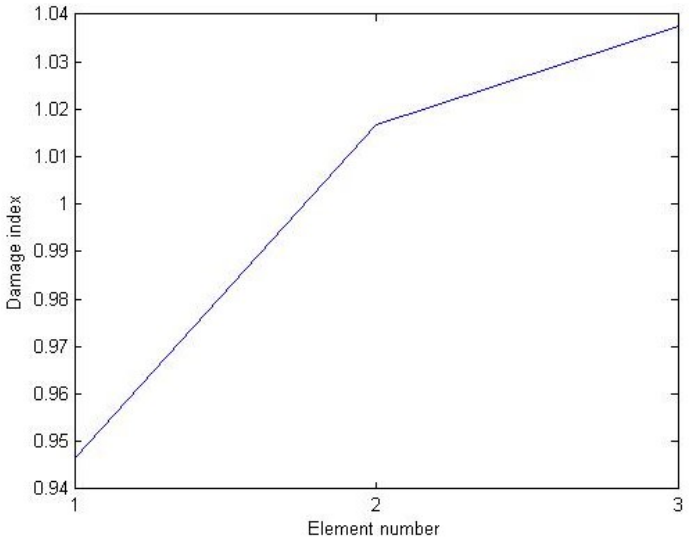

(a) Damage indices

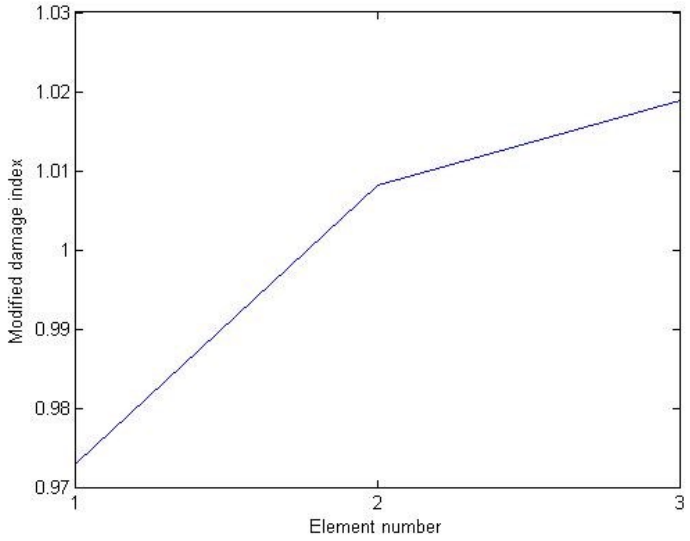

(b) Modified damage indices

Fig. 6.25 Damage indices

6.4.7 Matrix update method

For this method, M-FEM program developed in MATLAB (Bagchi et al. 2007) was used. An analytical model of the frame was modelled using beam elements. Each four column was simplified by only one frame because above VBDI methods used only four nodes and three frames. Fig. 6.26 shows the original structure and the simplified structure and Fig. 6.27 shows the first three mode shapes.

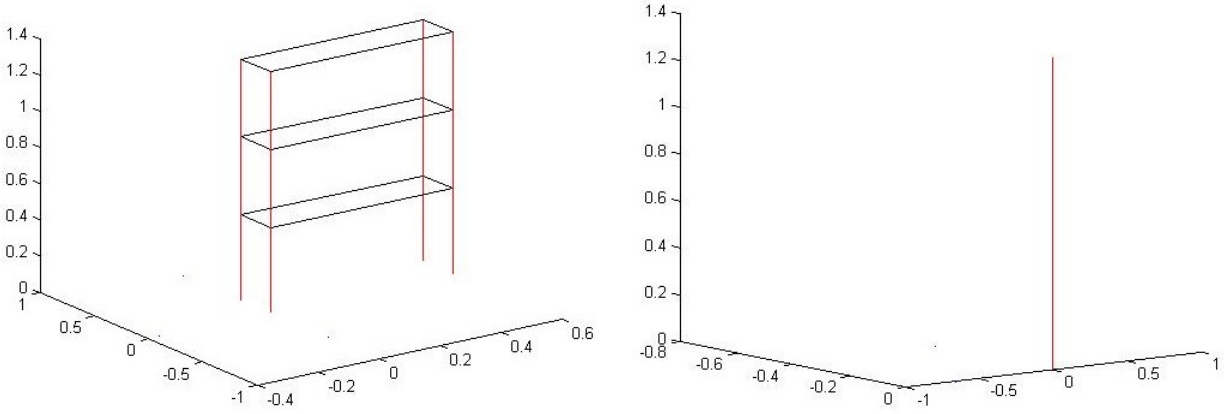

(a) Original structure (b) Simplified structure

Fig. 6.26 FE model for M-FEM

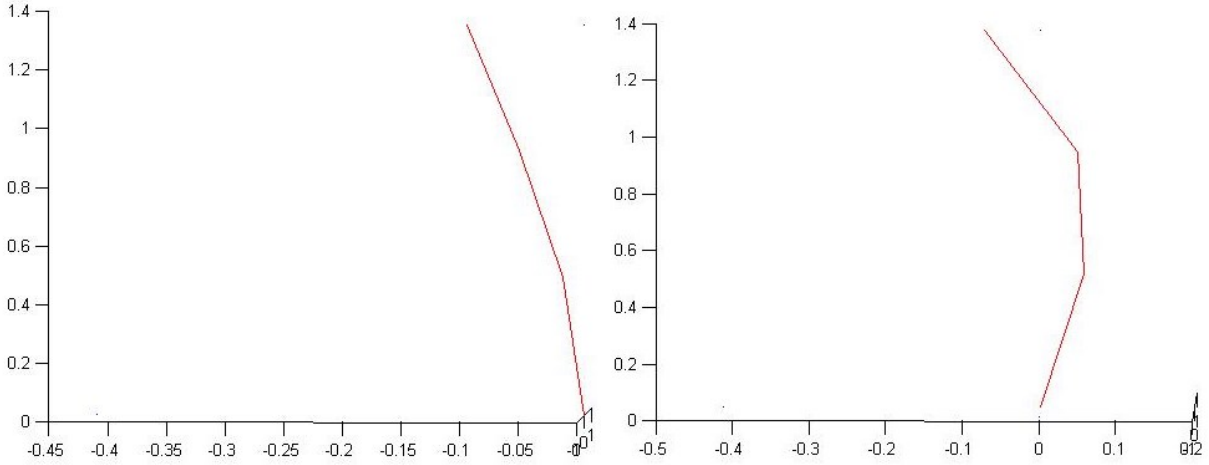

(a) Mode 1 (b) Mode 2

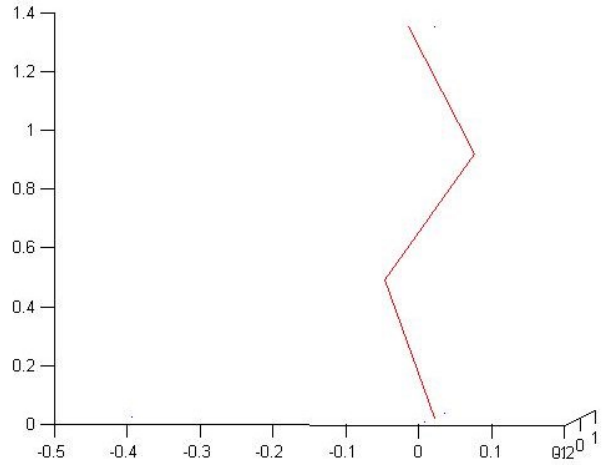

(c) Mode 3

Fig. 6.27 Mode shapes for frame structure

Fig. 6.28 shows the model updating results. During this process of model updating, the stiffness of every elements were modified to match the modal frequencies of the damaged structure's test results. The maximum difference between the initial finite element model and the test was 6.39% (at second mode). After two iterations, it was possible to achieve a correlated model, and Table 6.9 shows the changes of the stiffness after updating.

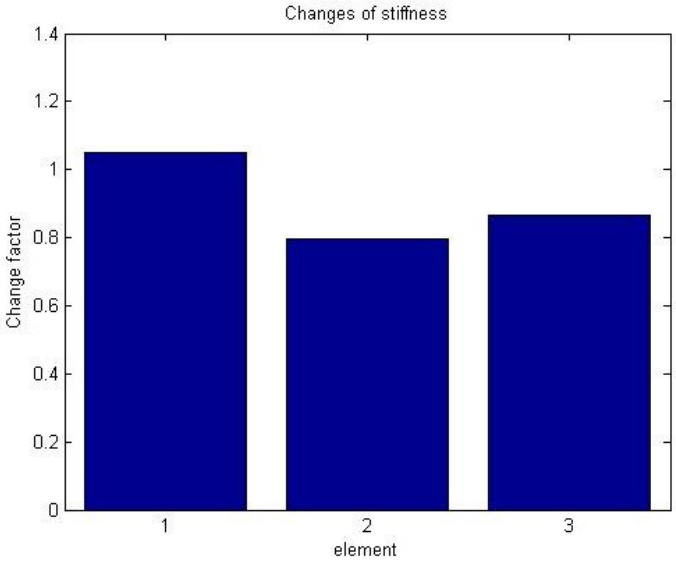

Fig. 6.28 Stiffness change factors

Table 6.9 Stiffness change factors

Element no.	1	2	3
Change Factor	1.0494	0.7958	0.8671

Fig. 6.29 shows the results by matrix update methods. Fig. 6.29 (a) and (b) correspond to matrix update method using the pseudo-inverse and optimized methods respectively. Both methods show proper damage locations properly. It shows that damage factor of element 2 and 3 are high and this indicates these elements are damaged.

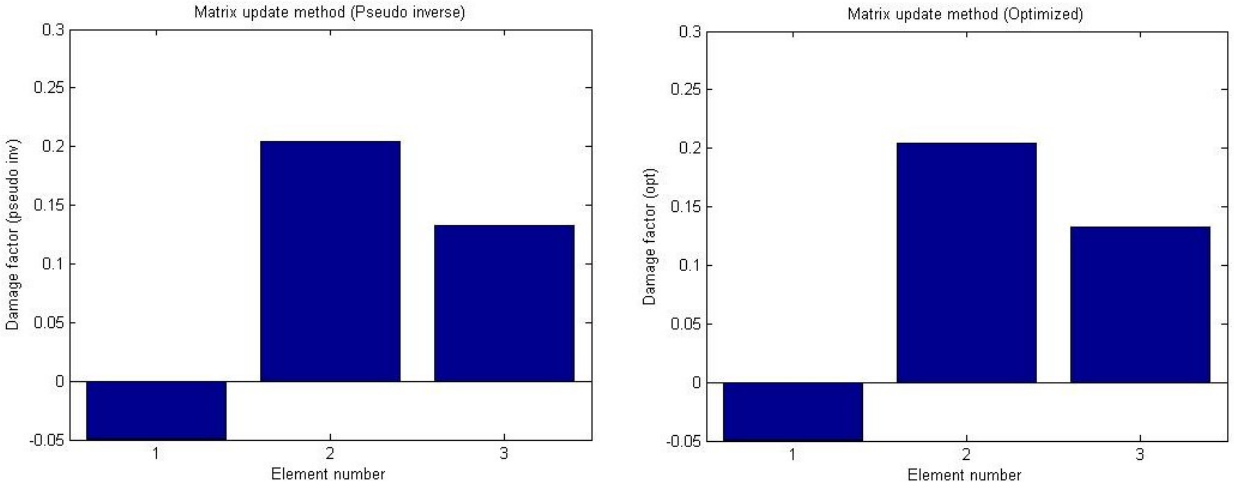

(a) Pseudo Inverse (b) Optimized

Fig. 6.29 Matrix update method

6.4.8 Genetic algorithm

The software for the genetic algorithm method was developed with MATLAB R2012b. This software uses iterative method by modifying the properties of the SAP2000 FE model. The values in objective function are calculated by frequencies and mode shapes in every iteration. This method is carried out by the dash board shown Fig. 6.30. This dash board is consisted of seven steps.

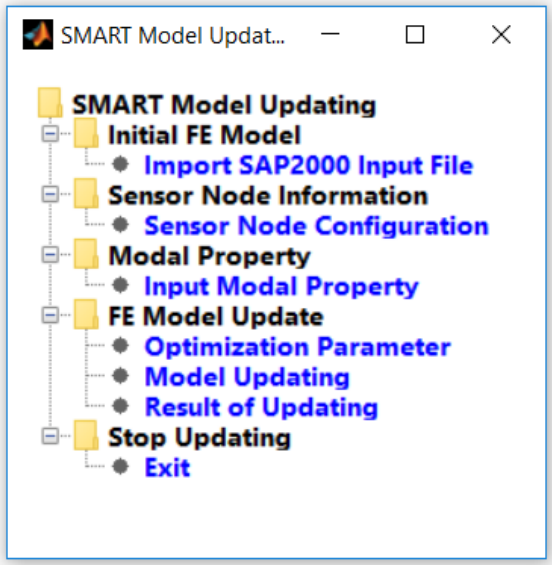

Fig. 6.30 Dash board

1) Import SAP 2000 Input File

In this step, the information of the SAP 2000 model is imported such as coordination of nodes and elements, properties of material and section, boundary conditions.

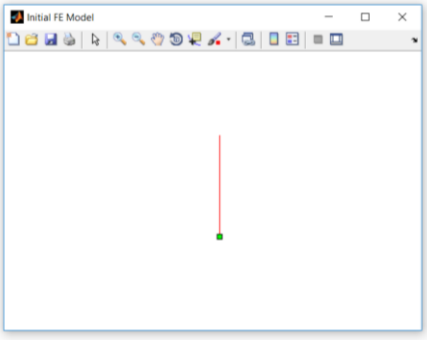

Fig. 6.31 Importing SAP 2000 model to MATLAB

2) Sensor Node Configuration

In this step, linking the sensor location to the FE model is carried out. Direction of measuring axis and restraint are determined.

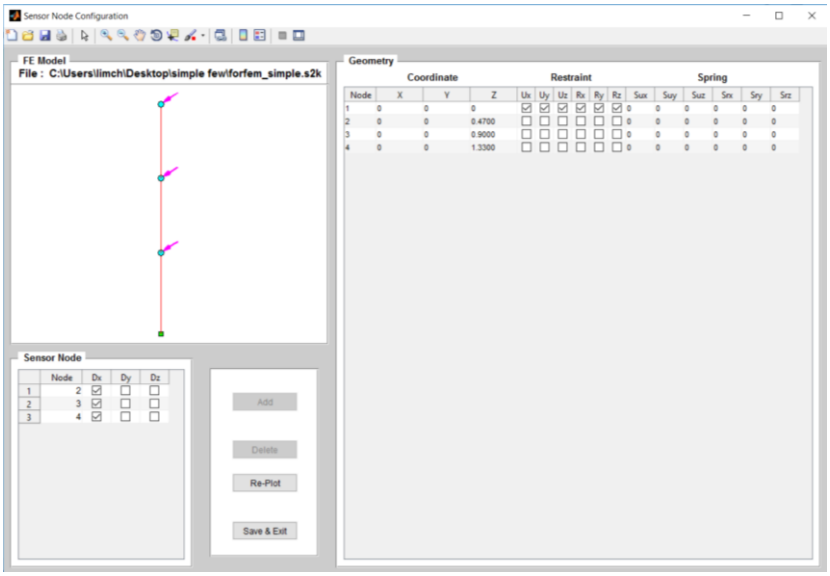

Fig. 6.32 Sensor configuration

3) Input Modal Property

In this step, objective frequencies and mode shapes are defined.

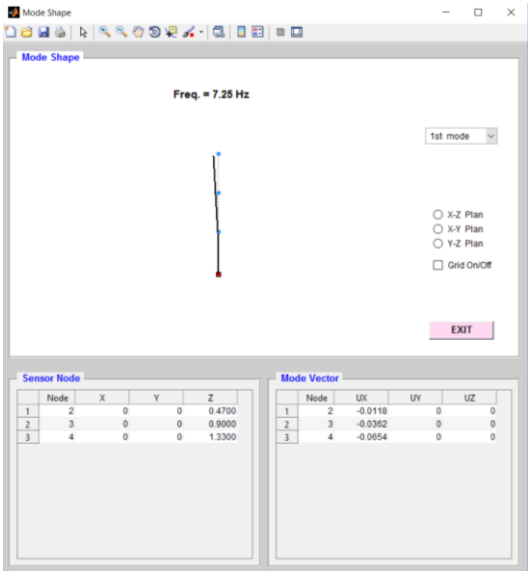

Fig. 6.33 Modal property

4) Optimization Parameter

In this step, parameters are chosen. For this, material properties of each frame are selected.

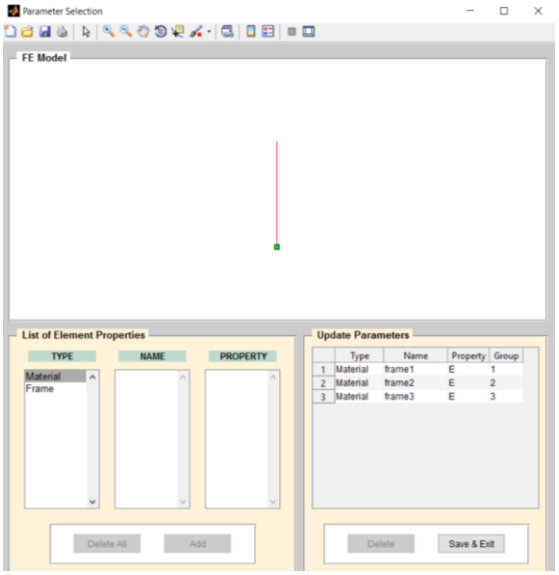

Fig. 6.34 Selection of updating parameters

5) Model Updating

Limits of chosen parameters, weighting factors for frequency and mode shape, population and generation numbers can be selected. Fig. 6.35 shows the selected options for this study.

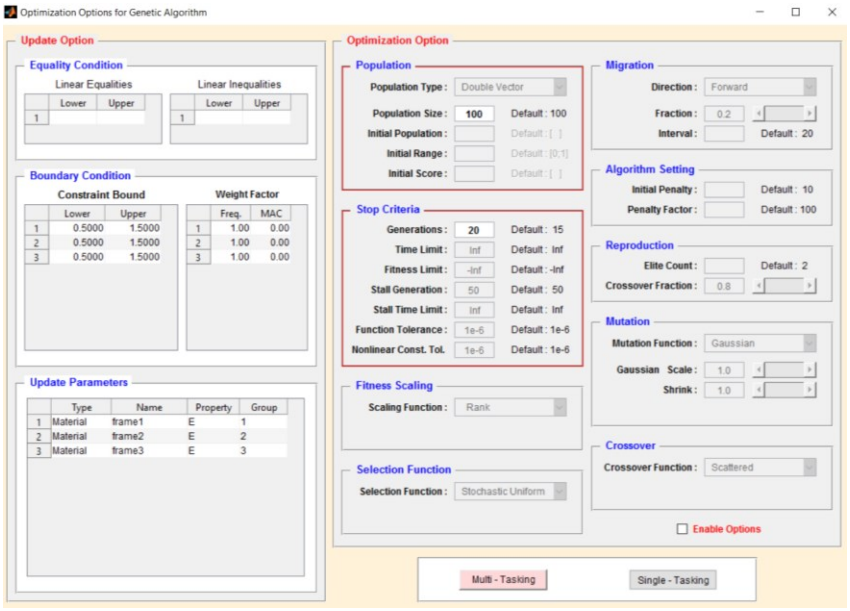

Fig. 6.35 Selection of optimization method

6) Result of Updating

Fig. 6.36 shows the result of GA method. Material property of frame 1 was increased to 1.0477 and other two frame's properties were decreased to 0.7986 and 0.8583. These values are very similar to those of matrix updating method (1.0494, 0.7958, 0.8671).

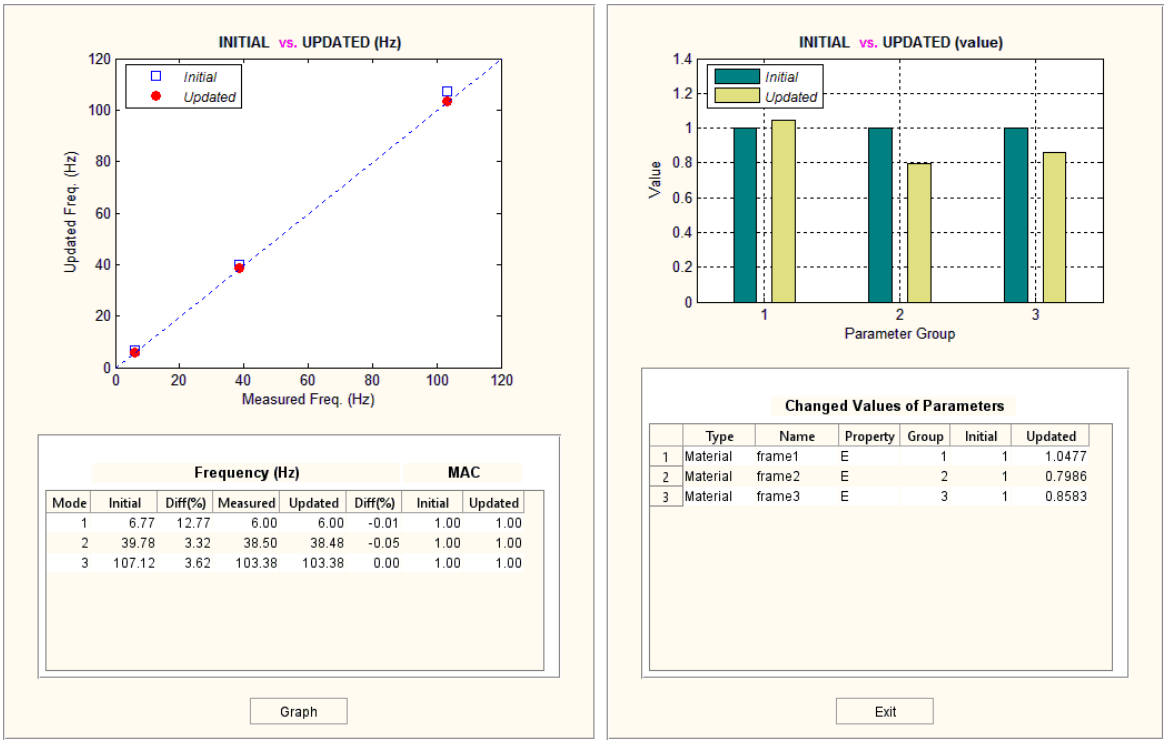

Fig. 6.36 Modal updating results

6.5 Conclusions

Some of the principal VBDI methods were carried out through the experimental test of the frame structure. With output-only information, the fundamental frequencies and mode shapes before and after damage were reasonably calculated. Some VBDI methods, the induced damage on the frame was detected and located in some degree. Practically, only a small number of sensors are feasible, and damage localization is depend on the number and spacing between sensors. The following conclusions can be drawn from this chapter.

1) The results of the two output-only modal identification methods were very similar and these results were matched well with the results of FEM. Therefore, both SSI and FDD methods are efficient modal identification method.

2) The induced damage was detected and located in matrix update and genetic algorithm methods. However, the results were not reasonable because a small number of sensors were used so only a limited number of modes were available.

Chapter 7. Conclusions and Future Research

7.1 Summary

This thesis is organized in two main parts: the first part is about Modal Identification with output-only information and the other part is related to Vibration-based Damage Identification (VBDI) techniques. The primary objective in this study was to investigate the capability of VBDI techniques to detect and locate damage using a small number of sensors.

Two modal identification methods (FDD and SSI) and eight VBDI techniques were used. These VBDI techniques include frequency changes, mode shape changes, mode shape curvature, flexibility matrix change, uniform flexibility shape curvature change, damage index, matrix update and genetic algorithm. All of these methods are non-model based VBDI methods except for matrix update and genetic algorithm. Non-model based method means that this method only rely on the measured frequencies and mode shapes.

The experimental tests were carried on modal identification for two types of highway bridges and VBDI for the steel frame structure. For these tests, wireless accelerometers were used to measure dynamic properties of the structures. Finite element models for the tested structures were generated for the numerical studies.

7.2 Conclusions

7.2.1 Modal identification

Two modal identification methods of output-only information (FDD and SSI) were used for modal identification. The results of each method were well matched in two types of highway bridges (PSCB and STB). Thought the modal properties identified from the ambient vibration test have been found to be fairly far from those obtained from the FE model (PSCB 8.6%, STB 8.3%), the main object of FE model was to verify the accordance of the mode shapes and the trends of the natural frequencies. These differences might be the FE model does not reflect the current structural condition.

The SSI method requires larger computation time and is more complicated than the FDD method. However, if adjacent modes were closely spaced, the SSI method is more accurate than the FDD method like the results of the STB bridge. So the FDD method can be used in the preliminary stage then, the SSI method can be used in the finalizing procedure to extract more accurate results.

7.2.2 VBDI

Some of the principal VBDI methods were carried out through the experimental test of the frame structure. With output-only information, the fundamental frequencies and mode shapes before and after damage were reasonably calculated. Some VBDI methods, the induced damage on the frame, was detected and located in some degree. The comparisons of the each VBDI technique's effectiveness are shown in Table 7.1. The following conclusions can be drawn from this study.

1) Results of this study show that the matrix update and the genetic algorithm methods are the best method of the eight VBDI techniques. These methods could successfully detect the severity and location of the induced damage. However, these methods are not non-model based methods, so the initial FEM model is required.

2) In order to produce the best results, mode shapes must be measured with a high level of accuracy because mode shape changes by low levels of damage are very small.

3) During the several times of the ambient vibration tests using hands or hammer, the results of the modal identification were various. The results might be depending on the source of excitation. This accuracy errors might result in a failure to successful detect of small scale damage. Repeated excitation and measurements should be used to reduce the error.

4) Different from non-model based VBDI methods, the accuracy of matrix update and genetic algorithm method depend on the determination of frequencies and mode shapes, and closeness of the FEM model to the real structure.

Table 7.1 Comparison of VBDI techniques

Method	Severity	Location	Detection
Frequency change	X	X	O
Mode shape change	X	X	▲
Mode curvature	X	X	▲
Flexibility matrix	X	O	O
Flexibility curvature	X	O	O
Damage index	▲	O	O
Matrix update	O	O	O
Genetic algorithm	O	O	O

7.3 Future research

The following items are suggested for future research concerning the modal identification and vibration-based damage identification:

1) VBDI in this study is focused on the simple frame structure. More complex and practical structures such as bridges, buildings should be investigated.

2) The damages were induced in this frame by loosening the bolts of the second floor in each directions. Other damage types such as frame section cutting, boundary conditions should be investigated.

3) Environmental effects especially temperature were not considered in this study. The effect of these elements on determining dynamic characteristics should be considered.

4) Other powerful VBDI methods such as wavelet, neural networks or combination of these methods should be considered. These methods would be successfully detect Level 3 damages (severity of the damage).

5) VBDI is based on the modal identification result from the vibration data. Therefore enhancements to modal identification method could improve VBDI results. So, more accurate modal identification methods should be investigated.

References

Aktan, E., Çatbas, N., Türer, A., and Zhang, Z. "Structural Identification: Analytical Aspects." *Journal of Structural Engineering* 124.7 (1998): 817-29.

Allemang, R. J., and Brown, D. "A Correlation Coefficient for Modal Vector Analysis". *Proceedings of the 1st international modal analysis conference.*

Allemang, R. J. "The Modal Assurance criterion–twenty Years of use and Abuse." *Sound and vibration* 37.8 (2003): 14-23.

Alvandi, A., and Cremona, C. "Assessment of Vibration-Based Damage Identification Techniques." *Journal of Sound and Vibration* 292.1 (2006): 179-202.

Au, F., Cheng, Y., Tham, L., and Bai, Z. "Structural Damage Detection Based on a Micro-Genetic Algorithm using Incomplete and Noisy Modal Test Data." *Journal of Sound and Vibration* 259.5 (2003): 1081-94.

Bagchi, A., Humar, J., and Noman, A. "Development of a Finite Element System for Vibration-based Damage Development of a Finite Element System for Vibration-based Damage Identification in Structures." *Journal of Applied Sciences* 7.17 (2007): 2404-13.

Bagchi, A. Updating the mathematical model of a structure using vibration data. *Journal of Vibration and Control, 11*(12), (2005) 1469-1486.

Baker, K. "Singular Value Decomposition Tutorial." *The Ohio State University* 24 (2005)

Bakht, B., Jaeger, L. G., Cheung, M. S., and Mufti, A. A. The state of the art in analysis of cellular and voided slab bridges. *Canadian Journal of Civil Engineering, 8*(3), (1981) 376-391.

Beck, J., and Katafygiotis, L. "Updating Models and their Uncertainties. I: Bayesian Statistical Framework." *Journal of Engineering Mechanics* 124.4 (1998): 455-61.

Beck, J., and Katafygiotis, L. "Probabilistic System Identification and Health Monitoring of Structures". *Proc., 10th World Conf. On Earthquake Engrg.*

Brincker, R., Zhang, L., and Andersen, P. "Modal identification from Ambient Responses using Frequency Domain Decomposition". *Proc. of the 18*'International Modal Analysis Conference (IMAC), San Antonio, Texas.*

Brownjohn, J. M., Xia, P., Hao, H., and Xia, Y. "Civil Structure Condition Assessment by FE Model Updating:: Methodology and Case Studies." *Finite Elements in Analysis and Design* 37.10 (2001): 761-75.

Casas, J. R., and Aparicio, A. C. "Structural Damage Identification from Dynamic-Test Data." *Journal of Structural Engineering* 120.8 (1994): 2437-50.

Catbas, F. N., Ciloglu, S. K., Hasancebi, O., Grimmelsman, K., and Aktan, A. E. "Limitations in Structural Identification of Large Constructed Structures." *Journal of Structural Engineering* 133.8 (2007): 1051-66.

Chance, J., Tomlinson, G., and Worden, K. "A Simplified Approach to the Numerical and Experimental Modelling of the Dynamics of a Cracked Beam". *Proceedings-SPIE the International Society for Optical Engineering.*

Chen, S., Venkatappa, S., Petro, S., and Ganga Rao, H. "Damage Detection using 2-D Strain Energy Distribution and Scanning Laser". *Society for Experimental Mechanics, Inc, 17 th International Modal Analysis Conference.*

Chou, J., and Ghaboussi, J. "Genetic Algorithm in Structural Damage Detection." *Computers and Structures* 79.14 (2001): 1335-53.

Ewins, D. *Modal Testing: Theory, Practice, and Application*. Research Studies Press, (2000).

Doebling, S. W., Farrar, C. R., Prime, M. B., and Shevitz, D. W. *Damage identification and health monitoring of structural and mechanical systems from changes in their vibration characteristics: a literature review* (1996)

Doebling, S. W., Farrar, C. R., and Prime, M. B. "A Summary Review of Vibration-Based Damage Identification Methods." *Shock and Vibration Digest* 30.2 (1998): 91-105.

Dos Santos, J. M., and Zimmerman, D. C. "Damage Detection in Complex Structures using Component Mode Synthesis and Residual Modal Force Vector". *Proceedings-spie the International Society for Optical Engineering.*

Farrar, C.R., Baker, W.E., Bell, T.M., Cone, K.M., Darling, T.W., Duffey, T.A., Eklund, A., and Migliori, A. *"Dynamic Characterization and Damage Detection in the I-40 Bridge Over the Rio Grande".* United States. doi:10.2172/10158042 Vol. , (1994).

Farrar, C. R., and Jauregui, D. A. "Comparative Study of Damage Identification Algorithms Applied to a Bridge: II. Numerical Study." *Smart Materials and Structures* 7.5 (1998): 720.

Farshchin, M. Frequency Domain Decomposition (FDD) MATLAB code, https://www.mathworks.com/matlabcentral/fileexchange/50988-frequency-domain-decomposition--fdd-, December, (2015).

Fox, C. "The Location of Defects in Structures: A Comparison of the use of Natural Frequency and Mode Shape Data". *Proceedings of the International Modal Analysis Conference.*

Friswell, M., Penny, J., and Garvey, S. "A Combined Genetic and Eigensensitivity Algorithm for the Location of Damage in Structures." *Computers and Structures* 69.5 (1998): 547-56.

Friswell, M., and Penny, J. "Is Damage Location using Vibration Measurements Practical?". *Proceedings of Euromech 365 international workshop: Damas.*

Guan, H., Karbhari, V. M., and Sikorsky, C. S. "Web-Based Structural Health Monitoring of an FRP Composite Bridge." *Computer‐Aided Civil and Infrastructure Engineering* 21.1 (2006): 39-56.

Hajela, P., and Soeiro, F. "Recent Developments in Damage Detection Based on System Identification Methods." *Structural Optimization* 2.1 (1990): 1-10.

Hermans, L., and Van der Auweraer, H. "Modal Testing and Analysis of Structures Under Operational Conditions: Industrial Applications." *Mechanical systems and signal processing* 13.2 (1999): 193-216.

Housner, G., Bergman, L. A., Caughey, T. K., Chassiakos, A. G., Claus, R. O., Masri, S. F., and Yao, J. T. "Structural Control: Past, Present, and Future." *Journal of Engineering Mechanics* 123.9 (1997): 897-971.

Hu, N., Wang, X., Fukunaga, H., Yao, Z., Zhang, H., and Wu, Z. "Damage Assessment of Structures using Modal Test Data." *International Journal of Solids and Structures* 38.18 (2001): 3111-26.

Humar, J., Bagchi, A., and Xu, H. "Performance of Vibration-Based Techniques for the Identification of Structural Damage." *Structural Health Monitoring* 5.3 (2006): 215-41.

Ibrahim, S. R., and Pappa, R. S. "Large Modal Survey Testing using the Ibrahim Time Domain Identification Technique." *Journal of Spacecraft and Rockets* 19.5 (1982): 459-65.

Jauregui, D. V., and Farrar, C. R. "Comparison of Damage Identification Algorithms on Experimental Modal Data from a Bridge". *Proceedings-spie the International Society for Optical Engineering.*

Juang, J., and Pappa, R. S. "An Eigensystem Realization Algorithm for Modal Parameter Identification and Model Reduction." *Journal of guidance, control, and dynamics* 8.5 (1985): 620-7.

Kabe, A. M. "Stiffness Matrix Adjustment using Mode Data." *AIAA Journal* 23.9 (1985): 1431-6.

Kaouk, M., and Zimmerman, D. C. "Structural Damage Assessment using a Generalized Minimum Rank Perturbation Theory." *AIAA Journal* 32.4 (1994): 836-42.

Kim, J., and Stubbs, N. "Model-Uncertainty Impact and Damage-Detection Accuracy in Plate Girder." *Journal of Structural Engineering* 121.10 (1995): 1409-17.

Kim, J., and Stubbs, N. "Non-destructive Crack Detection Algorithm for Full-Scale Bridges." *Journal of Structural Engineering* 129.10 (2003): 1358-66.

Li, J., Wu, B., Zeng, Q., and Lim, C. W. "A Generalized Flexibility Matrix Based Approach for Structural Damage Detection." *Journal of Sound and Vibration* 329.22 (2010): 4583-7.

Mares, C., and Surace, C. "An Application of Genetic Algorithms to Identify Damage in Elastic Structures." *Journal of Sound and Vibration* 195.2 (1996): 195-215.

Marwala, T. *Finite Element Model Updating using Computational Intelligence Techniques: Applications to Structural Dynamics*. Springer Science and Business Media, 2010.

Masri, S., Nakamura, M., Chassiakos, A., and Caughey, T. "Neural Network Approach to Detection of Changes in Structural Parameters." *Journal of Engineering Mechanics* 122.4 (1996): 350-60.

MATLAB user manual. The Mathworks Inc. Natick. MA. USA (2008).

Midas-Civil. Online manual. Midas Information Technology Co. Ltd. http://www.midasit.com. (2012).

Mottershead, J., and Friswell, M. Model updating in structural dynamics: A survey. *Journal of Sound and Vibration, 167*(2), (1993) 347-375.

Nabil, F., and Roula, M. "A Probabilistic Framework for Detecting and Identifying Anomalies." *Engng Mech.* 12.2 (1997): 63-73. Print.

Newland, D. E. *An Introduction to Random Vibrations, Spectral and Wavelet Analysis*. Courier Corporation, 2012.

Obrien, E. J., Keogh, D., and O'Connor, A. *Bridge deck analysis* CRC Press (2014).

Oran Brigham, E. "The Fast Fourier Transform and its Applications." *UK: Prentice Hall* (1988)

Pandey, A., Biswas, M., and Samman, M. "Damage Detection from Changes in Curvature Mode Shapes." *Journal of Sound and Vibration* 145.2 (1991): 321-32.

Pandey, A., and Biswas, M. "Damage Detection in Structures using Changes in Flexibility." *Journal of Sound and Vibration* 169.1 (1994): 3-17.

Ramirez, R. W. "The FFT. Fundamentals and Concepts." *Englewood Cliffs: Prentice-Hall, 1985* 1 (1985)

Rytter, A. "Vibrational Based Inspection of Civil Engineering Structures." (1993)

Salawu, O., and Williams, C. "Damage Location using Vibration Mode Shapes". *Proceedings of the 12th International Modal Analysis.*

Salawu, O. "Detection of Structural Damage through Changes in Frequency: A Review." *Engineering Structures* 19.9 (1997): 718-23.

Siddique, A., Sparling, B., and Wegner, L. "Assessment of Vibration-Based Damage Detection for an Integral Abutment Bridge." *Canadian Journal of Civil Engineering* 34.3 (2007): 438-52.

Sohn, H., Farrar, C. R., Hemez, F. M., Shunk, D. D., Stinemates, D. W., Nadler, B. R., and Czarnecki, J. J. "A Review of Structural Health Monitoring Literature: 1996–2001." *Los Alamos National Laboratory, USA* (2003)

Steenackers, G., and Guillaume, P. "Structural Health Monitoring of the Z24 Bridge in Presence of Environmental Changes using Modal Analysis". *Proceedings of IMAC.*

Storey, B. D. "Computing Fourier Series and Power Spectrum with Matlab." *TEX Paper* (2002)

Stubbs, N., Kim, J., and Farrar, C. "Field Verification of a Non Destructive Damage Localization and Sensitivity Estimator Algorithm." *IMAC XIII* 196: 210-8.

West, W. M. "Illustration of the use of Modal Assurance Criterion to Detect Structural Changes in an Orbiter Test Specimen". *International Modal Analysis Conference, 4 th, Los Angeles, CA, Proceedings.*

Wu, X., Ghaboussi, J., and Garrett, J. H. "Use of Neural Networks in Detection of Structural Damage." *Computers and Structures* 42.4 (1992): 649-59.

Xia, Y., and Hao, H. "A Genetic Algorithm for Structural Damage Detection Based on Vibration Data". *Proceedings of SPIE, the International Society for Optical Engineering.*

Yang, Q., and Sun, B. "Structural Damage Identification Based on Best Achievable Flexibility Change." *Applied Mathematical Modelling* 35.10 (2011): 5217-24.

Yi, J., and Yun, C. "Comparative Study on Modal Identification Methods using Output-Only Information." *Structural Engineering and Mechanics* 17.3_4 (2004): 445-66.

Zhang, Z., and Aktan, A. "The Damage Indices for the Constructed Facilities". *Proceedings-spie the International Society for Optical Engineering.*

Zimmerman, D. C., and Kaouk, M. "Structural Damage Detection using a Minimum Rank Update Theory." *Journal of Vibration and Acoustics* 116.2 (1994): 222-31.

Appendix A: Acceleration response and PSD of PSCB Bridge

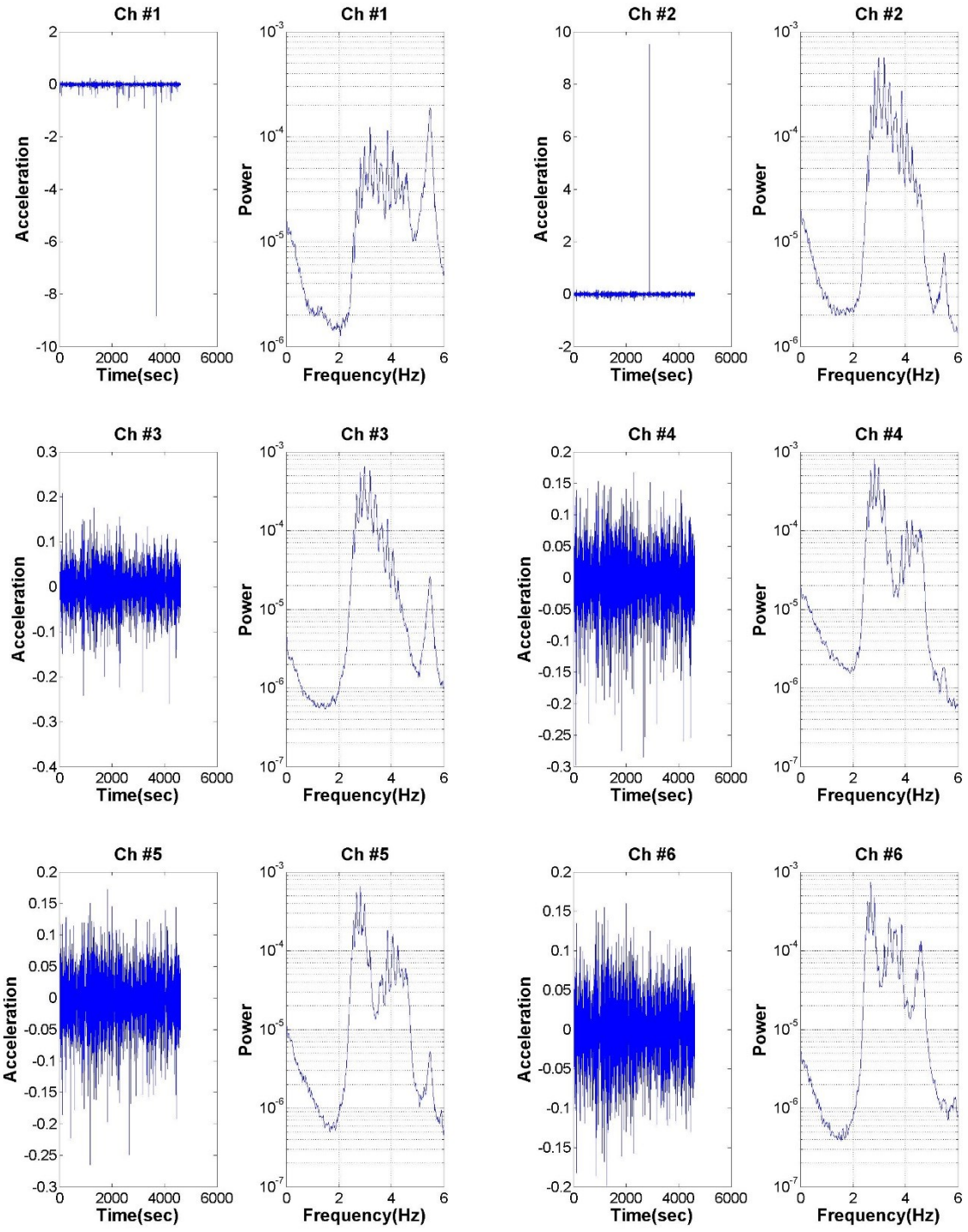

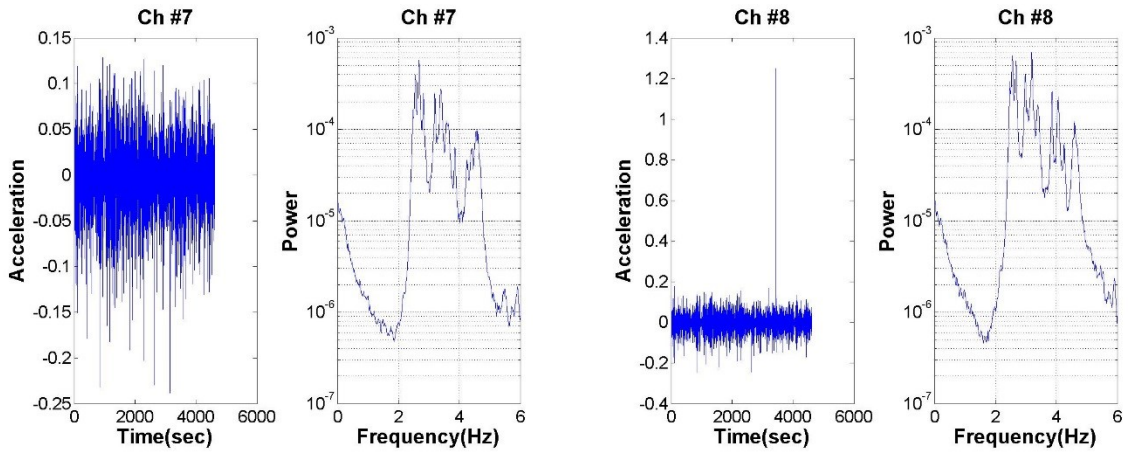
Ch #7
Acceleration
Time(sec)
Ch #7
Power
Frequency(Hz)
Ch #8
Acceleration
Time(sec)
Ch #8
Power
Frequency(Hz)

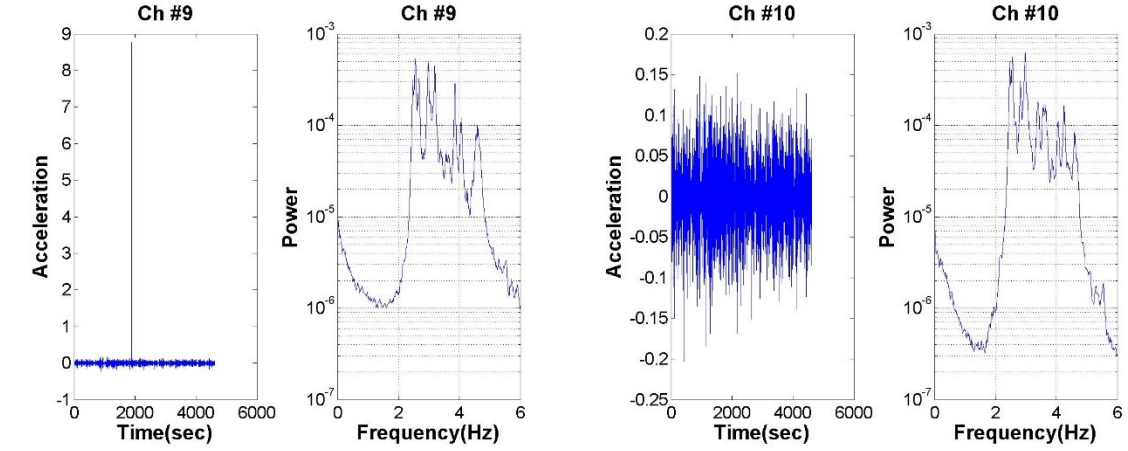
Ch #9
Acceleration
Time(sec)
Ch #9
Power
Frequency(Hz)
Ch #10
Acceleration
Time(sec)
Ch #10
Power
Frequency(Hz)

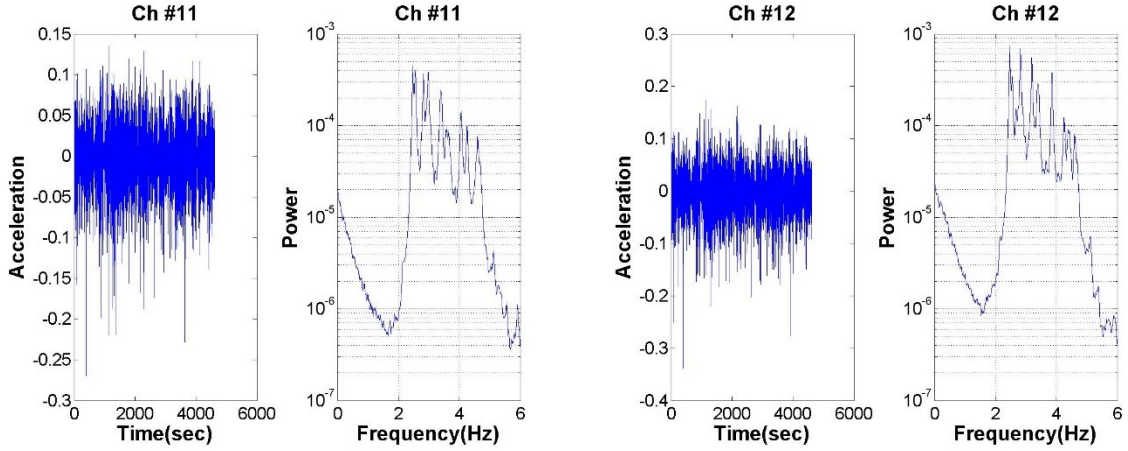
Ch #11
Acceleration
Time(sec)
Ch #11
Power
Frequency(Hz)
Ch #12
Acceleration
Time(sec)
Ch #12
Power
Frequency(Hz)

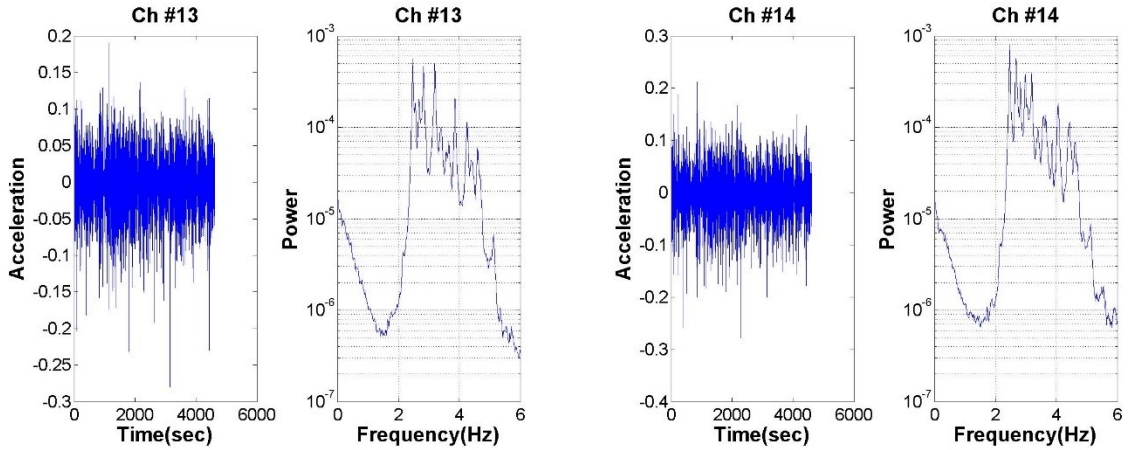
Ch #13
Acceleration
Time(sec)
Ch #13
Power
Frequency(Hz)
Ch #14
Acceleration
Time(sec)
Ch #14
Power
Frequency(Hz)

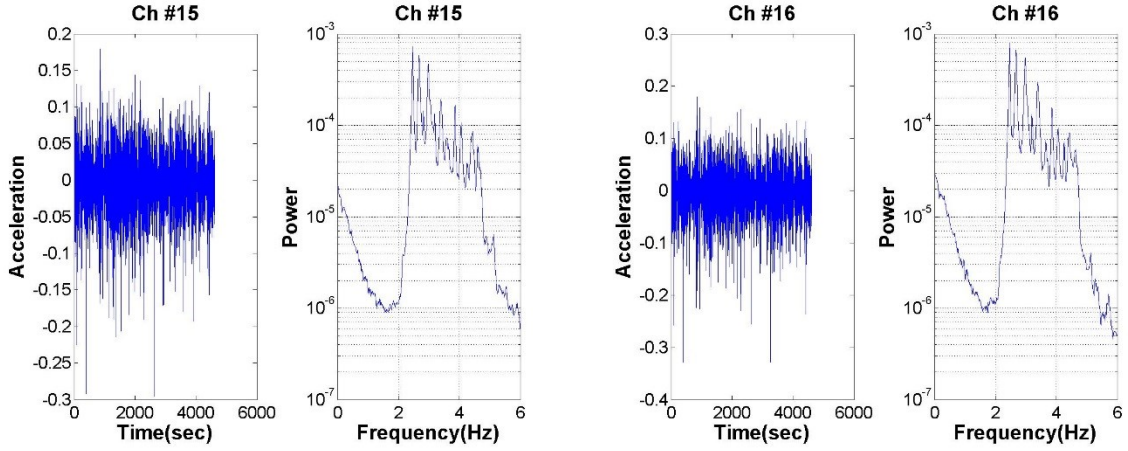
Ch #15
Acceleration
Time(sec)
Ch #15
Power
Frequency(Hz)
Ch #16
Acceleration
Time(sec)
Ch #16
Power
Frequency(Hz)

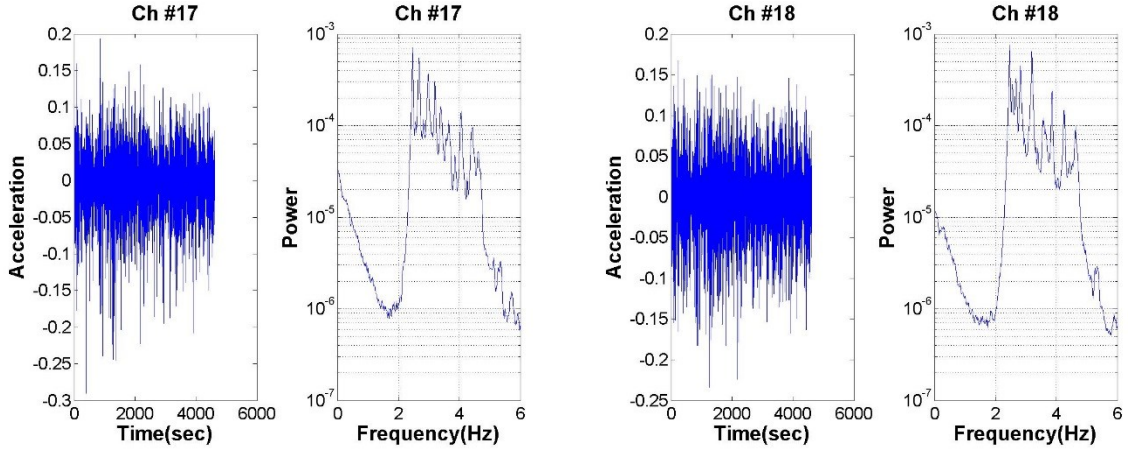
Ch #17
Acceleration
Time(sec)
Ch #17
Power
Frequency(Hz)
Ch #18
Acceleration
Time(sec)
Ch #18
Power
Frequency(Hz)

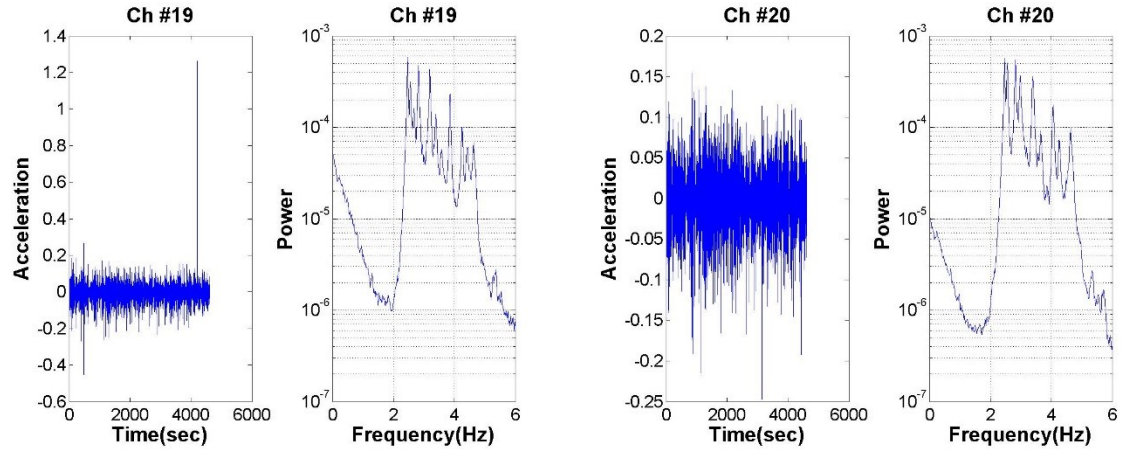
Ch #19
Acceleration
Time(sec)
Ch #19
Power
Frequency(Hz)
Ch #20
Acceleration
Time(sec)
Ch #20
Power
Frequency(Hz)

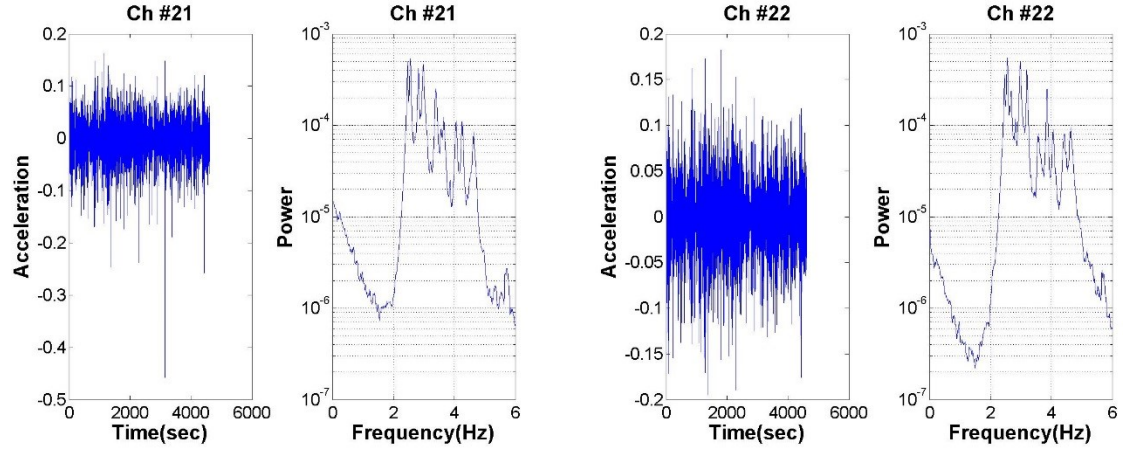
Ch #21
Acceleration
Time(sec)
Ch #21
Power
Frequency(Hz)
Ch #22
Acceleration
Time(sec)
Ch #22
Power
Frequency(Hz)

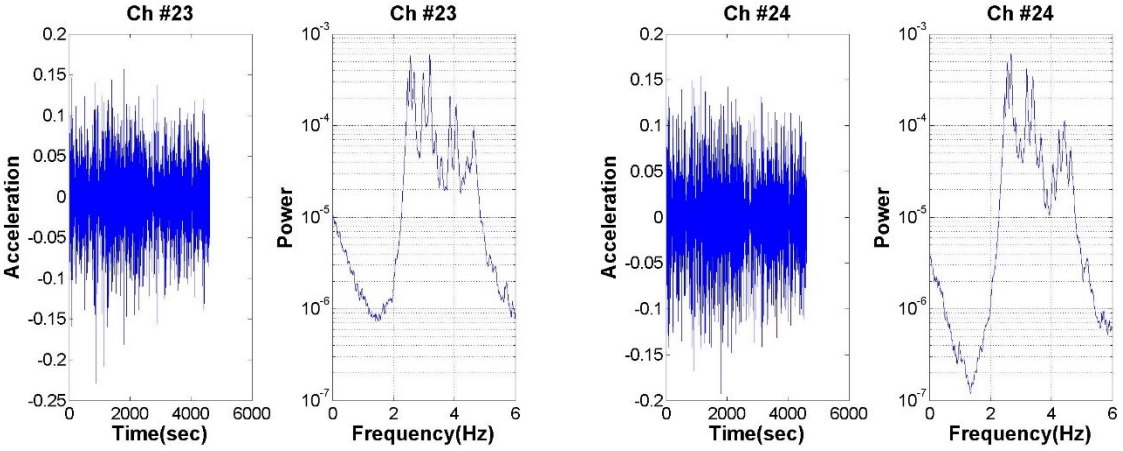
Ch #23
Acceleration
Time(sec)
Ch #23
Power
Frequency(Hz)
Ch #24
Acceleration
Time(sec)
Ch #24
Power
Frequency(Hz)

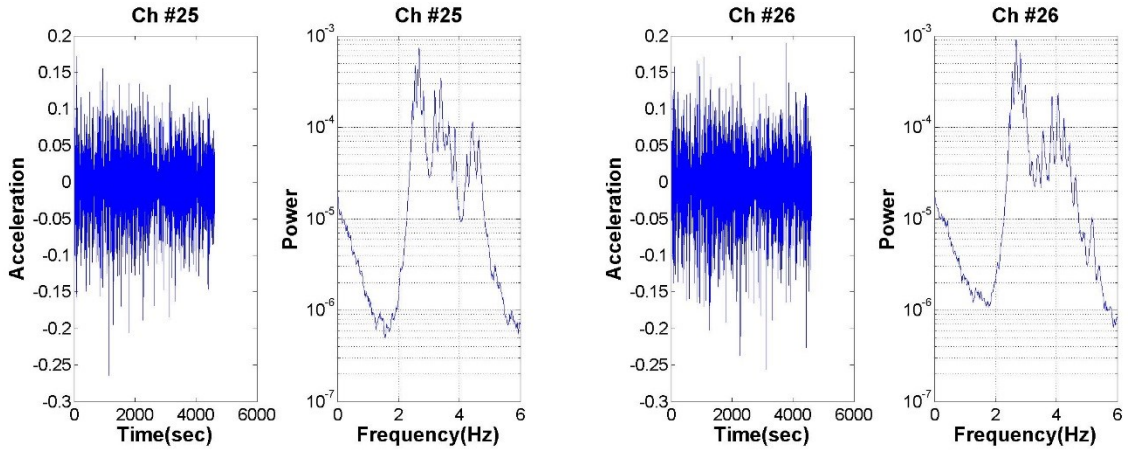
Ch #25
Acceleration
Time(sec)
Ch #25
Power
Frequency(Hz)
Ch #26
Acceleration
Time(sec)
Ch #26
Power
Frequency(Hz)

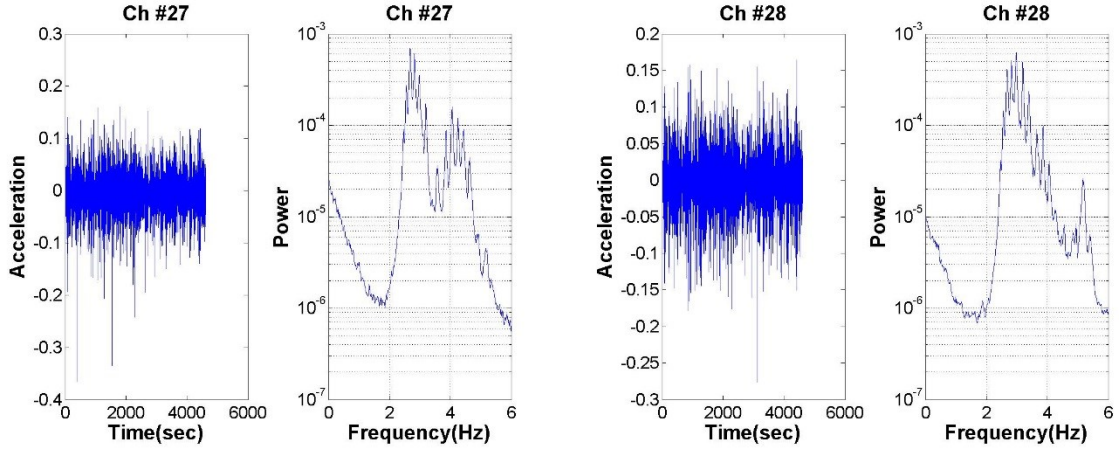
Ch #27
Acceleration
Time(sec)
Ch #27
Power
Frequency(Hz)
Ch #28
Acceleration
Time(sec)
Ch #28
Power
Frequency(Hz)

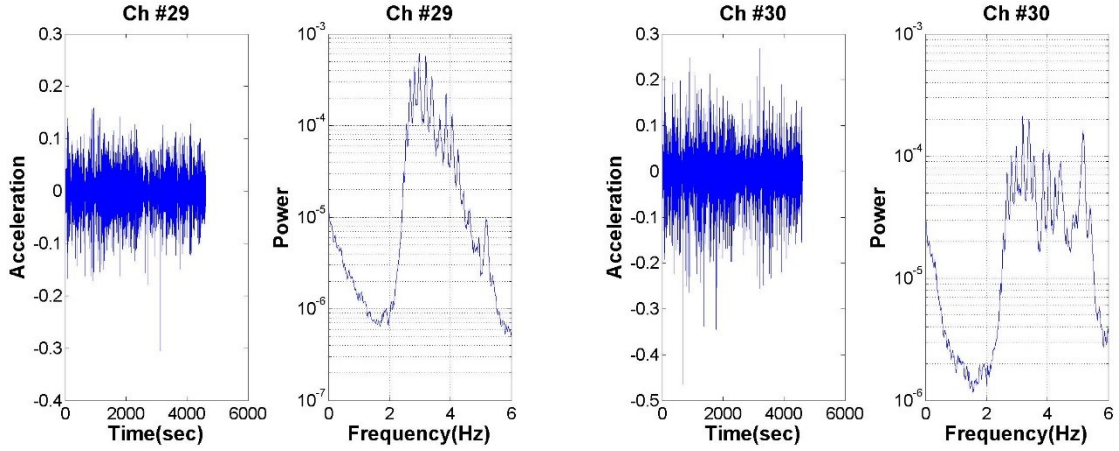
Ch #29
Acceleration
Time(sec)
Ch #29
Power
Frequency(Hz)
Ch #30
Acceleration
Time(sec)
Ch #30
Power
Frequency(Hz)

Appendix B: Acceleration response and PSD of STB bridge

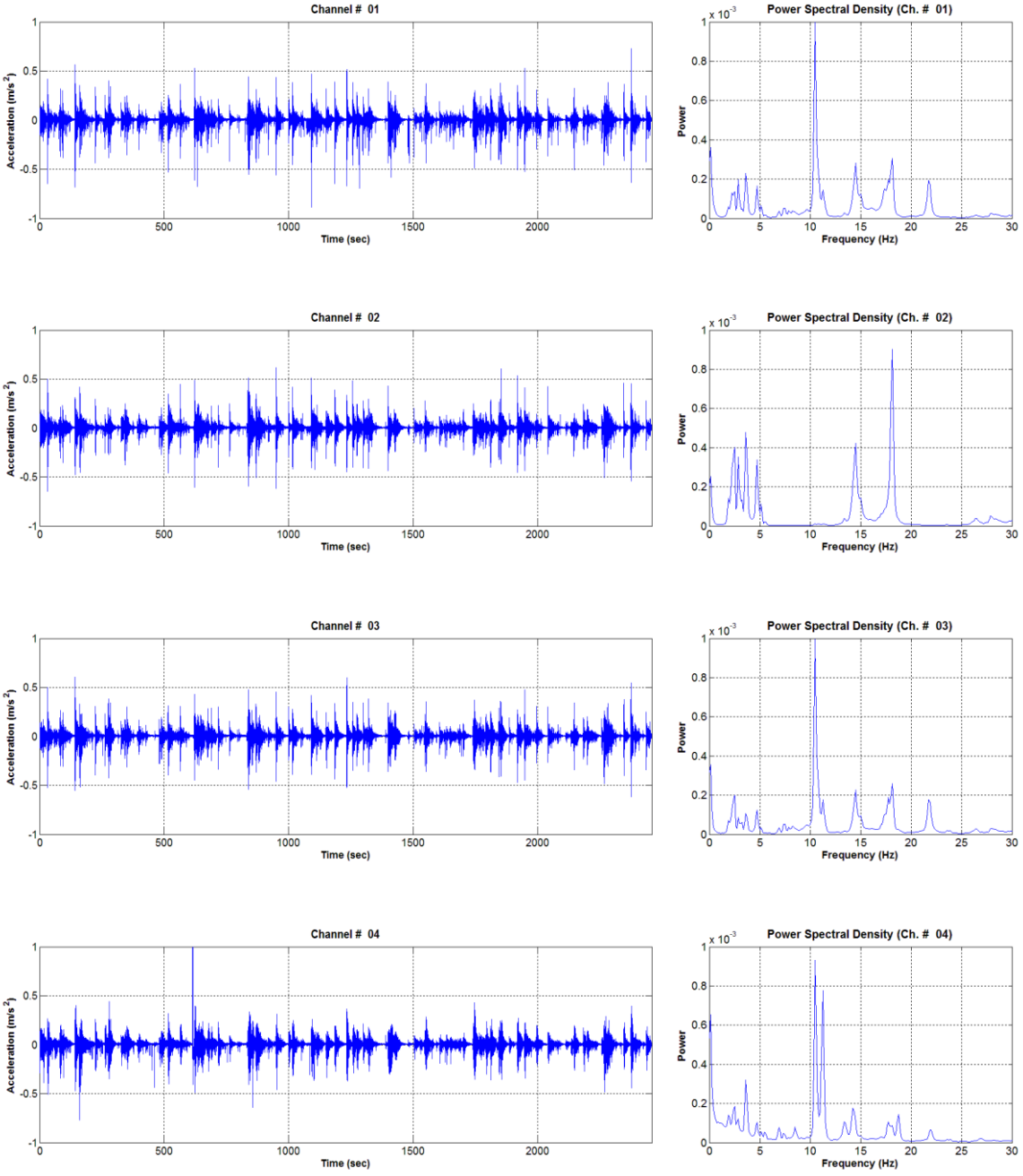

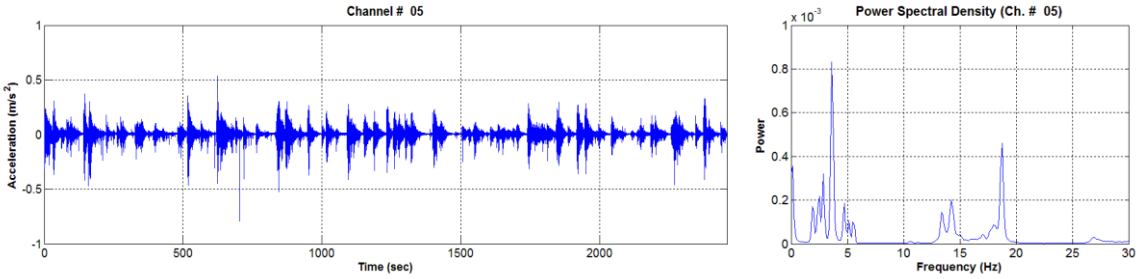
Channel # 05
Acceleration (m/s^2)
Time (sec)
Power Spectral Density (Ch. # 05)
x 10^{-3}
Power
Frequency (Hz)

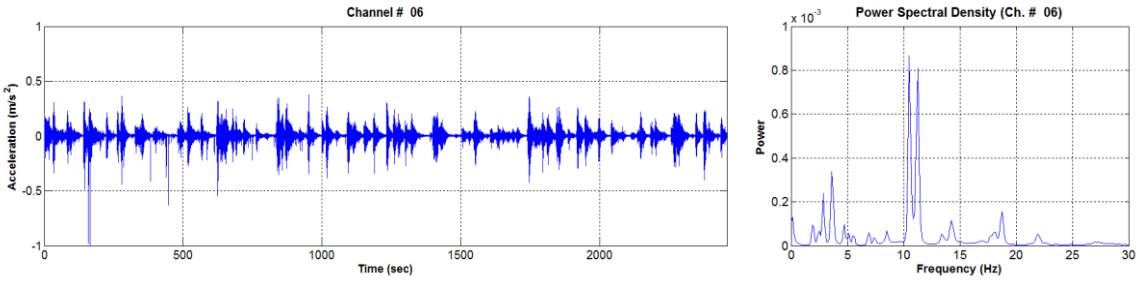
Channel # 06
Acceleration (m/s^2)
Time (sec)
Power Spectral Density (Ch. # 06)
x 10^{-3}
Power
Frequency (Hz)

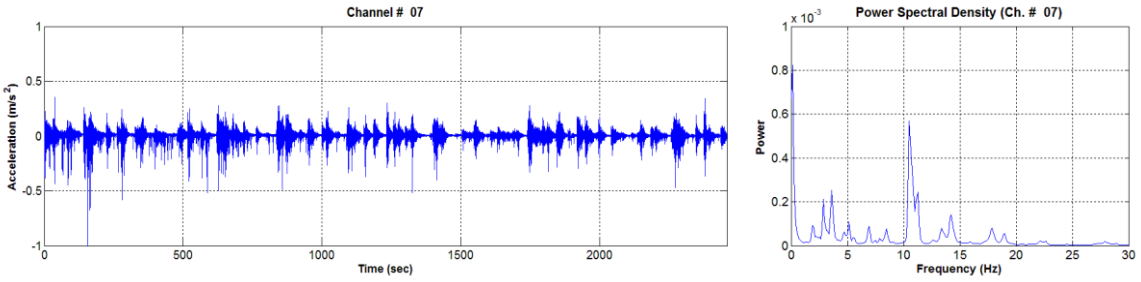
Channel # 07
Acceleration (m/s^2)
Time (sec)
Power Spectral Density (Ch. # 07)
x 10^{-3}
Power
Frequency (Hz)

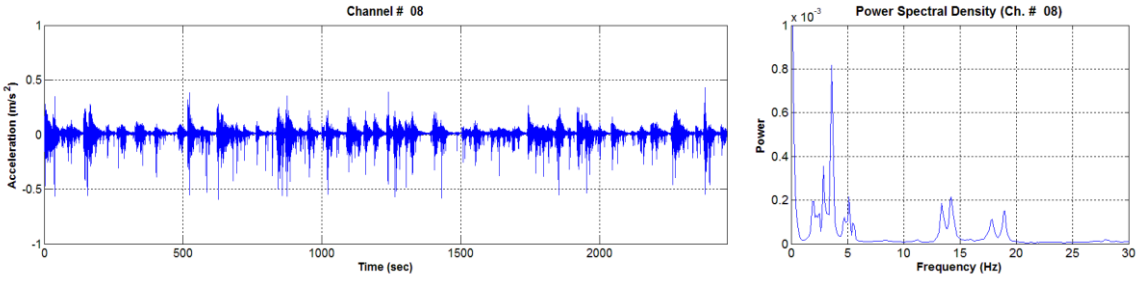
Channel # 08
Acceleration (m/s^2)
Time (sec)
Power Spectral Density (Ch. # 08)
x 10^{-3}
Power
Frequency (Hz)

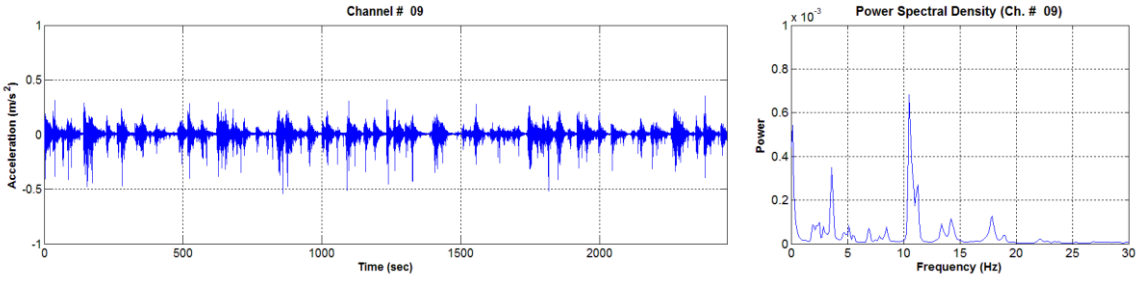
Channel # 09
Acceleration (m/s^2)
Time (sec)
Power Spectral Density (Ch. # 09)
x 10^{-3}
Power
Frequency (Hz)

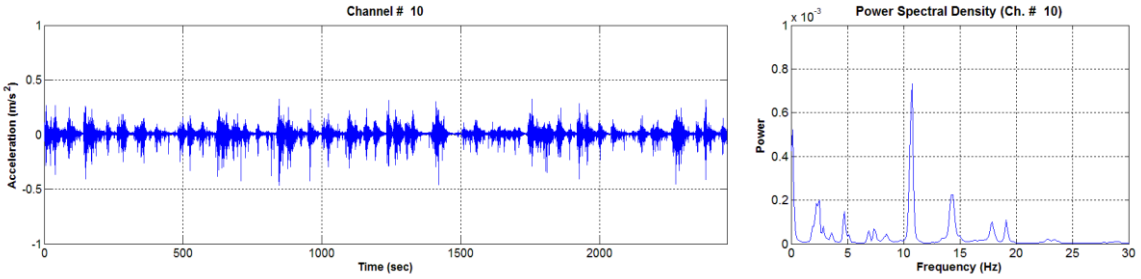
Channel # 10
Acceleration (m/s^2)
Time (sec)
Power Spectral Density (Ch. # 10)
x 10^{-3}
Power
Frequency (Hz)

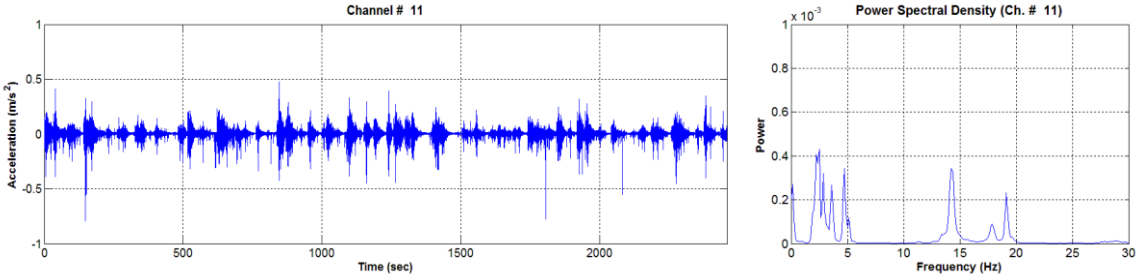
Channel # 11
Acceleration (m/s^2)
Time (sec)
Power Spectral Density (Ch. # 11)
x 10^{-3}
Power
Frequency (Hz)

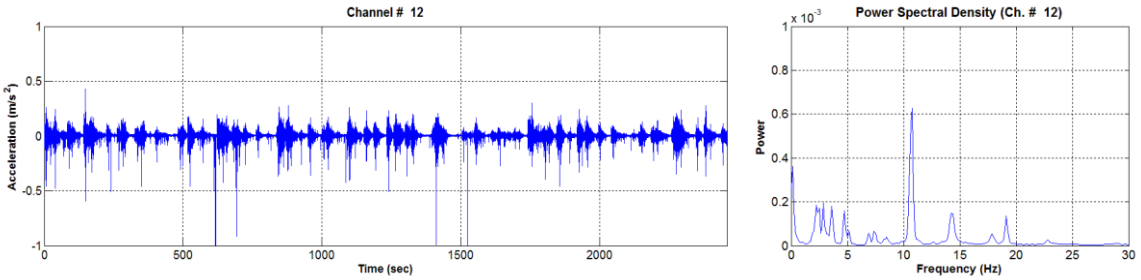
Channel # 12
Acceleration (m/s^2)
Time (sec)
Power Spectral Density (Ch. # 12)
x 10^{-3}
Power
Frequency (Hz)

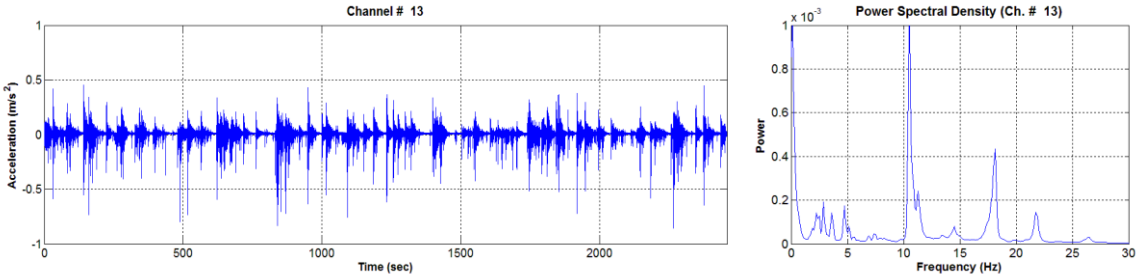
Channel # 13
Acceleration (m/s^2)
Time (sec)
Power Spectral Density (Ch. # 13)
x 10^{-3}
Power
Frequency (Hz)

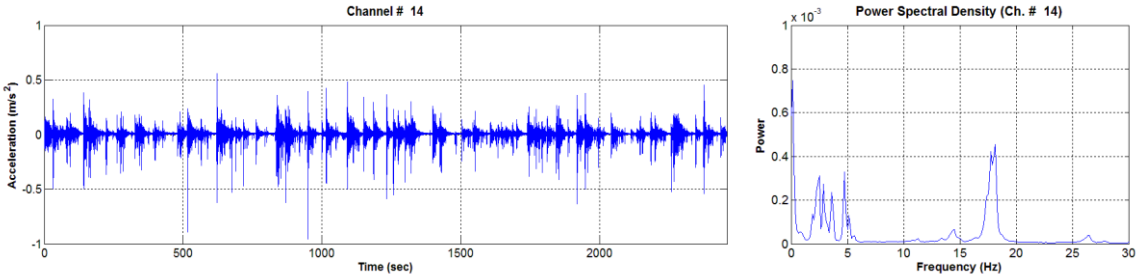
Channel # 14
Acceleration (m/s^2)
Time (sec)
Power Spectral Density (Ch. # 14)
x 10^{-3}
Power
Frequency (Hz)

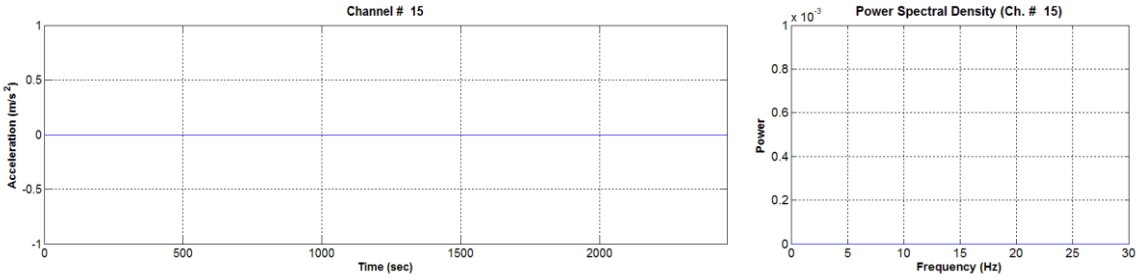

* Channel # 15 could not save data because of power off

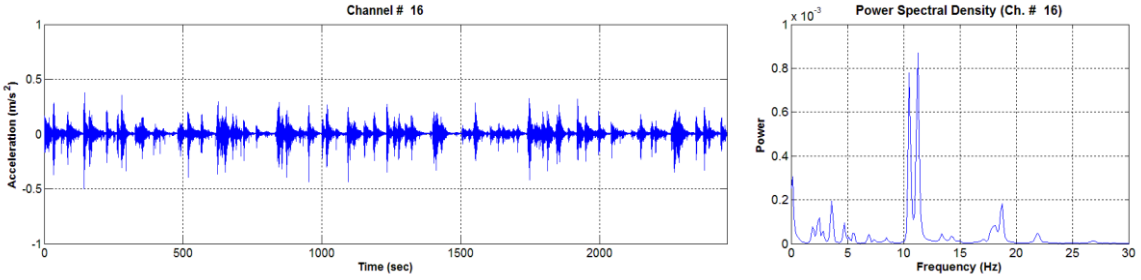

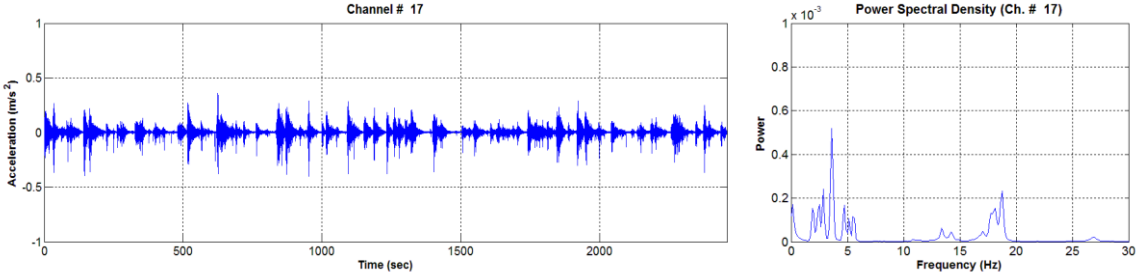

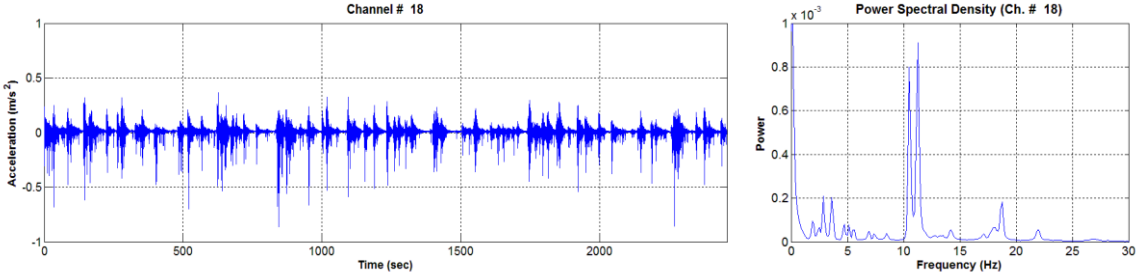

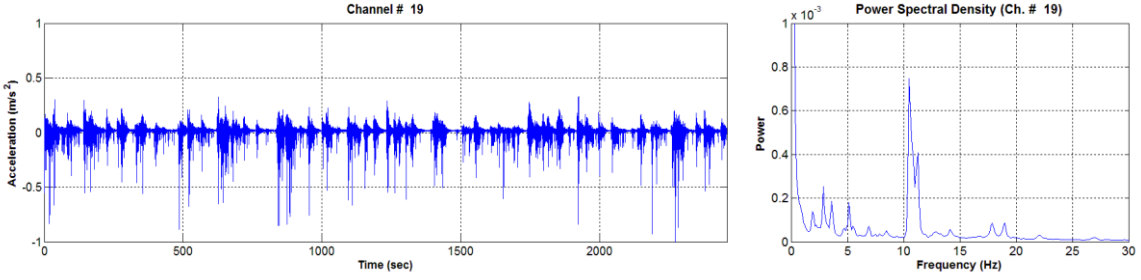

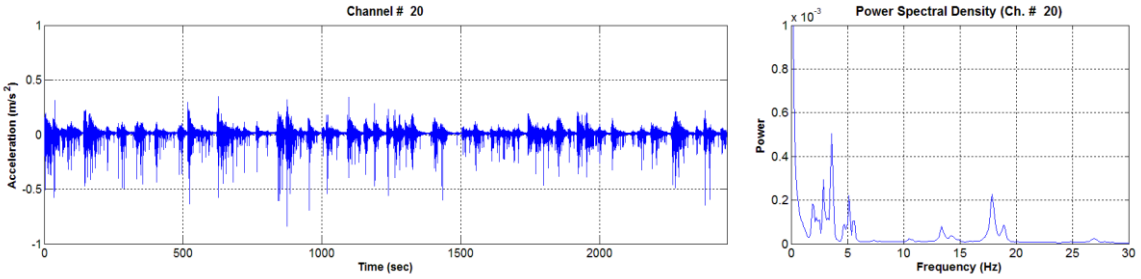
Channel # 20
Acceleration (m/s^2)
Time (sec)
Power Spectral Density (Ch. # 20)
x 10^{-3}
Power
Frequency (Hz)

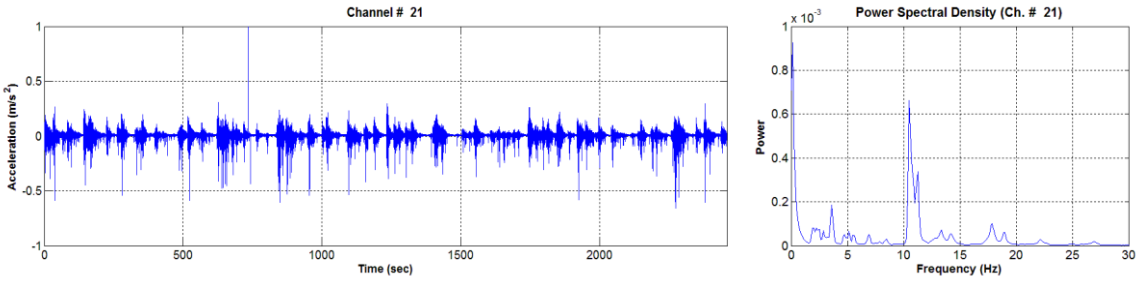
Channel # 21
Acceleration (m/s^2)
Time (sec)
Power Spectral Density (Ch. # 21)
x 10^{-3}
Power
Frequency (Hz)

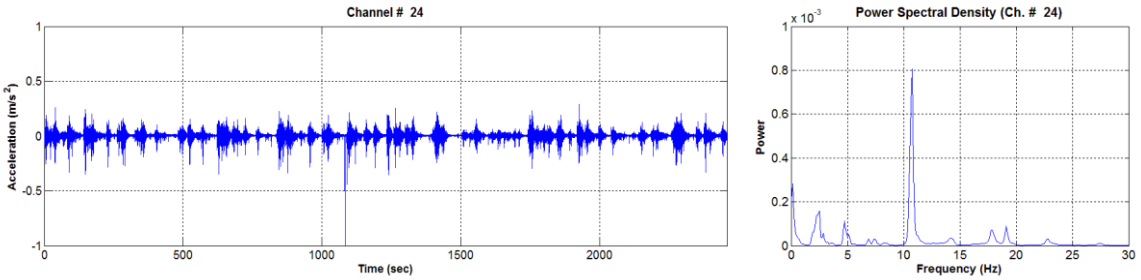
Channel # 24
Acceleration (m/s^2)
Time (sec)
Power Spectral Density (Ch. # 24)
x 10^{-3}
Power
Frequency (Hz)

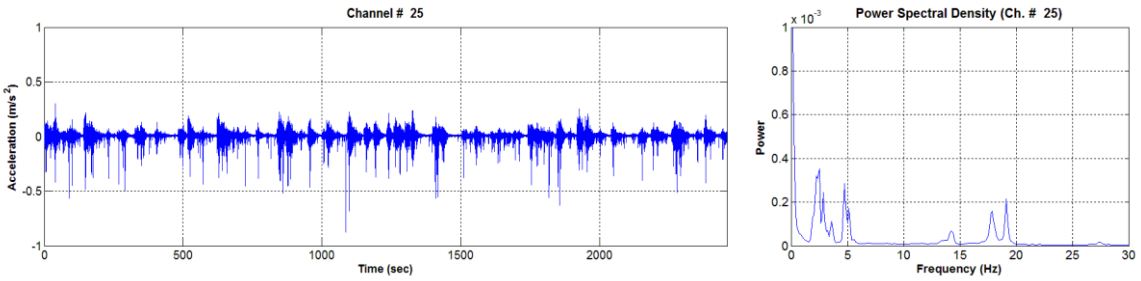
Channel # 25
Acceleration (m/s^2)
Time (sec)
Power Spectral Density (Ch. # 25)
x 10^{-3}
Power
Frequency (Hz)

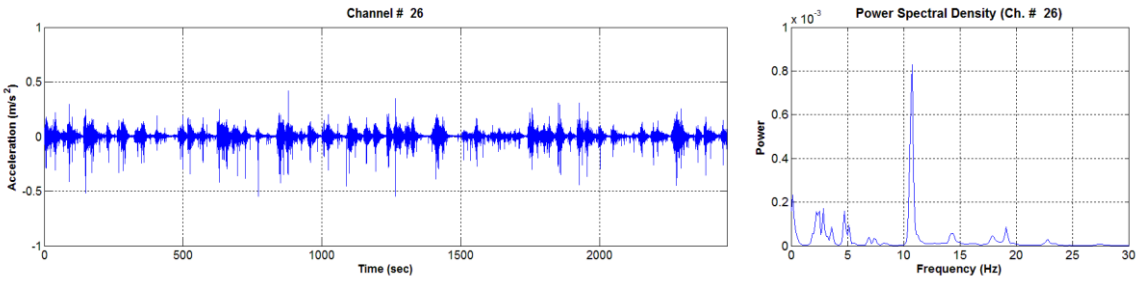
Channel # 26
Acceleration (m/s^2)
Time (sec)
Power Spectral Density (Ch. # 26)
x 10^{-3}
Power
Frequency (Hz)

Appendix C: Damage identification of PSCB bridge

C.1 Introduction

Most of literature deals with the application of theoretical damage identification or laboratory test. Applications on real structures such as bridges or buildings are very rare. So, the PSCB bridge used in chapter 5.2 is used again for comparing of various damage detection techniques through computer simulation studies because there was no damage by visual inspection Moreover, frequencies of the ambient test were higher than those of FEM model, this means that the current condition of the bridge is stronger than the design strength. The bridge is assumed that damage reduces the stiffness of element 166, 167 (span 4) and 566, 567 (span 12) by 20% and that of element 366, 367 (span 8) by 30%. Fig. C.1 shows the undamaged and damaged (20%, 30%) material properties by reducing modulus of elasticity. Computer simulation based on a FEM of the bridge provides both undamaged and damaged vibration characteristics.

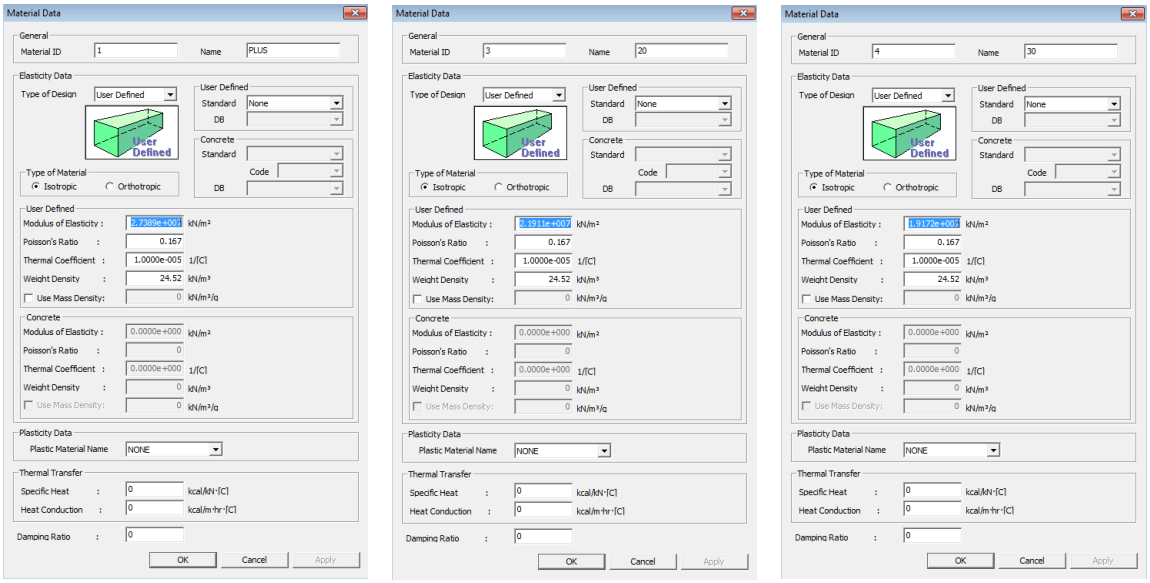

(a) Undamaged (b) Damaged (20%) (c) Damaged (30%)

Fig. C.1 Material properties for undamaged and damaged bridge

C.2 Methods based on frequency changes

Frequency changes come from structural property changes such as mass, stiffness and damping. Frequencies of this bridge would be decreased by the reduced stiffness. The bridge has been modeled with Midas Civil and applied damage to get the difference of frequencies. Table C.1 shows frequencies of undamaged and damaged bridge. It can be seen that all frequencies are reduced after damage, but the differences are very subtle and location of damage cannot be identified.

Table C.1 Frequencies of undamaged and damaged bridge

Mode no.	undamaged (Hz)	damaged (Hz)	Difference (%)
1st	2.275	2.268	0.32
2nd	2.342	2.337	0.22
3rd	2.448	2.441	0.27
4th	2.588	2.587	0.06
5th	2.757	2.752	0.21
6th	2.950	2.945	0.17

C.3 Methods based on mode shape changes

Damage reduces the stiffness of structures and it alters the mode shapes. Mode shape changes are good indicators as the damage identification and the location of the damage. The Modal Assurance Criterion (MAC) values were used to compare between two mode shapes (damaged and undamaged). A value close to 1 suggests that the two mode shapes are well correlated, while a value close to 0 indicates that the mode shapes are not correlated. However, mode shape changes are usually so small that detection of damage is impractical (Humar et al. 2006). Fig. C.2 and Table C.2 show MAC values between the undamaged and damaged mode shapes. In this study, damages were subtle, so mode shape method was not available because all MAC values were close to 1.

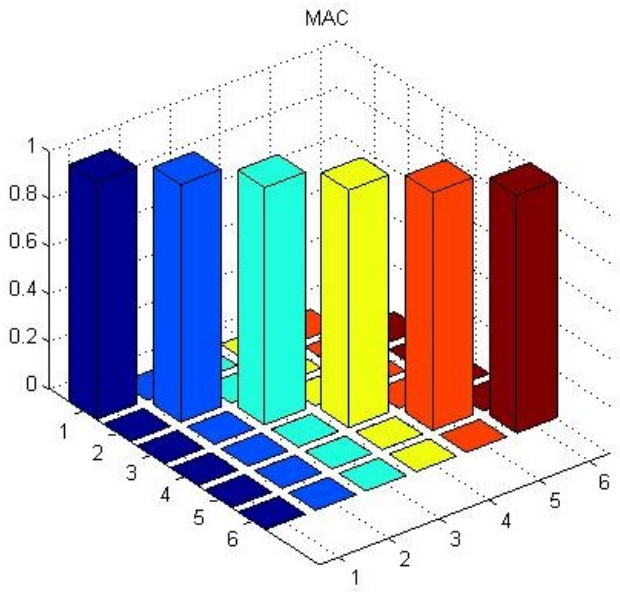

Fig. C.2 MAC values of the undamaged and damaged bridge

Table C.2 MAC values of the undamaged and damaged bridge

Mode no.	1st	2nd	3rd	4th	5th	6th
1st	0.99970	0.00007	0.00012	0.00000	0.00001	0.00002
2nd	0.00007	0.99982	0.00000	0.00000	0.00004	0.00004
3rd	0.00012	0.00000	0.99907	0.00042	0.00031	0.00004
4th	0.00000	0.00000	0.00044	0.99930	0.00024	0.00001
5th	0.00001	0.00004	0.00030	0.00026	0.99931	0.00001
6th	0.00002	0.00004	0.00004	0.00001	0.00001	0.99981

C.4 Mode shape curvature method

Instead of using methods based on mode shape changes to obtain spatial information, mode shape curvature method is an alternative method. This method is better than mode shape changes to detect damage for a beam type structure. The curvature values can be computed from the measured displacement mode shapes by using a central difference operator (Eq. (4.2)).

Fig. C.3 shows the mode shape curvature for mode 1 and 3 both before and after damage. It is evident that the modal curvature has significantly increased span 4, 8 and 12 (elements 166, 167, 366, 367, 566, 567), correctly indicating the damage at these areas.

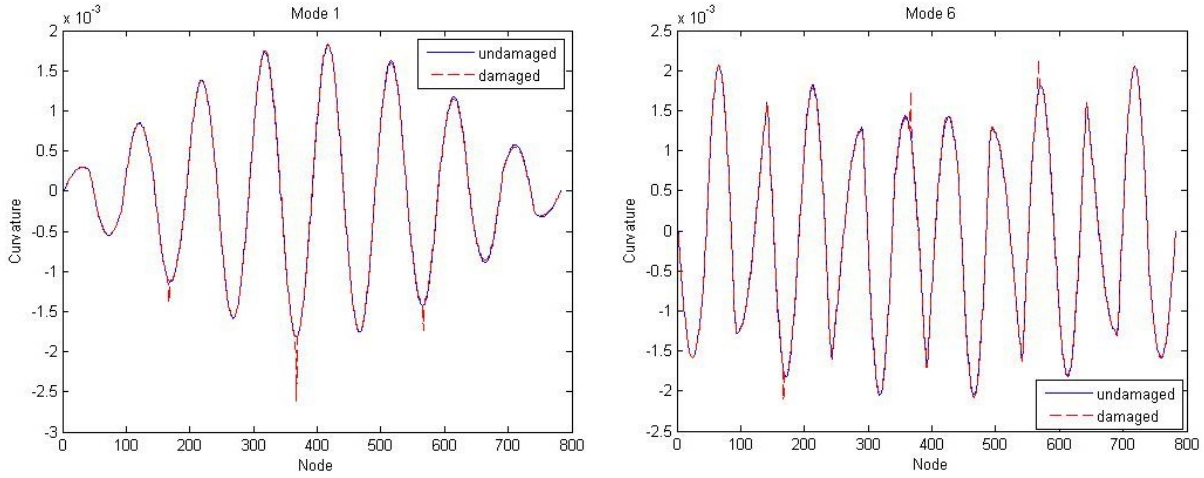

(a) Mode 1 (b) Mode 6

Fig. C.3 Modal curvatures of mode 1 and mode 3

C.5 Methods based on change in flexibility matrix

In this flexibility change method, damage is detected by comparing the flexibility matrix measured from the mode shapes of the damaged and undamaged structure. The flexibility matrix is the inverse matrix of the static stiffness matrix. Therefore, the flexibility matrix is relations between the applied static force and displacement. The measured flexibility matrix can be estimated from the mass-normalized measured mode shapes and frequencies. The flexibility matrix of the undamaged (F) and damaged (F_d) structure is obtained from Eq. (4.3) and (4.4). The difference between flexibility matrices of the damaged and undamaged structure is obtained from Eq. (4.5). Then, the largest absolute value(δ_j) in the row vector whose jth element is equal to the element with the largest absolute value in the jth column of ΔF is obtained from Eq. (4.6). The flexibility differences δ_j are plotted in Fig. C.4. It is apparent that span 4, 8 and 12 (elements 166, 167, 366, 367, 566, 567) have been affected by damage.

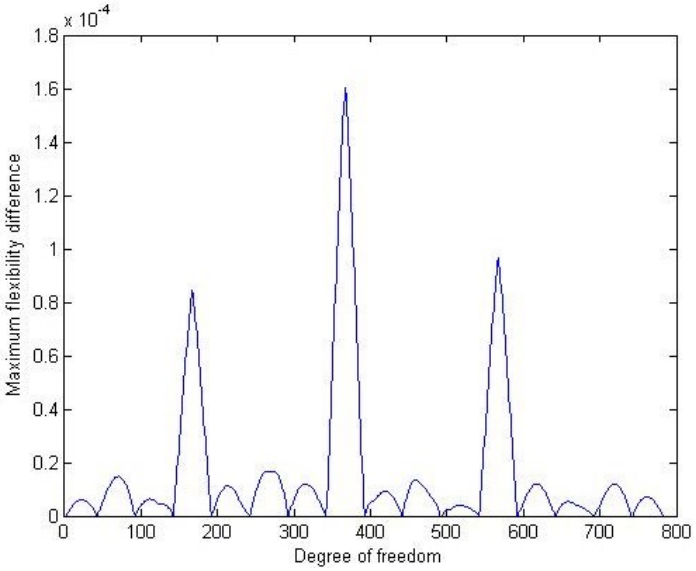

Fig. C.4 Maximum differences of flexibility matrices of damaged and undamaged bridge

C.6 Methods based on changes in uniform flexibility shape curvature

A displacement curvature shape can be obtained corresponding to each column of F and F_d. The difference of curvatures between damaged and undamaged can be obtained from Eq. (4.7). The uniform flexibility shape curvature differences obtained from the flexibility matrix are plotted in Fig. C.5 It is apparent that span 4, 8 and 12 (elements 166, 167, 366, 367, 566, 567) have been affected by the damage.

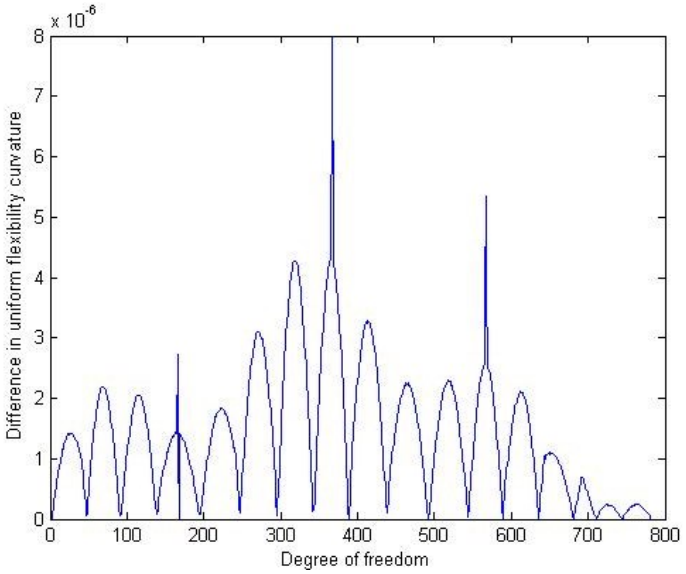

Fig. C.5 Differences in uniform flexibility curvatures of damaged and undamaged bridge

C.7 Damage index method

Damage index is defined as the change in strain energy of the structure when it is deformed. This modal strain energy of the undamaged and damaged structure can be derived from the curvature of the measured mode shapes (Eq. (4.8 ~ 4.10)). The damage index is obtained from Eq. (4.12) and elements with relatively large damage index are likely to be damaged. The damage index method is applied to detect damage for PSCB bridge. Six mode shapes are used for this method. Using Eq. (4.12), damage indices are obtained for the elements and are plotted in Fig. C.6. It is apparent from the plot that damage is expected in span 4, 8 and 12 (elements 166, 167, 366, 367, 566, 567).

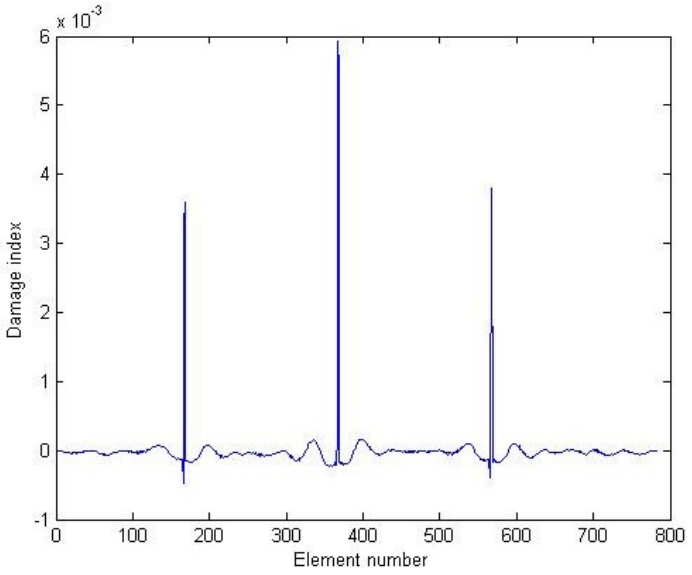

Fig. C.6 Damage indices of the PSCB bridge

C.8 Method based on modal residual vector

This method was performed with M-FEM (Bagchi et al. 2007). The changed stiffness by damage can be obtained by Eq. (4.20). The changed stiffness can be expressed as the weighted sum of the damaged elements' stiffness matrices. This weighting factors show the severity of damage. The stiffness reduction of element is expressed by Eq. (4.21) and the summation is carried out over the all damaged elements. Then the modal residual vector can be expressed by Eq. (4.22). The

calculated modal residuals are shown in Fig. C.7. The predominant values correctly identify the damage in in span 4, 8 and 12 (elements 166, 167, 366, 367, 566, 567).

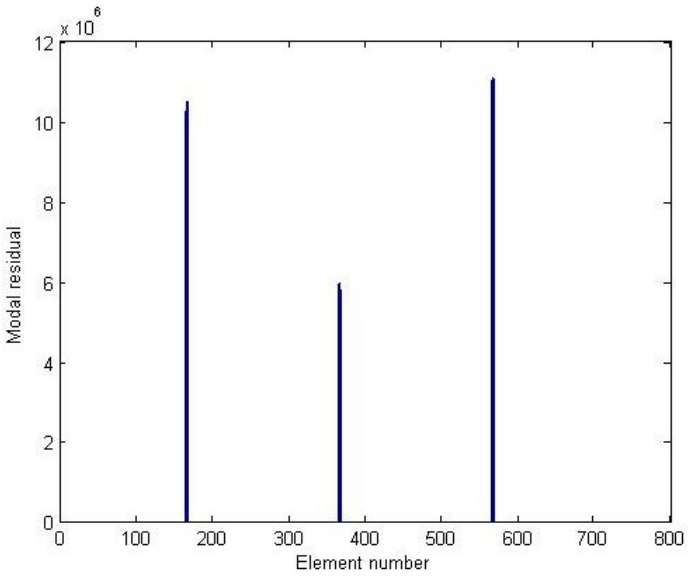

Fig. C.7 Modal residuals from six-mode of the PSCB bridge

C.9 Matrix update method

For this method, M-FEM program was used again. An analytical model of the PSC Box was modelled using beam elements as Fig. C.8. Fig. C.9 shows the results by matrix update methods. Fig. C.9 (a) and (b) correspond to matrix update method using the pseudo-inverse and optimized methods respectively. Both methods show proper damage locations properly. It shows that damage factor of element elements 166, 167, 366, 367, 566 and 567 are high and this indicates these elements are damaged.

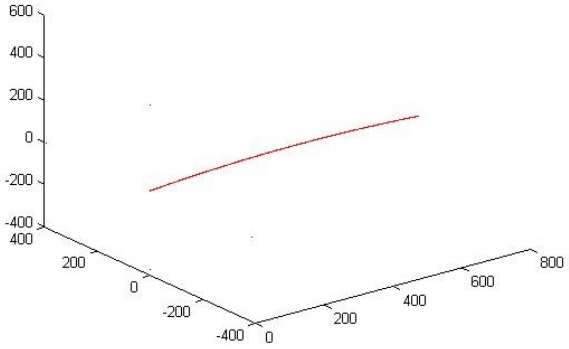

Fig. C.8 FE model for M-FEM

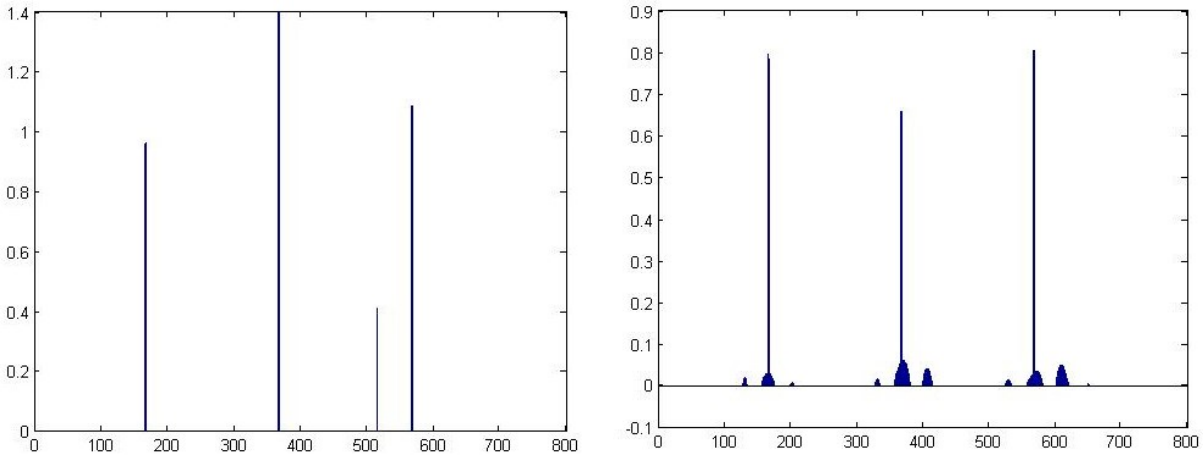

(a) Pseudo Inverse (b) Optimized

Fig. C.9 Damage factors of the PSCB bridge

C.10 Genetic algorithm method

Genetic Algorithm (GA) is a population-based, probabilistic technique such as natural selection and evolution by mimicking the nature. For genetic algorithm method, undamaged frequencies and mode vectors are considered as objective value. Damaged frequencies and mode vectors are set as initial values. Fig. C.10 shows the results of GA method. The stiffness of damaged elements has changed 1.32 and 1.31 for 20 % and 30 % damaged elements respectively and other elements show subtle changes (0.99 and 1.03). This indicates that elements of changed value are damaged.

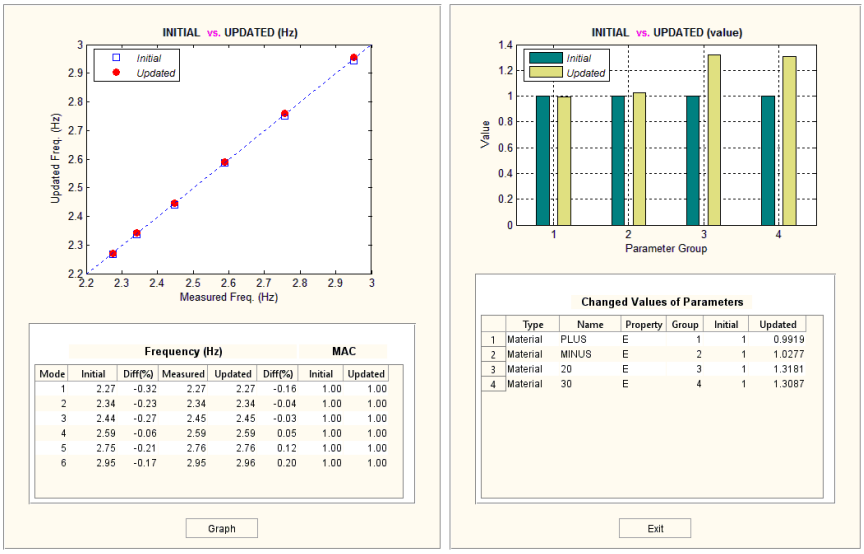

Fig. C.10 Genetic algorithm results and changed values

C.11 Conclusion

All of VBDI methods used in this study were possibly predict damage exist and location of the damage. However, the damage was simulated for this study so, there would be differences in real and simulated structures. These gaps could be reduced by many measurement points and measuring higher modes. Table C.3 shows summaries of VBDI techniques used in this study.

Table C.3 Comparison of VBDI techniques

Method	Severity	Location	Detection
Frequency change	X	X	▲
Mode shape change	X	X	X
Mode curvature	X	O	O
Flexibility matrix	X	O	O
Flexibility curvature	X	O	O
Damage index	▲	O	O
Modal residual	▲	O	O
Matrix update	O	O	O
Genetic algorithm	O	O	O

Appendix D: Case study of model updating techniques

D.1 Introduction

As it is mentioned in chapter 5.2.4 and 5.3.4, there are differences between the ambient test results and the FEM analysis results. These differences might be caused by the differences of design strength and current strength of the structures. However, these differences can be removed by model updating method such as matrix update method and genetic algorithm method. The purpose of model updating is to modify the mass, stiffness and damping parameters of the numerical model in order to obtain better agreement between numerical results and test data (Mottershead and Friswell, 1993). Updated models can then be used to predict operational displacements and stresses due to simulated loads, or to identify damage based on the operational response of the structure (Bagchi, 2005). Three types of bridge were considered to perform model updating techniques: PSCB bridge and Voided slab bridge. The PSCB bridge is the same bridge used in this thesis.

D.2 PSCB bridge

The PSCB bridge used in chapter 5.2 was employed again for the model updating technique. So, the test results and modal identification results were same. In this study, the SSI method was used as modal identification results.

D.2.1 Matrix model update method

The PSCB Bridge was modeled with the M-FEM program (Bagchi et al. 2007) that is a MATLAB-based finite element system for structural model updating and vibration-based damage identification. The bridge has only bending modes because the bridge is relatively long and the section is slander. So the bridge was modeled beam elements. The model comprises a total of 782 frame elements and 1565 nodes (additional 782 nodes were used to define the plane because the

bridge is curved, each beam elements need its additional node). Fig. D.1 shows the M-FEM model for model updating.

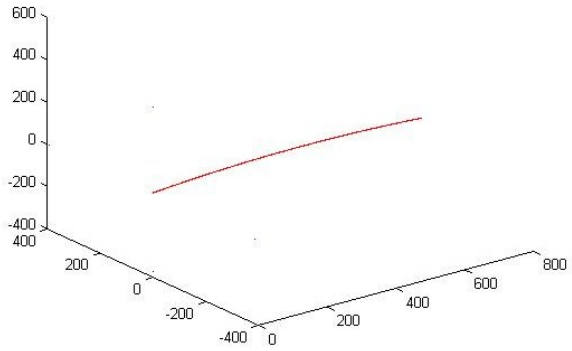

Fig. D.1 M-FEM model for model updating

As seen in Table D.1, the analysis model showed the differences of 5.55% in the first mode and 2.92% in the sixth mode. In spite of these differences, the overall calculation of the natural frequencies and mode shapes could be said to be consistent in both approaches by considering the sequences and level of differences in lower modes.

Table D.1 Comparison of initial models and test

Mode no	SSI (Hz)	Initial M-FEM (Hz)	Difference (%)
1st	2.46	2.33	5.55
2nd	2.56	2.41	5.93
3rd	2.68	2.53	5.70
4th	2.83	2.69	5.11
5th	2.99	2.88	3.77
6th	3.19	3.10	2.92

Fig. D.2 and Table D.2 show the updated results. The natural frequencies of the updated FE model become closer to the measured natural frequencies than those of the initial FE model. Table

D.2 includes natural frequencies from updated model and corresponding error rate to the test result. The bound for correlation is 0.8 to 1.2 and tolerance is 0.1%. Maximum number of iteration is 100 times but it ended its iteration after 12 times because it reached the tolerance. In this case, most elements' stiffness was increased.

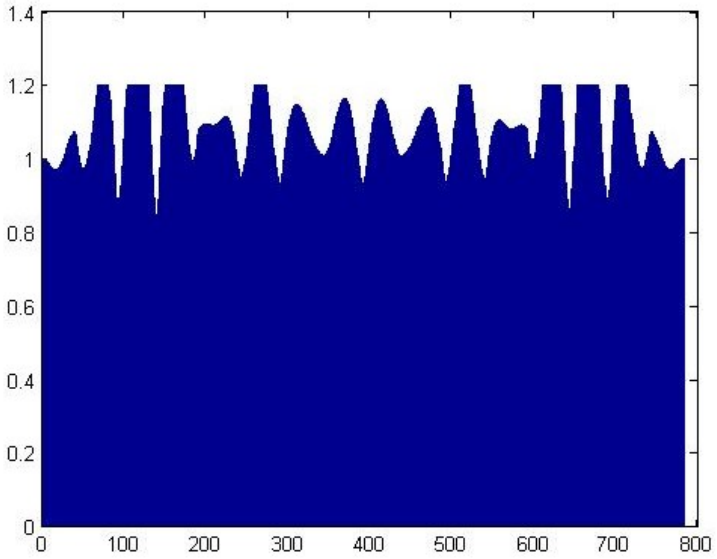

Fig. D.2 Changes of the stiffness

Table D.2 Comparison of updated models and test

Mode no	SSI (Hz)	Updated M-FEM (Hz)	Difference (%)
1st	2.46	2.46	-0.04
2nd	2.56	2.56	-0.07
3rd	2.68	2.68	-0.07
4th	2.83	2.83	-0.07
5th	2.99	2.99	-0.03
6th	3.19	3.19	-0.03

D 2.2 Genetic algorithm method

The target bridge is modeled using Midas Civil like chapter 5.2.4 based on drawings and the model comprises a total of 782 frame elements. As seen in Table D.3, the analysis model showed the differences of 7.72% in the first mode and 7.52% in the sixth mode. In spite of these differences, the overall calculation of the natural frequencies and mode shapes can be said to be consistent in both approaches by considering the sequences and level of differences in lower modes. In addition, the natural frequency responses from analytical model were relatively lower than those from measured results. It demonstrates that the flexural stiffness increased in current state condition compared to As-Built condition.

Table D.3 Comparison of initial models and test

Mode no	SSI (Hz)	Initial Midas (Hz)	Difference (%)
1st	2.46	2.27	7.72
2nd	2.56	2.34	8.59
3rd	2.68	2.45	8.58
4th	2.83	2.59	8.48
5th	2.99	2.76	7.69
6th	3.19	2.95	7.52

Careful selection of design variables is important since the number of unknown parameters is very large in real cases. A grouping scheme was utilized in this project to reduce the number of design variables. Two update variables were selected; Flexural stiffness of positive area girder and negative area girder. Fig. D3 and Table D.4 show the updated results. The natural frequencies of the updated FE model become closer to the measured natural frequencies than those of the initial FE model. Table D.4 includes natural frequencies from updated model and corresponding error rate to the test result.

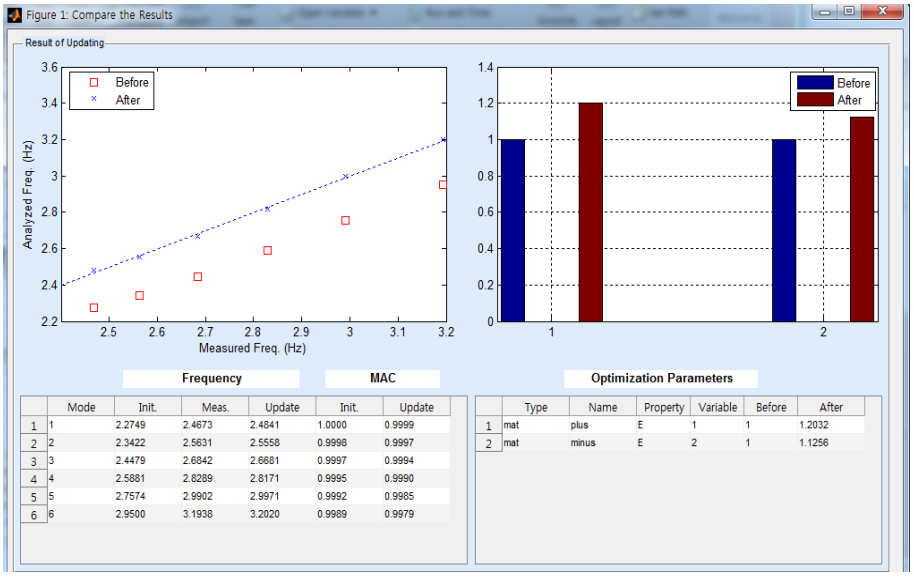

Fig. D.3 Results of genetic update method

Table D.4 Comparison of updated models and test

Mode no	SSI (Hz)	Updated Midas (Hz)	Difference (%)
1st	2.47	2.48	0.80
2nd	2.56	2.56	-0.28
3rd	2.68	2.67	-0.60
4th	2.83	2.82	-0.42
5th	2.99	3.00	0.23
6th	3.19	3.20	0.26

D.3 Voided slab bridge

The voided slab bridge is a three-span bridge and the total length is 65 m (20 m + 25 m + 20 m). Fig. D.4 shows this bridge.

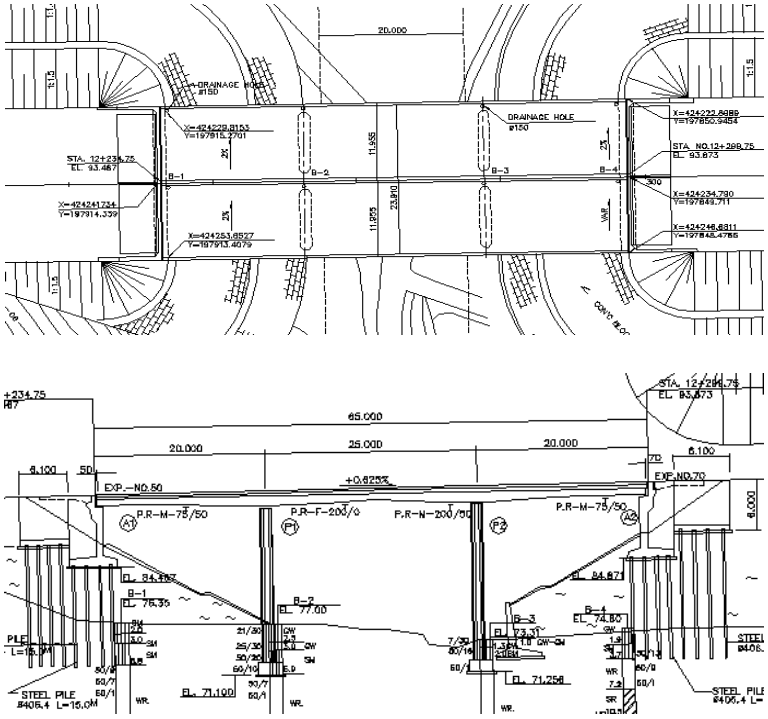

(a) General elevation plan

(b) Side view of the bridge

Fig. D.4 General elevation and image of Voided slab bridge

D.3.1 Ambient vibration test and modal identification

To measure the ambient vibration of the bridge, 18 wireless accelerometers were spaced along the full-length of the bridge for the duration of 90 minutes with sampling rates of 128 Hz in order to collect sufficient vibration data for modal parameter extraction. Fig. D.5 shows the wireless accelerometer and Fig. D.6 plots the some measured acceleration signals and corresponding Power Spectrum Density (PSD).

Fig. D.5 Wireless accelerometer for ambient vibration test

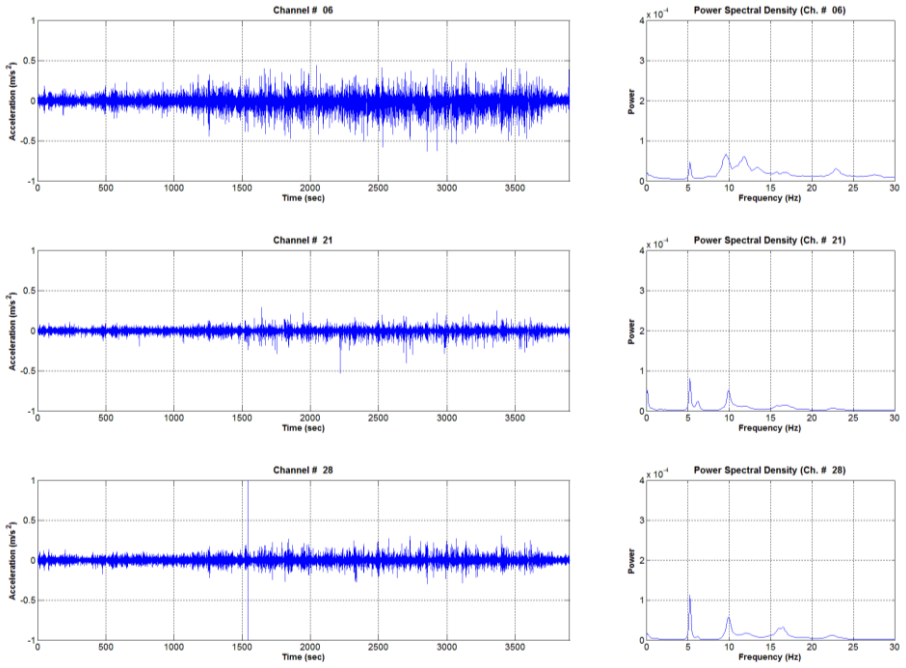

Fig. D.6 Measured acceleration data and corresponding PSD

The SSI modal identification method was carried out using the 18 acceleration. Fig. D.7 shows the stabilization chart obtained by the SSI analysis and indicates the location of natural modes. Three of the main low frequency modes were extracted and Fig. D.8 shows the identified operational mode shapes with their corresponding natural frequencies.

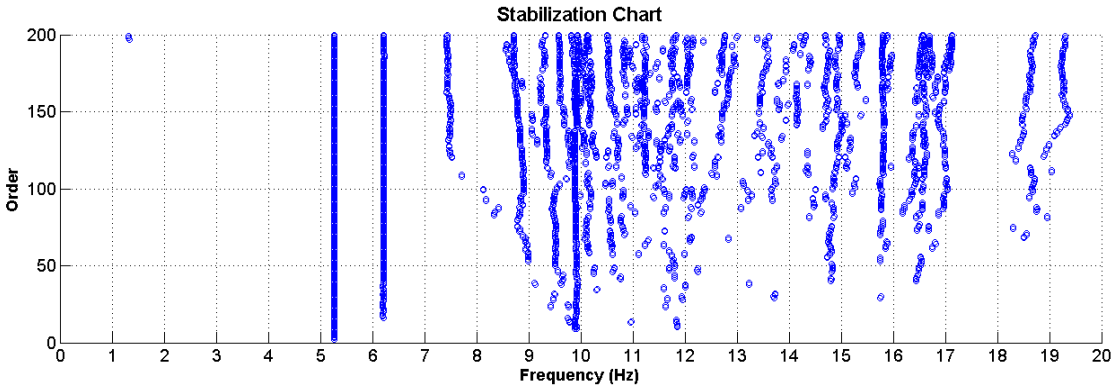

Fig. D.7 Stabilization chart obtained by SSI method

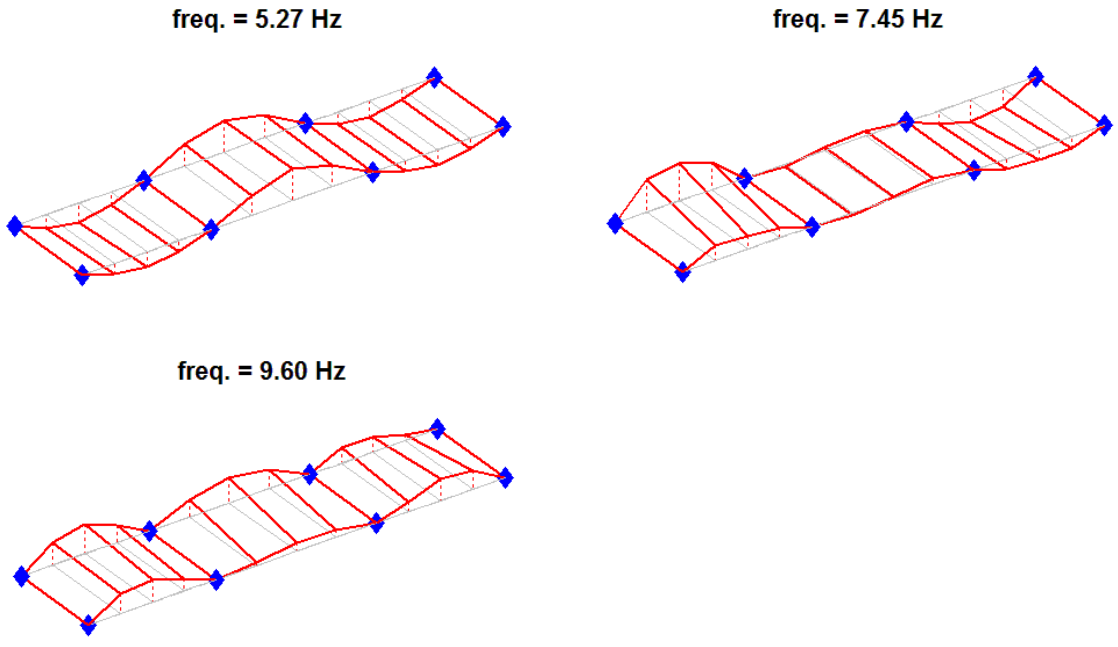

Fig. D.8 Identified modal properties from vibration test

D.3.2 Matrix model update method

The voided slab bridge is modeled using M-FEM. The model comprises a total of 2461 frame elements and 1358 nodes. The voided slab bridge was modeled as grillage mesh. Fig. D.9 shows the typical voided slab section. The transverse second moment of area, Bakht et al. (1981) recommend the method of Elliott (Eq. D.1) which gives this quantity in terms of the depth of the slab (d) and the diameter of the voids (d_v). For the torsional stiffness of voided slabs per unit depth, they recommend using the method of Ward and Cassell as Table D.5 (Eugene. 1999).). Fig. D.10 shows the M-FEM model for model updating.

$$i_y^{v-slab} = \frac{d^3}{12}\left[1 - 0.95\left(\frac{d_v}{d}\right)^4\right] \tag{D.1}$$

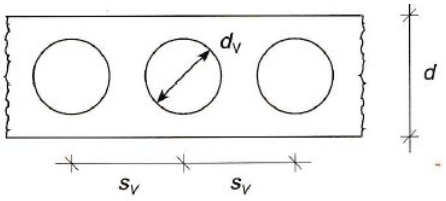

Fig. D.9 Cross-section through segment of voided slab bridge

Table D.5 Ratio of torsional stiffness of voided slab to that of solid slab

		$\frac{d_v}{s_v}$				
		0.9	0.8	0.7	0.6	0.5
$\frac{d_v}{d}$	0.90	0.45	0.48	0.51	0.56	0.62
	0.85	0.55	0.58	0.61	0.64	0.69
	0.80	0.64	0.66	0.68	0.71	0.75
	0.75	0.70	0.72	0.74	0.77	0.80
	0.70	0.76	0.78	0.79	0.82	0.84
	0.65	0.81	0.82	0.84	0.86	0.88
	0.60	0.85	0.86	0.87	0.89	0.90

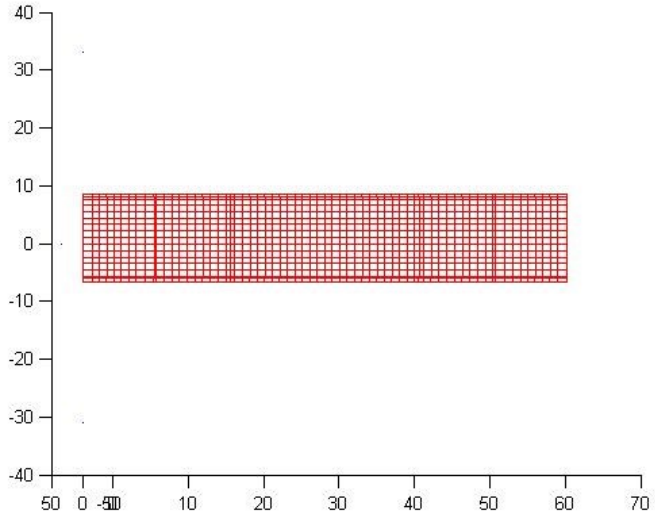

Fig. D.10 M-FEM model for model updating

As seen in Table D.6, the analysis model shows the differences of 11.80% in the first mode and 0.21% in the third mode. In spite of these differences, the overall calculation of the natural frequencies and mode shapes can be said to be consistent in both approaches by considering the sequences and level of differences in lower modes.

Table D.6 Comparison of initial models in terms and test

Mode no	SSI (Hz)	Initial M-FEM (Hz)	Difference (%)
1st	5.27	4.65	-11.80
2nd	7.45	7.38	-0.90
3rd	9.60	9.62	0.21

Fig. D.11 and Table D.7 show the updated results. The natural frequencies of the updated FE model become closer to the measured natural frequencies than those of the initial FE model. Table D.7 includes natural frequencies from updated model and corresponding error rate to the test result. The bound for correlation is 0.6 to 1.4 and tolerance is 0.1%. Maximum number of iteration is

2461 times and it ended its iteration after 2461 times because it didn't reach the tolerance. In this case, longitudinal grillage elements' stiffness was increased

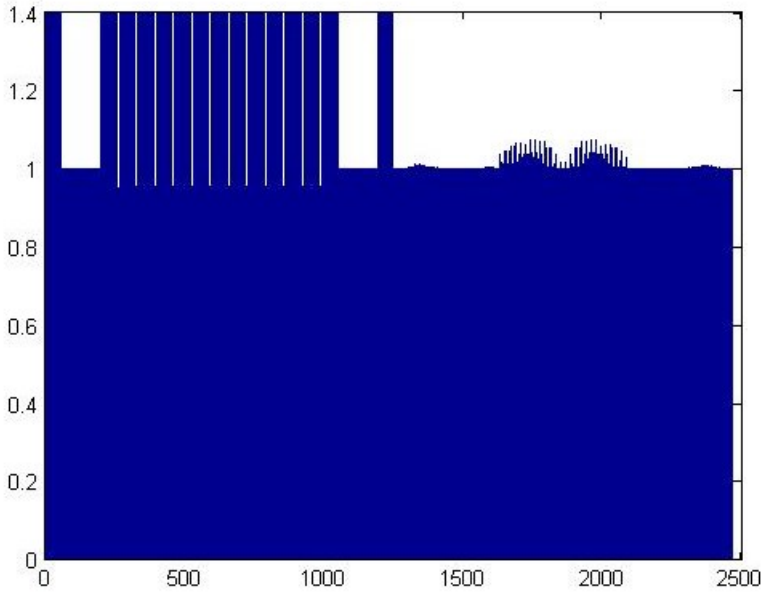

Fig. D11 Changes of the stiffness

Table D.7 Comparison of updated models and test

Mode no	SSI (Hz)	Updated M-FEM (Hz)	Difference (%)
1st	5.27	5.26	-0.15
2nd	7.45	7.45	-0.03
3rd	9.60	9.59	-0.06

D.3.3 Genetic algorithm method

The target bridge is modeled using Midas Civil based on drawings as shown in Fig. D.12. The voided slab bridge is modeled using frame elements. The model comprises a total of 2461 frame elements.

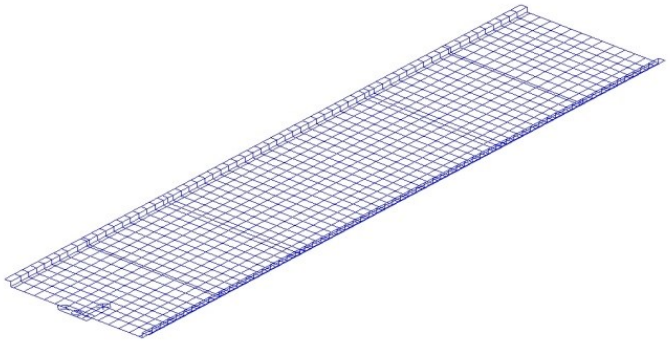

Fig. D.12 FE Model for genetic algorithm method

As seen in Table D.8, the analysis model shows the differences of 12.85% in the first mode and 3.55% in the third mode. In spite of these differences, the overall calculation of the natural frequencies and mode shapes can be said to be consistent in both approaches by considering the sequences and level of differences in lower modes. In addition, the natural frequency responses from analytical model were relatively lower than those from measured results. It demonstrates that the flexural stiffness increased in current state condition compared to As-Built condition.

Table D.8 Comparison of initial models and test

Mode no	SSI (Hz)	Initial Midas (Hz)	Difference (%)
1st	5.27	4.59	-12.85
2nd	7.45	7.21	-3.18
3rd	9.60	9.26	-3.55

A grouping scheme was utilized in this study to reduce the number of design variables. Eight update variables are selected; Flexural stiffness of positive area longitudinal and transverse section, flexural stiffness of negative area longitudinal and transverse section, flexural longitudinal and transverse cantilever section, etc.

Figure D.13 and Table D.9 show the updated results. The natural frequencies of the updated FE model become closer to the measured natural frequencies than those of the initial FE model. Table 8 includes natural frequencies from updated model and corresponding error rate to the test result.

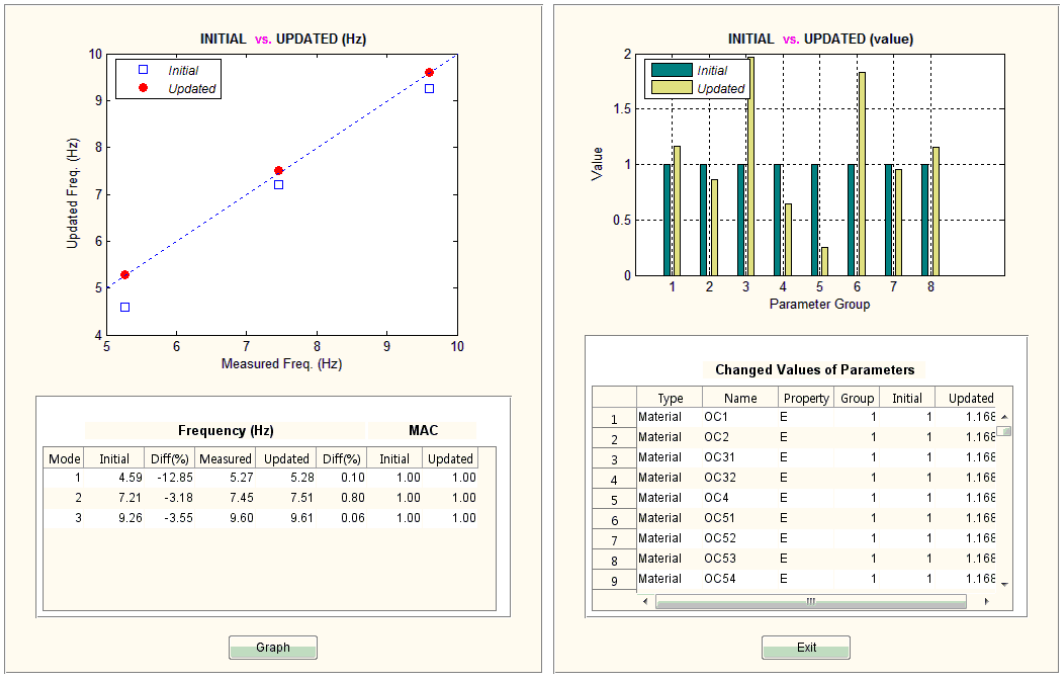

Fig D.13 Results of genetic update method

Table D.9 Comparison of updated models and test

Mode no	SSI (Hz)	Updated Midas (Hz)	Difference (%)
1st	5.27	5.28	0.10
2nd	7.45	7.51	0.80
3rd	9.60	9.61	0.06

D.4 Conclusion

D.4.1 PSCB bridge

Table D.10 shows that the difference between matrix update and genetic algorithm method. In this table we can see that matrix update method is more precise than genetic algorithm method in both of initial and updated results. Moreover, matrix update method ended with 12 iterations because it reached its tolerance value (0.1%). In the other hand, genetic algorithm ended after 1200 iterations (80 populations × 15 generations) as the user defined. However, in case of matrix update method, stiffness of 144 elements changed from 1.0 to 1.2 (upper boundary) (70~82, 105~130, 151~172, 261~273, 510~518, 611~632, 653~678, 701~713). It means that the stiffness of these elements could increase more over the boundary 1.2. Fig. D.14 shows highly increased elements.

Table D.10 Comparison of PSCB bridge results

Modes	Test	Matrix update		Genetic algorithm	
		Initial	Update	Initial	Update
1	2.47	2.33(-5.55%)	2.47(-0.04%)	2.27(-7.80%)	2.48(0.80%)
2	2.56	2.41(-5.93%)	2.56(-0.07%)	2.34(-8.62%)	2.56(-0.28%)
3	2.68	2.53(-5.70%)	2.68(-0.07%)	2.45(-8.80%)	2.67(-0.60%)
4	2.83	2.69(-5.11%)	2.83(-0.07%)	2.59(-8.51%)	2.82(-0.42%)
5	2.99	2.88(-3.77%)	2.99(-0.03%)	2.76(-7.79%)	3.00(0.23%)
6	3.19	3.10(-2.92%)	3.19(-0.03%)	2.95(-7.63%)	3.20(0.26%)

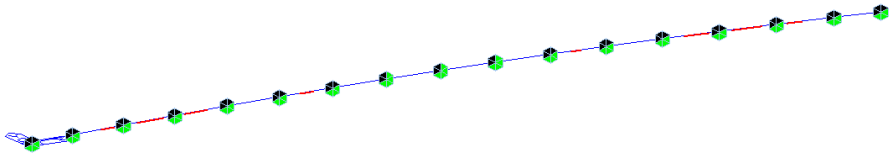

Fig. D.14 Location of highly increased elements (red)

D.4.2 Voided slab bridge

Table D.11 shows that matrix update method is more precise than genetic algorithm method in both of initial and updated results too. matrix update method ended with 2461 iterations and it didn't reach its tolerance value (0.1%). In the other hand, Genetic Algorithm ended after iterations 3000 (200 populations × 15 generations) as the user defined. However, in case of matrix update method, stiffness of 181 elements changed to 0.6 (lower boundary) and 807 elements changed to 1.4 (upper boundary). It means that the stiffness of these elements could change more. The elements that changed to1.4 were longitudinal grillage elements. Fig. D.15 shows that most of longitudinal grillage's stiffness factor changed to 1.4.

Table D.11 Comparison of Voided slab bridge results

Modes	Test	Matrix Update		Genetic Algorithm	
		Initial	Update	Initial	Update
1	5.27	4.65(-11.80%)	5.26(-0.15%)	4.59(-12.85%)	5.28(0.10%)
2	7.45	7.38(-0.90%)	7.45(-0.03%)	7.21(-3.18%)	7.51(0.80%)
3	9.60	9.62(0.21%)	9.59(-0.06%)	9.26(-3.55%)	9.61(0.06%)

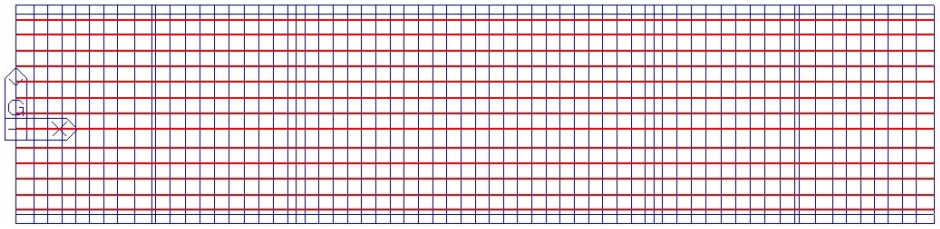

Fig. D.15 Longitudinal grillage's stiffness changed to 1.4

D.4.2 Conclusion

The results of those of two model update methods were relatively satisfactory. The different results of initial model of matrix update method and genetic algorithm are caused by the solver and boundary condition. These are my opinion of strengths and weaknesses of two methods.

1. Matrix Update Method

- If the results reached tolerance, it stops its iteration → calculation time shortening

- Tolerance can be defined

- Initial and updated results are more accurate than those of GA

- It is difficult to model FE (code-based modelling)

- Stiffness of all elements are changed (can't select variables, selecting variables is useful when some elements would not be needed to change their stiffness)

2. Genetic Algorithm Method

- It is convenient to model FE because of using Midas Civil

- It is possible to select variables and make groups

- It runs to the defined iteration numbers

- Initial and updated results are less accurate than those of Matrix Update Method